Changes of *in vivo* functional properties of microglia in aging and Alzheimer's disease

Thesis submitted as requirement to fulfill the degree „Doctor of Philosophy" (Ph.D.)

at the
Faculty of Medicine
Eberhard Karls University
Tübingen

by

Olmedillas del Moral, Rosa Maria

from

Lima, Perú

December 2019

Dean: Professor Dr. B. Pichler

1. Reviewer: Universitätsprofessorin Dr. rer. nat. Olga Garaschuk
2. Reviewer: Universitätsprofessorin Dr. med. Manuela Neumann

A mis padres,
Mariano y Mercedes

Table of contents

List of Abbreviations

$[Ca^{2+}]_i$	intracellular free calcium concentration
AD	Alzheimer's disease
ADP	Adenosine 5'-diphosphate
AF	Alexa Fluor
ANOVA	analysis of variance
APP	amyloid precursor protein
ATP	Adenosine 5'-triphosphate
AUC	area under the curve
Aβ	Amyloid beta
BACE	β-secretase
BAPTA	1,2-bis(2-aminophenoxy)ethene
BBB	Blood brain barrier
BDNF	brain-derived neurotrophic factor
BW	body weight
CNS	central nervous system
CRAC	Ca^{2+} release-activated Ca^{2+} channel
DAM	disease-associated microglia
DAMP	damage-associated molecular pattern
DAPI	4′,6-diamidin-2-phenylindo
DNA	desoxyribonucleic acid
DREADD	Designer Receptor Exclusively Activated by a Designer Drug
e.g.	exempli gratia / for example
ECM	extracellular matrix
eGFP	enhanced green fluorescent protein
ER	endoplasmic reticulum
FAD	familial Alzheimer's disease
FOV	field of view
GABA	gamma-amino butyric acid
GECI	genetically-encoded Ca^{2+} indicator
HEPES	4-(2-hydroxyethyl)-1-piperazineethanesulfonic acid
i.e.	id est / that is to say
i.p.	intraperitoneal

Iba	Ionized calcium binding adaptor molecule
IHC	immunohistochemistry
IL	interleukin
IP$_3$R	inositol 1,4,5-trisphosphate receptors
IQR	interquartile range
LOAD	late onset Alzheimer's disease
LPS	Lipopolysaccharide
LV	lentivirus vector
mC	mCherry
MHC	major histocompatibility complex
MIP	maximum intensity projection
miR-9	microRNA-9
mRNA	messenger RNA
mTq2	mTurquoise2
mVN	mVenus
NA	numerical aperture
NFT	neurofibrilary tangles
NLRP3	NLR family pyrin domain containing 3
NO	nitric oxide
OGB	Oregon Green BAPTA
PAMP	pathogen-associated molecular pattern
PBS	phosphate-buffered saline
PFA	paraformaldehyde
PGK	phosphoglycerate kinase
PLC	phospholipase C
PMCA	plasma membrane Ca^{2+} ATPase
PRR	pattern recognition receptor
PS1	presenilin-1
PS2	presenilin-2
rAAV	recombinant adeno-associated virus
RGB	red green blue
RNA	ribonucleic acid
ROI	region of interest

s.c.	subcutaneous
SEM	standard error of the mean
SERCA	sarco/endoplasmic reticulum Ca^{2+} ATPase
SOCE	store-operated calcium entry
Tg	transgenic
TNF-α	Tumor necrosis factor-alpha
TRP	transient receptor potential
UDP	uridine 5'-diphosphate
WPRE	woodchuck hepatitis virus posttranscriptional regulatory element
WT	wild-type
ΔF/F	relative change in fluorescence over time

List of Figures

List of Tables

x

CHAPTER 1

Introduction

1.1. Microglial cells: origins and phenotype

Microglial cells are the primary resident macrophages of the Central Nervous System (CNS) and, as such, they are exquisitely sensitive to any change in their local environment, providing the first line of immune defense in response to injury or disease (Río-Hortega 1919; Sierra, Paolicelli, & Kettenmann 2019).

Microglia population represents, depending on the region studied, 5-12% of the total number of cells in the mouse brain (Lawson et al. 1990) and 0.5-16.6% in the human brain (Mittelbronn et al. 2001), and it has been estimated to comprise a population almost as numerous as the neuronal (Sousa et al. 2017).

In mice, microglia derive from a population of yolk-sac myeloid progenitor cells that migrate into the CNS at ~E9.5, before the establishment of the blood-brain barrier (BBB) (Alliot et al. 1999; Ginhoux et al. 2010; Ginhoux & Prinz 2015; Ferrero et al. 2018). The first wave of entry of microglia precursors into the developing brain coincides with the peak of neurogenesis and predates synaptogenesis (Menassa and Gomez-Nicola 2018; Garaschuk and Verkhratsky 2019). At this point, microglia display an amoeboid morphology with very high migratory and proliferative capacity that allows them to spread and colonize the whole brain (Zusso et al. 2012). Around the second postnatal week, microglia gradually acquire their typical ramified morphology of mature microglia (Zusso et al. 2012) and, due to its strong proliferation potential, their population will be maintained by lifetime local self-renewal, with no bone-marrow derived progenitor contribution needed (Ajami et al. 2007). In the mouse brain, the microglia turnover rates also depend on the brain region, with the highest rates found in the olfactory bulb (Askew et al. 2017; Tay et al. 2017) and the lowest in the cortex (Füger et al. 2017; Tay et al. 2017).

The molecular signature of acutely isolated microglia has been characterized using RNA-sequencing, and include genes encoding surface receptors such as *P2ry12*, *Tmem119* and *Trem2* (Galatro et al. 2017; Olah et al. 2018; Hickman et al. 2013; Butovsky et al. 2014). Microglia's origin and

their unique transcriptional signature distinguish them from other non-parenchymal macrophages (i.e., meningeal, perivascular, and choroid plexus macrophages) in the brain (Li & Barres 2018; Lopez-Atalaya et al. 2018). Importantly, in order to maintain their homeostatic identity, microglia need continuous crosstalk with neurons, astrocytes and oligodendrocytes (Butovsky et al. 2014; Hoek et al. 2000; Brionne et al. 2003; Cardona et al. 2006). One example of a crosstalk mediator is the neuronal chemokine fractalkine (Cx_3CL1), which is detected by the fractalkine receptor (Cx_3CR1) located in the plasma membrane of microglial cells. The Cx3CL1-Cx3CR1 signaling not only inhibits the production of pro-inflammatory cytokines by microglia (Cardona et al. 2006) but also regulates a broad spectrum of microglial properties under homeostatic conditions, such as the maturation and plasticity of neural circuits (Paolicelli et al. 2014).

Besides the extracellular signals, microglial phenotype is also regulated by intrinsic factors such as sexual identity and age. For example, adult-derived microglia have been shown to display transcriptional sex-differences, with a higher expression of genes associated with inflammatory responses, such as MHC II and the transcription factor NF-κB, in males compared to females (Guneykaya et al. 2018; Villa et al. 2018; Villa et al. 2019). Adult females, instead, have been shown to display a neuroprotective phenotype, since acute focal cerebral ischemia causes a reduced damage in female compared to male mice (Villa et al. 2018). Interestingly, sex differences are independent of estrogens and are retained both *in vitro* and after transplantation into the brain of the opposite sex (Villa et al. 2018).

Aging is another factor that shapes microglial phenotype. For example, aged microglia increase their expression of the major histocompatibility complex II (MHC-II) antigen (Overmyer et al. 1999; Henry et al. 2009; Streit et al. 2014), pro-inflammatory (TNF-α, IL-1β, IL-6) and anti-inflammatory (IL-10 and TFG-β) cytokines (Dinarello 2006; Sierra et al. 2007; Singh & Newman 2011), and they increase their soma size and shorten their processes (Damani et al. 2011; Hefendehl et al. 2014). Yet the functional

consequences for these changes and their interaction with sex remain obscure.

In the following section, I will introduce the known functional properties of adult microglia under homeostatic conditions and during tissue damage or infection.

1.2. Functional properties of adult microglia

In adult mice under physiological conditions (i.e. in the absence of any immune stimulus), microglial cells display a ramified morphology with a small soma and fine processes, and occupy non-overlapping territorial domains (Nimmerjahn et al. 2005). For many years it was believed that microglia are quiescent or resting under homeostatic conditions, but in 2005 Nimmerjahn et al. and Davalos et al. reported for the first time that microglia are highly motile *in vivo* (Nimmerjahn et al. 2005; Davalos et al. 2005). Although their somata was reported to be largely sessile, microglial processes were shown to have a constant radial extension and retraction at an average rate of 2.2 ± 0.2 µm/min, which was proposed to reflect a microglial's surveillant state (Nimmerjahn et al. 2005; Davalos et al. 2005; Kettenmann et al. 2011). Soon after, it was shown that microglia are not only the first line of brain's immune defense but they are also involved in a variety physiological functions. For example, during CNS development, microglia remove immature synaptic connections and apoptotic neurons (Marín-Teva et al. 2004; Stevens et al. 2007; Schafer et al. 2012). In adulthood, microglia are involved in the activity-dependent synaptic elimination in the visual cortex (Wake et al. 2009; Tremblay et al. 2010; Y. Li et al. 2012), and in the induction of synapse formation during learning by secretion of BDNF (Parkhurst et al. 2013). In adult neurogenic niches (i.e. olfactory bulb and hippocampus), microglia phagocyte adult born neurons that failed to survive, without inducing inflammation (Sierra et al. 2010; Lazarini et al. 2012; Denizet et al. 2017). Thus, far from being resting, microglia play crucial roles in maintaining and modifying the neuronal networks.

Upon infection or tissue damage, microglia recognize exogenous pathogen- and/or endogenous damage-associated molecular patterns (PAMPs and DAMPs, respectively). PAMPs are components from virus or bacteria, whereas DAMPs are self-molecules released by injured or stressed cells in abnormal amounts (Garaschuk & Verkhratsky 2019). Examples of PAMPs are the Gram-negative bacteria cell-wall component lipopolysaccharide (LPS), exogenous viral or bacterial DNA and RNA, and bacterial flagellin (Mogensen 2009). Among DAMPs, heat-shock proteins, endogenous DNA or RNA and adenosine triphosphate (ATP) trigger damage-associated response (Di Virgilio 2005). Depending on the stimulus, microglia may respond with the secretion of inflammatory mediators such as cytokines, chemokines, reactive oxygen species (ROS), nitric oxide (NO), and will increase their phagocytic, migratory and proliferative activity (Kettenmann et al. 2011). Concomitant to changes in protein expression, microglia change their morphology toward an amoeboid/hypertrophic shape, which is characterized by shortening of their processes, an increase in soma size and a decrease in dendritic density (Garaschuk 2017).

This response to PAMPs or DAMPs is known as neuroinflammation, i.e. a transient immune response to fight against the harmful signals (Wohleb & Godbout 2013). From a simplistic point of view, this response comprises two phases: an initial pro-inflammatory phase, characterized by secretion of inflammatory mediators, and a late anti-inflammatory phase, in which they promote angiogenesis, debris clearance and extracellular matrix deposition in order to restore the homeostatic balance (Sochocka et al. 2017; Cherry et al. 2014). The duration of the neuroinflammatory response may depend on the nature and intensity of the triggering stimulus (Wohleb & Godbout 2013) but if it is persistent and/or the system has difficulties to restore the homeostatic balance, this acute response converts to a chronic neuroinflammatory state which can eventually lead to tissue degeneration (Sochocka et al. 2017; Wohleb & Godbout 2013).

Microglia function as surveillant or sentinel cells is also reflected in the great variety of channels and receptors located in their cell membrane.

Receptors expressed on the surface of microglia under physiological conditions belong to the microglial 'sensome' (Hickman et al. 2013). Gene ontology analysis revealed that many of the receptors belonging to the sensome are associated with the immunocompetent properties of microglial cells: pattern recognition receptors (PRRs) account for 25% of the microglial sensome, while other receptor groups include cytokine receptors (10%), receptors involved in cell-cell interaction (10%), chemokine receptors (10%), purinergic receptors (8%), receptors for extracellular matrix (ECM) proteins (6%), Fc receptors (7%), and other less well characterized receptors (24%) (Hickman et al. 2013).

In addition, microglia display a remarkable array of ion channels and other receptors which are also involved in sensing the brain's milieu (Stebbing et al. 2015; Garaschuk and Verkhratsky 2019). Although microglia are non-excitable cells, there is evidence showing the presence of Na^+ channels, voltage-gated Ca^{2+} channels, H^+ channels, voltage-dependent and voltage-independent Cl^- channels, and at least six different types of K^+ channels in microglial cells *in vitro* (Stebbing et al. 2015). Moreover, microglia also express many ion channels and receptors for neurotransmitters and neuromodulators, with multiple subtypes of both ionotropic and metabotropic receptors for glutamate, ATP, adenosine, acetylcholine, GABA, adrenaline, noradrenaline, serotonin and histamine (Garaschuk and Verkhratsky 2019; Brawek and Garaschuk 2013). The presence of some of these channels/receptors *in vivo* is yet to be demonstrated but it is possible that fewer are expressed or functional compared to *in vitro* conditions (Garaschuk and Verkhratsky 2019; Brawek and Garaschuk 2013). In any case, many microglial functions depend directly on these channels.

In summary, microglia have a great variety of functions not only as immunocompetent cells, but also as key players in the maintenance of brain homeostasis. Many of these functions are reflected by the channels and receptors they express under physiological conditions, which may help to unveil novel functions of these cells.

1.2.1. Ca^{2+} signaling in microglia

Intracellular free Ca^{2+} ions are used as second messengers by virtually all cells. In microglia, many of the receptors and channels induce an increase in the intracellular free Ca^{2+} concentration ([Ca^{2+}]$_i$) (Figure 1). Indeed, many executive functions of microglia, such as release of inflammatory mediators, phagocytosis and process chemotaxis are dependent on Ca^{2+} elevations (Färber & Kettenmann 2006; Stebbing et al. 2015). The most prominent microglial receptors linked to an increase in [Ca^{2+}]$_i$ are both the ionotropic P2X and metabotropic P2Y purinergic receptors (Färber and Kettenmann 2006). For example, the purinergic P2Y$_{12}$ receptor, essential for process chemotaxis, detects extracellular ATP which leads to an increase of [Ca^{2+}]$_i$ via the PI3K/Akt/PLC pathway (Irino et al. 2008).
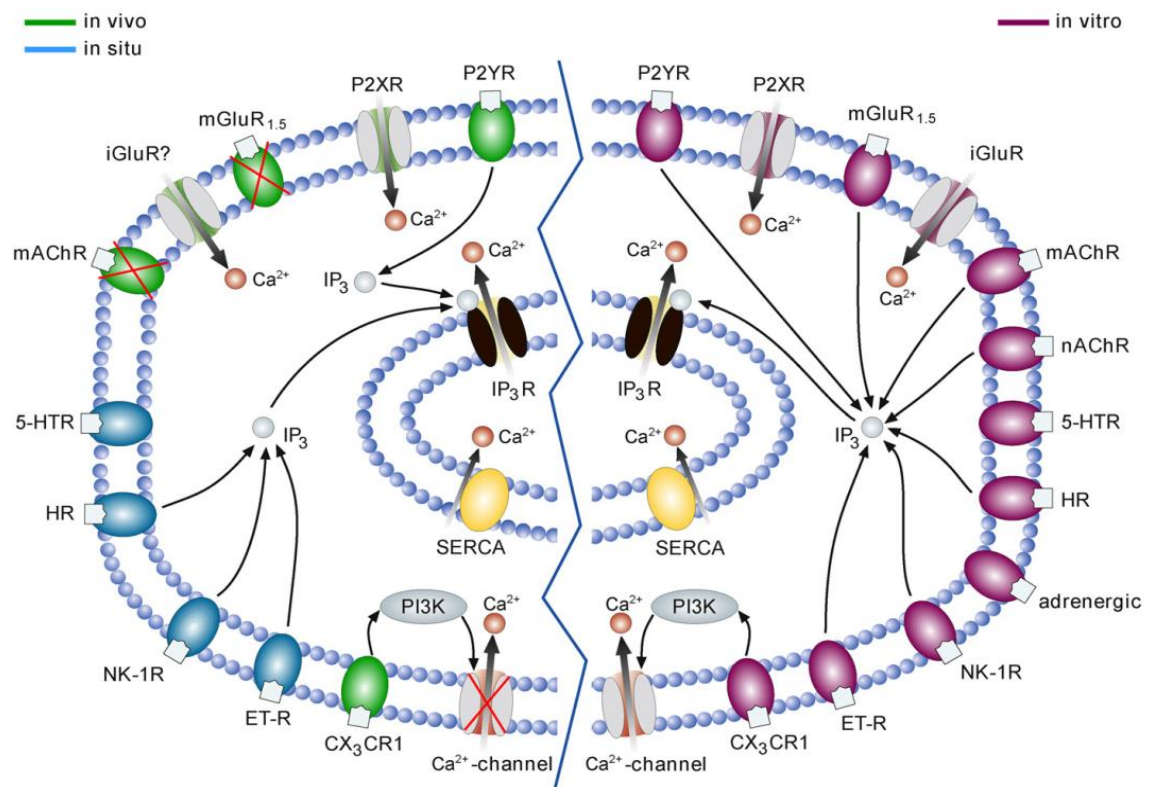
Figure 1. Agonist-induced Ca^{2+} signaling in microglia. Schematic drawing of a microglial cell illustrating receptors and channels known to increase [Ca^{2+}]$_i$ *in vivo* (green), *in situ* (blue) and *in vitro* (purple). Image is taken from Brawek & Garaschuk 2013.

Microglia's $[Ca^{2+}]_i$ ranges between 50-100 nM *in vitro*, which is much lower compared to the $[Ca^{2+}]$ in the extracellular space and other intracellular compartments such as the endoplasmic reticulum (ER) (Korvers et al. 2016). This Ca^{2+} distribution is maintained by Ca^{2+} ATPases located in the plasma and ER membranes (PMCA and SERCA, respectively) (Korvers et al. 2016).

Despite the presence of voltage-gated Ca^{2+} channels and non-selective cation channels such as transient receptor potential (TRP) channels, intracellular Ca^{2+} elevations in microglial cells are primarily due to the Ca^{2+} release from the ER stores, induced by the activation of most of their metabotropic receptors (Kettenmann et al. 2011; Korvers et al. 2016). In microglial cells, this release is mainly mediated by inositol 1,4,5-trisphosphate receptors (IP$_3$R), which are Ca^{2+}-permeable channels located in the ER membrane (Kettenmann et al. 2011; Garaschuk and Verkhratsky 2019). Store depletion causes a transient cytosolic elevation of $[Ca^{2+}]_i$ followed by the refilling of ER stores with Ca^{2+} from the extracellular space entering the cell via highly Ca^{2+} selective Ca^{2+} release-activated Ca^{2+} (CRAC) channels or cation-permeable non-selective store-operated Ca^{2+} entry (SOCE) channels located in the plasma membrane (Verkhratsky and Parpura 2014).

Microglia Ca^{2+} signaling can also occur spontaneously. *In vivo*, these spontaneous Ca^{2+} signals have been reported in both ramified and hyperthrophic microglia and directly depend on activation of P2 receptors followed by release of Ca^{2+} from the ER stores (Eichhoff et al 2011; Brawek et al. 2014). These Ca^{2+} signals are independent of astrocytic Ca^{2+} waves, but increase their frequency in the absence of neuronal activity and upon induced localized damage in their vicinity (Eichhoff et al. 2011; Brawek et al. 2014). It was hypothesized that these "spontaneous" Ca^{2+} transients were triggered by damage-induced ATP release from neurons (Eichhoff et al. 2011). However, spontaneous Ca^{2+} transients has been also observed in purified microglia cultures with no neuronal or astroglial contamination (Korvers et al. 2016). The mechanisms underlying spontaneous Ca^{2+} signaling in microglia *in vitro* remain unknown but it was proposed to be

caused by ATP released from astrocytes (Verderio and Matteoli 2001) or from microglia itself in an autocrine manner (Korvers et al. 2016).

In the brain of healthy adult mice, spontaneous somatic Ca^{2+} transients in cortical microglia have been reported to be infrequent *in vivo* (Brawek et al. 2014; Eichhoff et al. 2011; Pozner et al. 2015). However, Ca^{2+} signaling increases upon the disruption of physiological conditions, such as in induced neuronal damage, laser tissue ablation, LPS challenge or application of ATP (Tvrdik and Kalani 2017). Eichhoff et al. showed that, upon inducing damage of a single neuron *in vivo* with a glass micropipette, microglia located in the vicinity responded rapidly with a large Ca^{2+} transient (Eichhoff et al. 2011). Similarly, *in vivo* laser-mediated tissue ablation induced an increase in the fraction of microglial cells displaying spontaneous Ca^{2+} transients (Pozner et al. 2015). Acute systemic inflammation induced by subcutaneous injection of LPS also increased the fraction of microglia displaying spontaneous Ca^{2+} transients 12h after the injection (Pozner et al. 2015). *In vitro*, LPS application on microglial cells caused a sustained increase in $[Ca^{2+}]_i$ (Hoffmann et al. 2003), and extracellular ATP application induces an immediate, transient increase in $[Ca^{2+}]_i$ both *in vitro* and *in vivo* (Stebbing et al. 2015; Eichhoff et al. 2011; Walz et al. 1993).

In summary, Ca^{2+} signaling in microglia represents the most common mechanism by which these cells respond to extracellular changes. Therefore, the study of Ca^{2+} represents a powerful approach to infer the microglia's functional state.

1.3. Methods to study microglia physiology

As mentioned above, microglia keep their homeostatic state by the continuous input received from their local environment (Butovsky et al. 2014; Amit et al. 2016; Gosselin et al. 2017; Bohlen et al. 2017). This is of particular importance when designing experiments to study microglia. Overall, microglia functions in the healthy or diseased brain are complex and, despite the rapid advances in the field, their behavior under physiological conditions is still far from being understood.

Because the currently available *in vitro* methods fail to recapitulate all the physiological hallmarks of homeostatic microglia (Timmerman et al. 2018), the most powerful tool to study microglial cells under physiological conditions necessarily involve the use of *in vivo* imaging methods, which I will briefly discuss in the following sections.

1.3.1. *In vivo* visualization of microglia

In the past two decades, there has been an great effort to visualize and study microglial cells in their native physiological environment, the intact brain (Brawek, Olmedillas del Moral, and Garaschuk 2019). The development of transgenic mouse lines constitutively expressing the green fluorescent protein (GFP) in microglial cells allowed the first *in vivo* visualization of these cells and the monitoring of their dynamics in both healthy and pathological conditions (Hirasawa et al. 2007; Jung et al. 2000; Nimmerjahn, Kirchhoff, and Helmchen 2005; Askew et al. 2017; Bolmont et al. 2008; Hefendehl et al. 2014; Davalos et al. 2005; Wake et al. 2009; Schafer et al. 2012; M. Ě. Tremblay, Lowery, and Majewska 2010; Parkhurst et al. 2013). In the most widely used mouse line, the $CX_3CR1^{GFP/+}$ mice, one copy of the receptor for the chemokine fractalkine (CX_3CR1) has been replaced by the gene encoding GFP under the control of the CX_3CR1 promoter (Jung et al. 2000). The other frequently used mouse line is Iba-eGFP, in which eGFP is expressed under the control of the ionized Ca^{2+} binding protein-1 (Iba1) promoter (Hirasawa et al. 2007). However, the main limitation of these mouse lines is that they also express GFP in other myeloid cells such as monocytes and peripheral macrophages. This is particularly problematic in conditions in which monocytic infiltration occurs, such as during pathological conditions (Simard et al. 2006; Michaud et al. 2013).

Another method that allows fast detection of resident microglial cells in the brain is their labeling with fluorophore-conjugated Tomato lectin (Schwendele et al. 2012; Brawek et al. 2019). This method can be easily used in acute *in vivo* experiments but it is not possible for longitudinal studies (Schwendele et al. 2012).

Among the viral strategies, Åkerblom et al. described the first lentiviral method for labeling resident microglia (Åkerblom et al. 2013). This method involved the transduction with microRNA-9-regulated vectors, which contain the GFP gene under the ubiquitous phosphoglycerate kinase (PGK) promoter, and microRNA-9 target sites downstream the cassette (Åkerblom et al. 2013). Because microglia do not express microRNA-9, the fluorescent reporter mRNAs in these cells are able to undergo translation. The latest study using lentiviral vectors was done by Nie et al. (Nie et al. 2018). The authors used the PGK-GFP-4miR.T construct as a starting vector and replaced the GFP transgene with a double-floxed inverted open reading frame (DIO) encoding mCherry and artificial microRNAs for *Tlr2* and *Tlr4* in tandem (pLV-PGK-DIO-mCherry-TLR4miR-TLR2miR). Then, they injected the virus into a mouse line expressing tamoxifen-inducible Cre-recombinase in CX$_3$CR1-positive cells in the prefrontal cortex, which resulted in microglia-specific knockdown of TLR2/4 in this area after injection with tamoxifen. After four weeks, microglia were specifically labeled with a transduction efficiency of 25% and 45% for control and RNAi, respectively (Nie et al. 2018). This discrepancy between efficiencies in control and RNAi-transduced mice was not explained.

The first use of recombinant adeno-viruses (rAAVs) for targeting microglia *in vivo* was done by Bartlett et al. in 1998. Their approach used Cy3-labeled capsids of AAV2, and infused them into the inferior colliculus and hippocampus. They repeated the method with rAAV-CMV-GFP virus, to test the correlation between virus uptake and transduction efficiency. Although Cy3 was found in microglia 24 h after virus infusion, GFP was however not expressed, suggesting that either the virus underwent degradation or the expression of the GFP protein was suppressed (Bartlett et al. 1998). Years later, Rosario et al. introduced capsid-modified rAAV6 virus to drive GFP expression in microglial cells both *in vitro* and *in vivo* (Rosario et al. 2016). Although this approach had a transduction efficiency of up to 95% *in vitro*, the efficiency *in vivo* was not reported by the authors. Lately, Grace et al. intrathecally transduced microglia in the spinal cord with AAV2/9

containing DREADD (Designer Receptor Exclusively Activated by a Designer Drug) driven under the CD68 promoter. The authors showed that DREADDs colocalize with Iba1+ cells, but not with NeuN+ neurons or GFAP+ astrocytes (Grace et al. 2016). Unfortunately, GFP background fluorescence was high, making difficult to rely on this conclusion.

Other approach to visualize microglia is the use of transgenic mouse lines. The mouse line Cx$_3$cr1^{CreER} expresses tamoxifen-inducible Cre-recombinase in CX$_3$CR1-positive cells and allows conditional labeling of resident microglia. These mice can be crossed with different reporter mouse lines (Yona et al. 2013; Goldmann et al. 2013; Parkhurst et al. 2013). Tamoxifen treatment induces the labeling of all monocytic cells including peripheral cells, however, due to their short half-life, monocytes rapidly lose their fluorescent expression, whereas the long-lived microglial cells express the fluorophore up to several weeks or months, like in the Cx3CR1$^{creER/+}$ R26R$^{Confetti/+}$ mice (Tay et al. 2017; Yona et al. 2013). The caveats for Cx$_3$cr1^{CreER} mice are the expression of unicolor reporter genes, which make difficult the individual tracking of microglia in longitudinal experiments. The low transduction efficiency rates in Cx3CR1$^{creER/+}$ R26R$^{Confetti/+}$ mice was also considered by the authors a limitation of the method.

Finally, Füger et al. generated a double transgenic Cd11b-CreERT2;R26-tdTomato mouse line, in which fluorescent protein tdTomato is induced by tamoxifen injection in Cd11b-positive cells (Füger et al. 2017). These mice can be crossed with Iba-GFP mice to generate the triple transgenic Cd11b-CreERT2;R26-tdTomato;Iba-GFP mouse line (Füger et al. 2017). By using these approaches coupled with long-term imaging, it was shown that cortical microglial cells can persist until the end of the mean lifespan of 26-28 months of C57BL/6 mice, and thus are long-lived cells in the mouse (Füger et al. 2017).

All of the above-mentioned methods for visualization of microglia, except for the Cx3CR1$^{creER/+}$ R26R$^{Confetti/+}$ mice, are unicolor reporter mouse models, thus not allowing the discrimination of individual cells for longitudinal tracking or clonal studies. In addition, the transduction efficiency of all viral

methods available is rather low. Therefore, in order to visualize microglia for longitudinal experiments there is a need for new labeling methods that i) mark resident microglia *in vivo* with high efficiency and ii) allow discrimination between neighboring cells to facilitate the single-cell tracking.

1.3.2. *In vivo* calcium imaging of microglia

Upon infection or damage microglia are known to change their morphology typically characterized by the increase in soma size, shortening and thicken of their processes. Thus, morphological changes observed upon infection or damage were often seen as changes in microglial function. However, it is becoming increasingly clear that functional properties of microglia are not always reflected in their morphological phenotype (Perry & Holmes 2014). Because of the great number of receptors linked to Ca^{2+} elevations, the study of Ca^{2+} signals represents a more reliable approach to infer the functional properties of microglia.

To study Ca^{2+} signaling properties of microglia *in vitro*, microglial cells can be loaded with the synthetic Ca^{2+} indicator Fura-2 (Walz et al. 1993; Hoffmann et al. 2003). However, it has been a challenge to label microglial cells *in vivo* with small molecule Ca^{2+} indicators. The first successful approach used single-cell electroporation of individual microglial cells with the Ca^{2+} indicator Oregon Green BAPTA-1 (Eichhoff et al. 2011), allowing the visualization of microglial Ca^{2+} signals *in vivo*.

The first viral approach to deliver a genetically-encoded Ca^{2+} indicator (GECI) in microglial cells involved the use of retroviruses encoding the Ca^{2+} sensor GCaMP2 (Seifert et al. 2011). However, due to its ability to infect dividing cells only, the authors had to induce microglia proliferation mechanically via stab wound injury (Seifert et al. 2011). Later, the PC::G5-tdT mouse line was generated, which expresses the Ca^{2+} indicator GCaMP5G and the red fluorescent reporter tdTomato (Pozner et al. 2015). More recently, Brawek et al. adapted the use of miRNA-9-regulated lentiviral vectors from Åkerblom et al. to drive the expression of the ratiometric Ca^{2+} indicator Twitch-2B (Åkerblom et al. 2013; Brawek et al. 2017).

In Table 1, I summarize the currently available methods for *in vivo* visualization of microglial cells and the approaches for labeling microglia *in vivo* with Ca²⁺ indicators.

Table 1. Summary of methods currently available to study microglial cells *in vivo*.

Purpose of labeling	Current options available
In vivo visualization	
- Direct methods	Plant lectin conjugated with fluorophores (tomato lectin, isolectin IB4) (Schwendele et al 2012, Eichoff et al 2011, Brawek et al 2019)
- Transgenic mouse lines	$Cx_3CR1^{GFP/+}$ and $Cx_3CR1^{eGFP/+}$ mice (Jung et al 2000) Iba-GFP mice (Hirasawa et al 2005) $Cx3cr1^{creER}R26R^{DsRed}$ mice (Parkhurst et al 2013) $Cx3cr1^{creER}R26^{YFP}$ mice (Yona et al 2013, Goldmann et al 2013) $Cx3CR1^{creER/+} R26R^{Confetti/+}$ mice (Tay et al 2017) Cd11b-CreERT2;R26-tdTomato (Füger et al 2017) Cd11b-CreERT2;R26-tdTomato;Iba-eGFP mice (Füger et al 2017)
- Viral labeling	miRNA-9-regulated lentiviral vectors (Akerblom et al 2013) PGK-DIO-mCherry-TLR2/4RNAi (Nie et al 2018) Recombinant adeno-associated viruses (rAAV) (Rosario et al 2016) AAV2/9 containing DREADD (Grace et al. 2016)
In vivo Ca²⁺ imaging	
- Direct loading methods	Single-cell electroporation of OGB-1 (Eichhoff et al 2011)
- GECIs	Retroviral delivery of GCaMP2 (Seifert et al 2011) Lentiviral delivery of Twitch-2B (Brawek et al 2017) GCaMP5G in PC::G5-tdT mice (Pozner et al 2015)

1.4. Microglia in aging and pathology

Brain aging is a normal biological process characterized by numerous morphological and functional alterations of cells, eventually leading to cognitive decline (Hof & Morrison 2004). However, the incidence of neurodegenerative diseases such as Alzheimer's disease (AD), the most common one, increases exponentially after the age of 65. With the rising life expectancy, AD is predicted to affect 115 million people by 2050 (Prince et al. 2016), thus causing a massive economic burden on our society. Developing effective therapeutic strategies for AD demands a better

understanding of the biological processes underlying both normal and pathological brain aging.

In the recent years, genome wide association studies (GWAS) and meta-analyses have pointed to microglial cells as key players in aging and AD (Song and Colonna 2018; Mukherjee et al. 2019). In the following sections, I will introduce what is the current knowledge about microglia phenotype in both aging and in AD, the most common form of dementia worldwide.

1.4.1. Age-related changes in microglia phenotype

A pervasive feature of aging is the presence of low-grade chronic inflammation, a phenomenon termed "inflammaging" almost 20 years ago (Franceschi et al. 2000). This inflammatory state is thought to be sterile, as it occurs in the absence of overt infection, and it correlates with increased likelihood of a diagnosis of AD and dementia (Schmidt et al. 2002; Dunn et al. 2005; Engelhart et al. 2004). The reasons for this correlation, however, are not known yet.

Much of our knowledge about neuroinflammation in aging comes from gerontological data in humans, which have extensively reported an increase of systemic levels of pro-inflammatory cytokines and other inflammatory mediators in human plasma or serum in cohorts of older people (Singh and Newman 2011).

As mentioned in section 1.1, aged microglial cells were shown to display a "reactive" phenotype, documented by an enhanced expression of pro-inflammatory (TNF-α, IL-1β, IL-6) and anti-inflammatory (IL-10 and TFG-β) cytokines (Dinarello 2006; Sierra et al. 2007; Singh & Newman 2011), major histocompatibility complex II (MHC-II) antigen (Overmyer et al. 1999; Henry et al. 2009; Streit et al. 2014), and an increase their soma size and shortening of their processes (Damani et al. 2011; Hefendehl et al. 2014). However, aged microglia have also been proposed to display a senescent or dysfunctional, rather than reactive phenotype. The first evidence supporting this hypothesis came from histological studies in 2004, where microglia from

50-70 year-old humans were shown to display signs of deramification, spheroid formations and a fragmented-like cytoplasm (Streit et al. 2004). This phenotype was believed to reflect the cell's inability to perform their normal homeostatic surveillance functions. Some years later, this hypothesis was supported by *in vivo* studies in mouse retina, in which microglial cells were shown to display are reduced process motility in old mice *in vivo* (Damani et al. 2011). In addition, microglia from old mice was shown to display smaller and less branched dendritic arbors than those from young mice (Damani et al. 2011). Similarly, cortical microglia were also shown to display an increase in soma volume and shortening of processes with aging (Hefendehl et al. 2014).

Microglia also seem to change their spatial distribution with aging. While in the adult brain microglia occupy non-overlapping territorial domains and are homogeneously distributed within the brain areas, microglia in the aged brain are often closely juxtaposed and appear to lose their homogeneous distribution, with more microglia-free areas found in the mouse visual and auditory cortices (Tremblay et al. 2012; Hefendehl et al. 2014).

Finally, recent transcriptomic studies revealed that microglia might display, however, a neuroprotective and immunotolerant phenotype with aging. Genome-wide transcriptome studies of mouse microglia have generated aging brain expression profiles in these cells. More than 81% of the microglia sensome transcripts that were downregulated with aging were associated with endogenous sensing, but those involved in phagocytosis or microbe recognition were unaffected (Hickman et al. 2013; Orre et al. 2014; Grabert et al. 2016). The gene ontology (GO) category "cytoskeletal protein binding" was significantly decreased in aged microglia, whereas the GO categories "inflammatory response" and "cytokine activity" were enriched (Orre et al. 2014). More recently, gene expression profiles of isolated human microglia showed reduced expression of many cytoskeleton-associated genes, sensome cell surface receptors $P2Y_{12}$, IL6R and TLR10, as well as components from the TGF-β pathway (Grabert et al. 2016; Galatro et al. 2017; Olah et al. 2018).

A summary of changes in microglia phenotype (transcriptomic, morphological and physiological) as well as their distribution within the brain are shown in Table 2.

Table 2. Summary of age-related changes in the microglia distribution, morphology and physiology *in vivo*.

Changes in the transcriptomic profile
- Downregulation of genes involved in sensing (Hickman et al. 2013) - Upregulation of inflammatory-response associated genes (Orre et al. 2014) - Downregulation of the expression of actin cytoskeleton-associated genes (Galatro et al. 2017)
Changes in microglia distribution
- Increase in microglial density in the cortex (Hefendehl et al. 2014) - Decrease of homogeneous distribution (Tremblay et al. 2012) - Translocation into areas not previously occupied by microglia (e.g. to outer layers of the retina) (Damani et al. 2011)
Morphological changes
- Decrease of microglial dendritic arbors (Damani et al. 2011, Hefendehl et al. 2014) - Increase of soma size (Damani et al. 2011, Hefendehl et al. 2014) - Dystrophic microglia in humans (Streit et al. 2004)
Changes in physiological properties
- Decrease rate of process movement (Hefendehl et al. 2014) - Reduced migration rate to focal tissue injury (Damani et al. 2011)

In order to integrate and understand the functional meaning of aging-related changes provided by transcriptomics and immunohistochemistry studies there is a need for functional studies of microglia, for which *in vivo* assessing of microglia is crucial.

1.4.2. Alzheimer's disease

Alzheimer disease (AD) is the most common form of dementia currently affecting about 35 million people worldwide. It is characterized by progressive neurodegeneration, memory deficits as well as ultimate loss of cognitive abilities and death (Albert 1996). Despite the grim epidemiological forecast, there is no effective drug for AD to date, with treatments providing only symptomatic benefits for a limited time. Unfortunately, more than 400 drug candidates have failed in clinical trials during the last two decades (Mangialasche et al. 2010), which brings an urgent need for a better

understanding of the mechanisms underlying this disease in order to develop alternative drug targets.

The two histopathological hallmarks of AD are the presence of abundant accumulations of the extracellular amyloid β (Aβ) plaques and intracellular neurofibrillary tangles (NFTs) in neurons (https://www.alz.co.uk). The mechanisms underlying AD have been only elucidated in hereditary AD, the so-called familial AD (FAD). FAD is linked to mutations located in the genes for amyloid precursor protein (APP), presenilin-1 (PS1) and presenilin-2 (PS2) (https://www.alz.co.uk).

APP is an integral membrane protein with both cell-adhesion and receptor-like properties, and it is preferentially localized at pre- and postsynapses (De Strooper & Annaert 2000; Montagna et al. 2017). The putative functions of APP are the regulation of synapse formation and spine plasticity (Moya et al. 1994; Bart De Strooper and Annaert 2000; Wang et al. 2009; Weyer et al. 2014; Hick et al. 2015; Priller et al. 2006; Tyan et al. 2012). The sequential proteolysis of APP by β-secretase (BACE1) followed by γ-secretase generates amyloid β (Aβ), the central component of Aβ plaques. γ-Secretase is a multiprotein complex composed of PS1 or PS2, nicastrin, Aph1 and presenilin enhancer 2 (PEN2). Most FAD mutations affect the proteolytic processing of APP, resulting in the formation of a Aβ peptide more prone to aggregate ($A\beta_{>40}$) (Selkoe and Hardy 2016).

Unfortunately, only 1% of all AD cases are FAD, with the remaining 99% being sporadic (i.e. with no defined etiology) and occurring at or after a mean age of 65 (https://www.alz.co.uk). Despite this late onset, it has been estimated that the disease is usually initiated at least two decades prior to the time point of diagnosis (Bateman et al. 2012). Thus, understanding the mechanisms underlying pathology during the preclinical stage in order to develop drugs for early intervention is considered a vital research goal (Sasaguri et al. 2017).

In the recent years, '-omics' studies of the human brain pointed to microglial cells as causal agents in the development of sporadic AD (Navarro et al., 2018), so it has been proposed that targeting microglia might provide

benefit for AD pathology. The role of microglia in the context of AD, however, is far from being elucidated. In this work, I aimed at providing knowledge about the physiological properties of microglia, guided by the principle that AD is a disease that should ideally be prevented in preclinical stages, in which there might still be an interventional window for treating the disease effectively.

1.4.2.1. Microglia phenotype in AD

In AD, microglia appear clustered around amyloid plaques, displaying an amoeboid morphology characterized by enlarged soma size and fewer, thicker processes than ramified microglia (Navarro et al. 2018). However, the functional status of these cells remains unclear. It is not known yet whether a microglia plays a detrimental or insufficiently protective role in the disease (Navarro et al. 2018).

There were several efforts to elucidate the molecular signature of β-amyloid-plaque associated microglia and recent RNA-seq data from the mouse brain have suggested that microglia display a neuroprotective and immunotolerant phenotype in AD (Zöller et al. 2018; Keren-Shaul et al. 2017; Sala Frigerio et al. 2019). This subpopoulation of microglia was named disease-associated microglia (DAM) (Keren-Shaul et al. 2017) and it is characterized by the expression of genes related to phagocytosis and modulation of cytokine production and secretion. DAM microglia downregulate the homeostatic genes such as CX_3CR1, $P2Y_{12}$ or $Tmem119$, and upregulate genes such as $Apoe$, $Ctsd$, Lpl and $Trem2$, which are known to be risk factors for AD (Keren-Shaul et al. 2017). Interestingly, DAM microglia were also found in old mice but the fraction was smaller compared to that found in AD (Keren-Shaul et al. 2017; Sala Frigerio et al. 2019).

At the functional level, analyses of intracellular Ca^{2+} signaling of microglial cells *in vivo* revealed an increased hyperactivity in the vicinity of β-amyloid plaques in another mouse model of AD (Brawek et al. 2014). This hyperactivity was proposed to be the mechanism underlying ongoing microglial responses to acute and/or chronic insults, such as the secretion of cytokines (Brawek et al. 2014). Moreover, chemotaxis was impaired in these

mice, suggesting that dysregulation of Ca^{2+} signaling reflected an overall impairment of amyloid-associated microglia (Krabbe et al. 2013; Brawek et al. 2014).

It has been demonstrated, though, that microglia are able to clear up Aβ (D'Andrea et al. 2004; Mandrekar et al. 2009). However, excessive Aβ uptake by surrounding microglia causes lysosomal accumulation and eventual microglial cell death, which in turn contributes to plaque growth (Baik et al. 2016). Moreover, the plaque-microglia interface has been shown to be highly dynamic (Bolmont et al. 2008), highlighting the role of microglia not only for plaque clearance but also for plaque maintenance. So far, only microglial migration in amyloid-depositing mice has been reported, showing that microglia migrate toward Aβ plaques over a period of 24-48h (Bolmont et al. 2008). Other dynamic properties of these cells could not be assessed, however, due to the limitations of the methods. Indeed, the microglial turnover rate in plaque vicinity and its contribution to the number of plaque-associated microglia is yet to be determined. Thus, additional studies to elucidate microglia phenotype in AD are needed, which will provide new insights into the functional mechanisms of AD pathology.

1.4.2.2. AD mouse models for preclinical studies

The most common approach to study AD in animal models is the use of transgenic (Tg) mice that recapitulate the amyloid pathology observed in FAD patients. Several Tg mouse lines overexpress APP with FAD mutations such as the Indiana (V717F), London (V717I) and Swedish (K670N/M671L) mutations (Jankowsky and Zheng 2017). Examples are the PDAPP (Games et al. 1995), Tg2576 (Hsiao et al. 1996), APP23 (Sturchler-Pierrat et al. 1997), J20 (Mucke et al. 2000) and TgCRND8 (Chishti et al. 2001) mice.

Mice overexpressing mutant PS with FAD mutations alone do not induce Aβ pathology (De Strooper et al. 1995). Combination of mutated PS and APP confers strong Aβ pathogenicity, behavioral deficits and neuronal death (Holcomb et al. 1998). These mice include the PS/APP (Holcomb et al. 1998), the 5XFAD (Oakley et al. 2006) and the APPPS1 (Radde et al. 2006) mice. All the above-mentioned mice, however, do not recapitulate NFT

pathology. A triple Tg model the 3xTg mice was generated, which combine the expression of FAD mutated APP and PS1 with a mutant form of tau found in frontotemporal dementia and parkinsonism linked to chromosome 17 (FTDP-17) (Oddo et al. 2003). The main caveat of this model is that it represents a composite of two distinct pathologies that do not naturally occur together, making very difficult the interpretation of the results. A summary of the most widely used Tg mouse models of AD is shown in Table 4.

In this thesis, I used the APPPS1 mouse model (Radde et al. 2006), which expresses the human APP transgene approximately 3 times more than the endogenous murine APP, with Aβ42 preferentially generated over Aβ40 (Radde et al. 2006). In the neocortex, amyloid plaque deposition starts approximately at the age of 6 weeks and increases progressively with aging. Cognitive impairment also emerges with aging: at seven months of age, these mice display a deficit in performance in Morris Water maze test (Serneels et al. 2009), and at eight months of age, a reversal learning of a food-rewarded four-arm spatial maze task is reported (Radde et al. 2006). Thus, APPPS1 mice represent a suitable mouse model to study amyloidosis-related changes in the brain, allowing relatively rapid experimental readouts.

Table 3. Selected examples of mouse models of AD.

Strain	Mutation	Promoter	Pathology	Reference
PDAPP	APP^{V717F}	PDGF-β	Aβ plaques at 6-9 months of age	Games et al. 1995
Tg2576	APP$^{KM670/671NL}$	PrP	Aβ plaques at 11-13 months of age	Hsiao et al. 1996
APP23	APP$^{KM670/671NL}$	Thy1	Aβ plaques at 6-9 months of age	Sturchler-Pierrat et al. 1997
J20	APP$^{KM670/671NL,V717F}$	PDGF-β	Aβ plaques at 5-7 months of age	Mucke et al. 2000
TgCRND8	APP$^{KM670/671NL,V717F}$	PrP	Aβ plaques by 3 months of age	Chsihti et al. 2001
PS/APP	APP$^{KM670/671NL}$ PS1^{M146L}	PrP PDGF-β	Aβ plaques by 6 months of age	Holcomb et al. 1998
5XFAD	APP$^{KM670/671NL,I716V,V717I}$ PS1^{M146L,L286V}	Thy1	Aβ plaques by 2 months of age	Oakley et al. 2006
APPPS1	APP$^{KM670/671NL}$ PS1^{L166P}	Thy1	Aβ plaques by 6-8 weeks of age	Radde et al. 2006
3xTg-AD	APP^{K670N,M671L} PS1^{M146V} MAPT^{P301L}	Thy1 (APP,Tau)	Aβ plaques by 6 monthss of age Tau pathology by 12 months of age	Oddo et al. 2003

21

1.5. Relevance and aim of the project

Brain aging is a normal biological process, but it is also the main risk factor for neurodegenerative diseases, such as Alzheimer's disease (AD). In the recent years, '-omics' studies of the human brain pointed out to microglia as causal agents of AD. Indeed, there is increasing evidence that targeting microglial cells might provide benefit for AD pathology. The functional role of microglia in the context of AD, however, is far from being elucidated. First, we still lack information about the functional properties of these cells during normal aging. And second, we do not understand how the pathology interacts with the organism's age. Detailed knowledge about cellular and physiological properties of microglia is therefore crucial, and this information can only be assessed by studying these cells in their native environment: the intact brain.

The main goal of this work was to provide a better understanding of the physiological changes, which microglial cells undergo during aging and AD, by using the following approaches:

- An *in vivo* characterization of the Ca^{2+} signaling properties of microglia during aging and AD, and understanding how these properties react to potential interaction between aging and amyloid deposition.

- An *in vivo* characterization of the dynamic properties of microglia during homeostatic conditions and in AD.

Materials and Methods

2.1. Mice

All animal experiments in this study were approved by the Regierungspraesidium Tuebingen of the federal state of Baden-Württemberg (Germany) and conducted in accordance with the corresponding institutional animal welfare guidelines. C57BL/6 mice (Charles River) served as wild-type (WT) animals in this work. Animals were housed in the animal facility with a 12 hours light/dark cycle and unlimited access to water and food.

For the aging experiments, 2- to 4-month-, 9- to 11-month-, and 18- to 22-month-old of either sex were used in all the experiments.

2.1.1. Transgenic mice

For aging experiments, $Cx_3CR1^{GFP/+}$ mice (Jung et al. 2000) were used in addition to WT mice. In these mice, one copy of the *CX₃CR1* gene was replaced by a green fluorescent protein (GFP) reporter gene (Jung et al. 2000), enabling its expression in monocytes, dendritic cells, NK cells, and brain microglia.

For studies of AD pathology, the APPPS1 transgenic mouse model (line 21) of AD was used (Radde et al. 2006). These mice contain human transgenes for the amyloid precursor protein (APP) with the KM670/671NL Swedish mutation and presenilin 1 (PS1) with the L166P mutation, both under the control of the Thy-1 promoter (Radde et al. 2006). APPPS1 and APPPS1/Iba-1–GFP mice were used for multicolor labeling of microglia in AD mice. APPPS1/Iba-1–GFP mice were obtained by crossing hemizygous Iba-1–GFP mice (Hirasawa et al. 2007) with hemizygous APPPS1 mice.

2.2. Animal surgery

2.2.1. Acute craniotomy

For acute craniotomy preparation, mice were anesthetized and monitored throughout the experiment by adjusting the concentration of isoflurane supplied (0.8 - 2% in O_2; CP-Pharma). Mice were placed on a heating plate throughout the experiment and breathing rates and body

temperature were kept between 90 and 140 BPM and 36-37 °C, respectively. The area of surgery was locally anesthetized with 2% Xylocaine (AstraZeneca) injected s.c. followed by skin excision above the region of interest.

After the skull was cleaned and dried, a custom-made recording chamber with an opening in the middle was glued with cyanoacrylic glue (UHU, Baden-Baden, Germany). The skull under the opening was gently thinned under a dissecting microscope using a dental drill (Ultimate 500, NSK, Japan). The animal was then transferred to the imaging setup and the recording chamber was perfused with warm (37 °C) extracellular solution containing (in mM): 125 NaCl, 4.5 KCl, 26 $NaHCO_3$, 1.25 NaH_2PO_4, 2 $CaCl_2$, 1 $MgCl_2$, 20 glucose, pH 7.4 when bubbled continuously with 95% O_2 and 5% CO_2 (Figure 2A). A thin (30 G) syringe needle was used to perform a small craniotomy (~1 mm^2) in an area devoid of big blood vessels. Dura mater was left intact (Olmedillas del Moral et al. 2019).

2.2.2. Chronic cranial window implantation

Mice were injected with an i.p. injection of fentanyl (0.05 mg/kg BW, Fentadon, Eurovet Animal Health, Netherlands), midazolam (5.0 mg/kg BW, Hameln Pharma Plus, Germany) and medetomidine (0.5 mg/kg BW, Dormilan, Alfavet, Germany). Then, the fur in the area of surgery was trimmed with a hair trimmer. Animals were placed onto a heating plate under a dissecting microscope and head was fixed within a stereotaxic frame. During the entire surgery, the body temperature was monitored and maintained between 36-37 °C. Mice received a s.c. injection with 5 mg/kg BW of the analgesic carprofen (Rymadil, Pfizer, USA). An i.p. injection of 4 mg/kg BW dexamethasone (Sigma-Aldrich, USA) was also injected before the surgery. All surgical instruments were pre-sterilized with a glass bead sterilizer (Fine Science Tools, USA) and cleaned with 70 % ethanol.

After skin disinfection with a povidone-iodine solution (Braunol, B. Braun, Germany) a local anesthetic (2 % xylocaine, AstraZeneca, UK) was injected s.c. in the area of surgery. Skin excision was performed above the

brain region of interest, and the skull was cleaned and dried. Then, a circular craniotomy of 3 mm diameter was performed above the motor cortex.

After virus injection, a sterile 3 mm circular glass coverslip was placed on opening. With the help of a syringe needle, the glass coverslip was pressed gently onto the brain and glued to the skull with cyanoacrylate glue (UHU, Germany). After fixation, the whole skull was covered with a thin layer of dental cement (Tetric Evoflow, Ivoclar Vivadent, Liechtenstein). Then, a custom-built titanium bar was attached posteriorly and dental cement was fixed with ultraviolet light. The bar was used for the fixation of the animal's head under the microscope during the imaging sessions. Mice were then transferred to the cage and received an s.c. injection of flumazenil (0.5 mg/kg BW, Fresenius, Germany) and atipamezole (2.5 mg/kg BW, Nosedorm, Alfavet, Germany) to antagonize the anesthesia. For the next 3 consecutive days, mice received s.c. injections of 5 mg/kg BW carprofen. Additionally, the drinking water was supplemented with 0.025 % of the antibiotic enrofloxacin (Baytril, Bayer, Germany) for 10 days. Mice were left 3-4 weeks in the animal facility for recovery time.

2.3. Immunohistochemistry (IHC)

At the end of each experiment, mouse brains were isolated and fixed with 4 % formaldehyde in phosphate-buffered saline (PBS) for 24 h at 4 °C, cryoprotected in 25 % sucrose in PBS (overnight, 4 °C), embedded in Tissue Tek (Sakura) and stored at −80 °C. Brains were cut in coronal 50 μm slices with a cryostat (Leica, Germany) and transferred to 24 well plates (Greiner Bio-One, Austria) containing PBS solution. All incubations and washing steps were carried out on free-floating sections at room temperature and on a horizontal shaker.

Brain slices were incubated 1 h in blocking solution (5 % normal donkey serum and 1 % Triton-X 100 in PBS). Then, the slices were incubated overnight with the primary antibody solution. A polyclonal goat anti-GFP antibody (1:2500, Rockland Immunochemicals, USA) was used in combination with a polyclonal rabbit anti-P2Y$_{12}$ antibody (1:500, AnaSpec,

USA). Then, slices were rinsed in PBS three times for 10 min and incubated with Alexa Fluor (AF) 594- and AF 488-conjugated secondary antibodies (1:1000 in PBS + 2 % bovine serum albumin; Invitrogen) for 2 h in darkness. After incubation, slices were washed in PBS three times. Cell nuclei were stained using 4′,6-diamidin-2-phenylindol (DAPI) (1:4,000; Thermo Scientific). Finally, the slices were washed three times in PBS, and mounted on fluorescence-free Superfrost Plus microscope slides (Langenbrinck, Germany) with Vectashield Mounting Medium (Vector Laboratories, USA).

2.4. *In vivo* labeling of microglia using Tomato lectin

In vivo labeling of microglia in WT mice was performed by means of fluorophore-conjugated Tomato lectin (Schwendele et al. 2012; Brawek, Olmedillas del Moral, and Garaschuk 2019). Tomato lectin is a 100 kDa protein isolated from tomato (*Lycopersicon esculentum)*, which binds to poly-N-acetylglucosamine located in the membrane from microglia and endothelial cells (Slifkin and Doyle 1990) and has been extensively used to identify microglial cells in cell culture and brain slices. Briefly, a solution of 25 µg/ml of dye-conjugated Tomato Lectin (Vector Laboratories, Burlingame, CA) was prepared in a standard pipette solution (140 mM K-Gluconate, 14 mM KCl, 4 mM NaCl and 10 mM HEPES, pH 7.4). After performing an acute craniotomy as described in section 2.2.1., the solution was filtered using a Millipore Ultrafree® centrifugal filter with a pore diameter of 0.45 µm and injected at depth of 100 µm below the brain surface by using a pressure application system with 60 kPa for 30 seconds. By using this protocol, a tissue volume with a diameter of approximately 100–150 µm is labeled. If a larger tissue volume was required to be labeled, an additional application was performed in another spot, avoiding the overlapping of the labeled areas (Brawek, Olmedillas del Moral, and Garaschuk 2019).

Following dye ejection, the pipette was withdrawn and 30 minutes was given for washout of the excess of solution.

2.5. *In vivo* single cell electroporation

For *in vivo* electroporation of microglia, an acute craniotomy was first performed as described in section 2.2.1. In WT mice, microglial cells were stained with Tomato lectin solution as described in the previous section. After 30 min washout of Tomato lectin, a glass micropipette with a tip diameter of <1 µm was filled with 10 mM OGB-1 hexapotassium salt dissolved in the standard pipette solution (see previous section). The resistance of the micropipette was ~5-7 MΩ (Brawek and Garaschuk 2019). Using a manipulator (LN Junior, Luigs & Neumann), individual microglial cells at a depth of 80-120 µm were approached with the micropipette until their surface was touched with the tip of the pipette (Figure 2B). Then, a negative current of 600 nA was applied for 10 ms using a MVCS-02C iontophoresis system (NPI Electronic). Immediately after the current application, the micropipette was carefully withdrawn and around 10-15 min was allowed for dye equilibration.
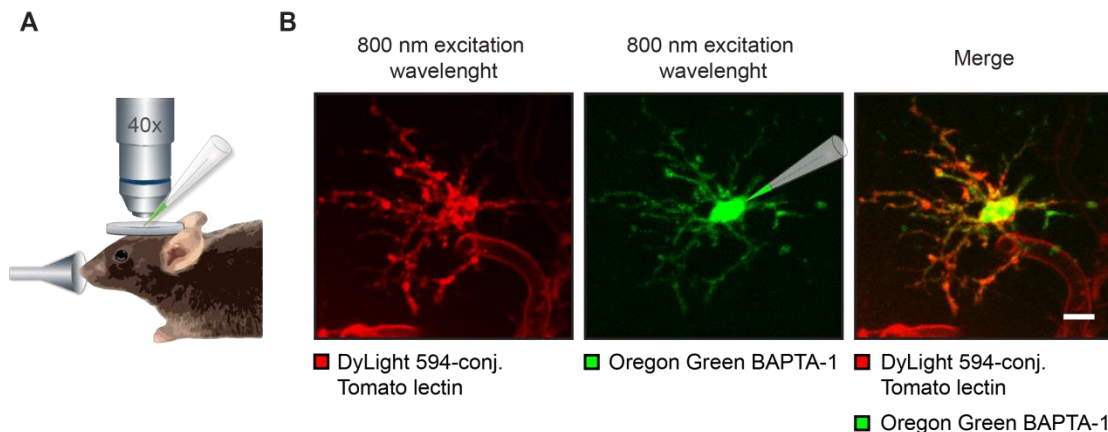
Figure 2. Single-cell electroporation technique for measuring microglial Ca²⁺ signaling
in vivo. (**A**) A glass micropipette containing the Ca²⁺ indicator Oregon Green BAPTA-1 (OGB-1) is inserted into the brain parenchyma through an acute craniotomy in an anesthetized mouse. (**B**) Maximum intensity projection (MIP) images of a representative microglial cell labeled with DyLight 594-conjugated Tomato lectin (left) and loaded with the Ca²⁺ indicator OGB-1 by means of single-cell electroporation in a WT mouse. Merged image is shown on the right. Scale bar: 5 µm. Panel (**B**) taken from Brawek, Olmedillas del Moral, and Garaschuk 2019.

To test the viability of the electroporated cells, 100 µM Uridine 5'-diphosphate (UDP, Sigma-Aldrich, USA) dissolved in standard pipette solution was injected in the vicinity of the cells to prove their ability to generate UDP-evoked Ca²⁺ transients. To allow the visualization of the

application pipette, 200 µM of AF 594 was added to the UDP-containing solution.

2.6. Multicolor labeling of microglia

In order to quantify the migration, proliferation and death events of microglia cells in both homeostatic conditions and in amyloid-depositing mice we designed a method that allowed *in vivo* color coding of individual microglial cells. To this purpose, we introduced a novel approach by means of microRNA-9-regulated vectors (Åkerblom et al. 2013). The structure of the starting lentiviral vector (LV.GFP.miR-9.T) has been described elsewhere (Åkerblom et al. 2013). Briefly, these vectors incorporate four target sites for microRNA-9 (miR-9) downstream to GFP. This leads to degradation of the GFP mRNA specifically in cells expressing miR-9. Since rodent microglia lacks miR-9 expression, miR-9-regulated vectors can be used for selective labeling of microglia (Åkerblom et al. 2013; Brawek et al. 2017) (Figure 3).
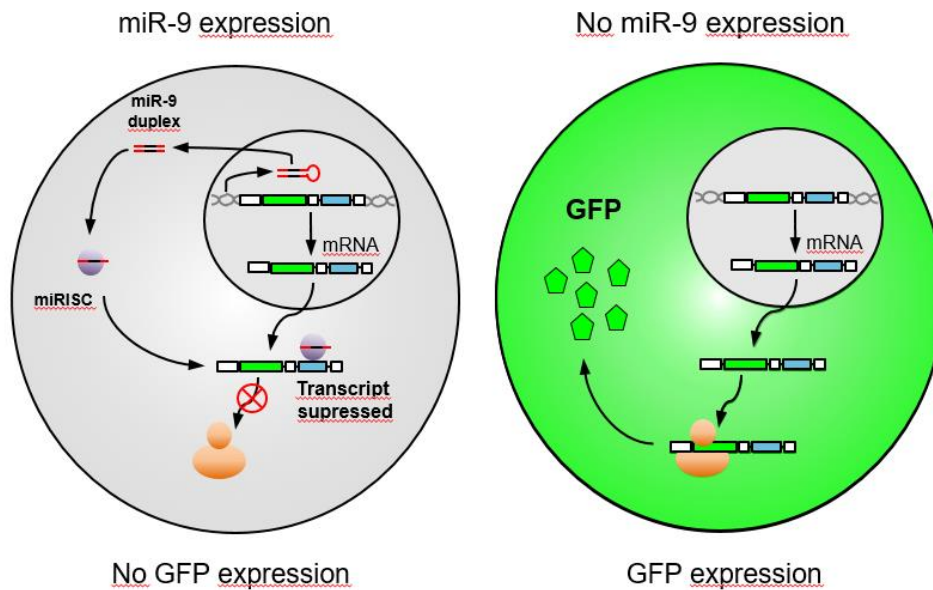
Figure 3. Mechanism of miR-9-regulated expression of GFP mRNA. Adapted from Åkerblom et al., 2013.

The structure of the starting lentiviral vector (LV.GFP.miR-9.T) was described by Åkerblom et al. (Åkerblom et al. 2013). Briefly, the target sites of miR-9 5′-TCATACAGCTAGATAACCAAAG-3′ were cloned immediately

downstream the woodchuck hepatitis virus post-transcriptional response element (WPRE) of a third-generation lentiviral vector. The fluorescence protein GFP in the original construct LV.GFP.miR.9.T was replaced by mCherry, or Venus, or mTurquoise2, generating the LV.FP.miR-9.T vectors. Cell-free supernatants containing viral particles were produced by transient transfection of HEK293T packaging cells with the lentiviral construct and helper plasmids (psPAX2 and pMD2G) as described previously (Kovalchuk et al. 2015; Brawek et al. 2017). After 48 h the virus-containing culture supernatant was collected, filtered through a 0.45 µm pore-sized filter and concentrated by centrifugation at 27,000 rpm for 2 h at 4 °C by using Thermofisher WX Ultra80 centrifuge (Waltham, MA, USA). Pellets were re-suspended in sterile PBS and stored at −80 °C. Viral solutions with a titer higher than 10^8 colony forming units/ml were used in this study. After purification of viruses released into the supernatant of cell culture medium, the three viruses were mixed together to make a 1:1:1 ratio of transduction efficacy which was named as the RGB viral solution.

After performing a 3-mm diameter craniotomy (as described in section 2.2.2) in the frontal/motor cortex, mice were injected with the RGB viral solution using a three-step procedure, in which 0.3 µl of the viral solution was injected at a depth of 0.53 mm, 0.3 µl at 0.4 mm and 0.3 µl at 0.22 mm with an application speed of 200 nl per min. Then, a cranial window was implanted as described in section 2.2.2. Mice were left 3 weeks in the animal facility for recovering.

2.7. *In vivo* image acquisitions and analysis

In vivo imaging was performed with a two-photon laser-scanning microscope (Olympus Fluoview 300, Olympus, Tokyo, Japan) coupled to a mode-locked laser operating at 690- to 1040-nm wavelength (MaiTai HP, Spectra Physics, Mountain View, CA) and equipped with a 40x water-immersion objective (0.80 NA, Nikon, Tokyo, Japan) (Olmedillas del Moral et al. 2019).

2.7.1. Ca^{2+} imaging

For imaging of spontaneous Ca^{2+} signals, OGB-1-loaded microglial cells were imaged at 800 nm at a sampling rate of 1 frame/s for a total recording period of 15 min. The chamber opening was covered with 2% agarose to suppress movement artifacts.

For measurement of UDP-evoked Ca^{2+} transients, the sampling rate was increased to 10 frames/s. OGB-1 and AF 594 (contained in the UDP solution) were excited at a wavelength of 800 nm. The emitted light was split by a beam splitter (580 nm) and sent through the BP510/84 and BP630/92 filters, respectively.

Image analyses were performed off-line using the Fiji (http://fiji.sc/Fiji) and/or Igor Pro (Wavemetrics, Lake Oswego, Oregon, United States) software. For measurements of Ca^{2+}-dependent changes in fluorescence, a region of interest (ROI) was drawn around the soma of OGB-labeled microglial cell and the mean fluorescence intensity was calculated within this area. The mean fluorescence intensity within a blood vessel area was used as background. Later, background-subtracted fluorescence intensity values were normalized and expressed as a relative change in fluorescence ($\Delta F/F$). Then, traces were filtered using a low-pass infinite impulse response (IIR) filter with a cut-off frequency of 0.2 Hz. A change in fluorescence was defined as a "Ca^{2+} transient" when its amplitude was higher than six times the standard deviation of the baseline noise. When estimating the number of Ca^{2+} transients encountered during a given time, we counted each Ca^{2+} transient whose fluorescence decayed to more than half of its amplitude. A microglial cell was considered spontaneously active when it displayed at least one spontaneous Ca^{2+} transient within a recording period of 15 min. Then, amplitude, duration (T-half) and areas under the curve (AUCs) of Ca^{2+} transients detected were measured for each transient (Olmedillas del Moral et al 2019).

2.7.2. Imaging of microglial process extension

For $Cx_3CR1^{GFP/+}$ mice, AF 594 was added into the ATP-containing solution. After application of ATP solution, a 3D stack (141 x 141 x 20 μm^3) of the region of interest was acquired every 30 s during ~20 min. GFP was excited at a wavelength of 900 nm. In all other mice, which were Tomato-lectin labeled, AF 488 was added to the ATP-containing solution instead. Both AF 488 and AF 594-conjugated Tomato lectin were excited at 800 nm. A beamsplitter (580 nm) was used to split the light emitted by AF 594 and AF 488, and sent through the BP510/84 and BP630/92 filters, respectively.

To analyse the ATP-evoked process extension of microglia, we measured the diameter of the containment formed by the processes as previously reported (Olmedillas del Moral et al 2019). Briefly, maximum intensity projections (MIPs) of time-lapsed 3D stacks were acquired every 30 seconds over a 15-min-long acquisition period at an x/y/z size of 141 x 141 x 20 μm^3 with a step size of 2 μm. The containment ring produced by microglial processes was fitted with an ellipse and its average diameter was calculated by measuring the mean of the major and minor diameters (Figure 4) at given time points. When the microglial processes converged around the pipette tip, the average diameter of the containment remained constant and it was read
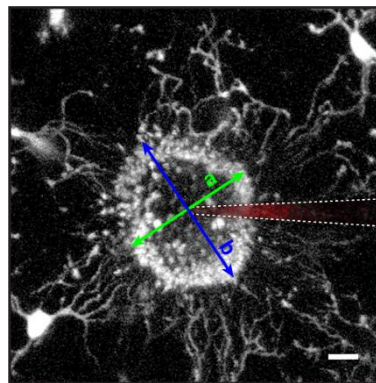
Figure 4. Measurement of the spherical containment generated around an ATP-containing pipette. MIP image of a Z stack (80–100 μm below the cortical surface, 2 μm step size), exemplifying the containment formation in a 2-month-old $Cx_3CR1^{GFP/+}$ mouse. The stack is taken 7 min after pressure application (50 ms, 30 kPa) of 5 mM ATP. Arrows indicate the minor (a) and major (b) diameters of the containment. White dashed lines emphasize the location of the ATP-containing pipette. Adapted from Olmedillas del Moral et al 2019). Scale bar: 5 μm.

out as the final diameter. The containment formation velocity (µm/min) was calculated as the reduction of the average diameter over a given time. To calculate the individual process velocities, we selected microglial processes, the tips of which could be unequivocally identified throughout at least seven consecutive time points. The processes were manually tracked over time using the ImageJ plug-in "MTrackJ" (https://imagescience.org/meijering/software/mtrackj/). The average process velocity (µm/min) was calculated by measuring the average distance travelled by a tracked tip between the two consecutive time points" (Olmedillas del Moral et al. 2019).

2.7.3. Longitudinal imaging sessions

After recovery time, RGB-injected mice (4-5 months old) were imaged once per day for 10-22 days by means of two-photon microscopy. Before each imaging session, mice were anesthetized with isoflurane (induction at 2% and immediately reduced and held constant at 0.8-1%), and then transferred to the imaging setup. Breathing rates and body temperature were monitored during every imaging session and kept between 90 and 140 BPM and 36-37 °C, respectively. Mouse head was fixed by screwing the custom-built titanium bar, implanted the day of surgery (see section 2.2.2), to the imaging setup. The window was then cleaned with 50% EtOH.

The fields of view (FOVs) were acquired at the periphery of the injection area (~100 µm distance from epicenter). In order to split the fluorescence emitted by RGB-labeled microglial cells, the following settings were used for excitation: mTurquoise2 and mCherry were excited at a wavelength of 800 nm, and the emitted light was split by a beam splitter (580 nm) and sent through the BP510/84 and BP630/92 filters, respectively. mVenus was excited at a wavelength of 990 nm, and the emitted light was split by a beam splitter (580 nm) and sent through the BP510/84 filter. Each FOV (235.7 µm x 235.7 µm, and 150 – 200 µm from dura) was sequentially scanned with 800 and 990 nm. Then, sulforhodamine B (0.1 ml/10 g BW, 1 mM in PBS, Sigma-Aldrich, St. Louis, MO, USA) was injected i.p. in order to generate a

fluorescent angiogram. One single shot enabled the visualization of blood vessels for approximately 2 h. Sulforhodamine B was excited at 900 nm, and the emitted signal was acquired through a LP channel of DM570. As shown previously (Liang et al. 2016) blood vessel pattern is very stable over prolonged periods of time, providing reliable landmarks for long-term tracking of individual cells.

In order to visualize amyloid plaques in APPPS1 or APPPS1/Iba-1-GFP mice, animals received an i.p. injection with 250 µl of amyloid staining solution (1% vol of 10 mg/ml methoxy-X04 (Klunk et al. 2002) in DMSO, and 2% vol CremophorEL (Sigma-Aldrich) in 97% vol PBS) every 10 days since the first day of the imaging session. Images were acquired 24 h after the injection. Methoxy-X04 was excited at 800 nm and the emitted light was registered through SP channel of DM515.

The 3D stacks acquired during the consecutive imaging sessions were combined off-line with the Fiji (http://fiji.sc/Fiji) software. Then, maximum projection images (MIPs) were generated from each stack and each cell was annotated with an identity number. A proliferation event was defined as the appearance of duplets consisting of two same-colored cells that lead to two independent cells in the consecutive days. A cell death event was defined as the disappearance of a cells and the deposition of cell debris on the consecutive day. Cell disappearance without debris deposition was considered cell loss but not included in the previous group.

For the analysis of migration events, the center of cell's soma within a 3D stack was marked as position point and the x, y, z coordinates were obtained. The x, y coordinates for each position point of a cell were read using the Fiji software. For Z axis coordinates, the depth of cells (Z_{ac}, actual depth of a cell) was the relative depth from the dura: $Z_{ac} = Z_{reading} - Z_{dura}$ (Liang et al 2016). Thus, the position history of each cell was generated. A change in soma position, or soma translocation, was understood as cell migration. With 3D coordinates for each position point, the migration distance (d) between two points in space was calculated by the following formula:

$$d = \sqrt{(x_2 - x_1)^2 + (y_2 - y_1)^2 + (z_2 - z_1)^2}$$

where (x_2, y_2, z_2) and (x_1, y_1, z_1) were the 3D coordinates of the cell position measured at time *n* and time *n-1*, respectively. Unless otherwise indicated, cell migration speed was defined as the translocation of the cell soma position between two consecutive days. Taking into account the 2-μm step size of the acquired stacks, a cell was considered migrating if the translocation of cell's soma between the two consecutive time points was ≥ 5 μm. To assess the direction of the movement, the maximal migration angle (θ) between the two immediately adjacent migration steps. If θ was ≤ 90°, then the migration of the cell was categorized as unidirectional; otherwise, as multidirectional. To calculate the fraction of migrating cells per time, the proportion of cells whose positions differed from that recorded at immediately preceding time point, was calculated in relation to the total number of cells in that stack (Liang et al. 2016).

2.8.   Statistics

For each experiment, the choice of the sample size was based on biometrical sample size estimation (Olmedillas del Moral et al. 2019). All statistical analyses were performed using either GraphPad Prism 6 (GraphPad Software Inc., La Jolla, CA, USA) or MATLAB (MathWorks, Inc., Natick, MA, USA). One-sample Kolmogorov-Smirnov and/or Shapiro-Wilk test were used to check for normality of the data distribution. Outliers were identified using the Tukey method in MATLAB (function "Quartiles") and excluded from data sets. Lines of box and whiskers represent 25th and 75th (box) and 10th and 90th (whiskers) percentile. In the text, all data are given as median ± interquartile range (IQR) unless otherwise indicated.

Comparisons of more than two independent variables were performed using the Kruskal–Wallis test followed by Dunn's post hoc test for multiple comparisons or one-way ANOVA followed by Bonferroni's post hoc test for multiple comparisons. Two-way ANOVA was used for testing the effect of two independent factors within the same dataset. All statistical tests were two-sided.

Spearman's rank correlation coefficient was calculated for estimating the relationship between the initial distance of a microglial process to the tip of an ATP-containing pipette and the average process velocity of extension.

To estimate the survival probability of each microglia cell tracked we used the Kaplan–Meier method. The disappearance of a tracked RGB-labeled microglia was marked as a death event. Statistical difference between the survival curves were determined by the log-rank Mantel-Cox test. In all statistical tests performed, difference was considered statistically significant if $p < 0.05$.

CHAPTER 3

Results

3.1. Age-dependent changes in microglial Ca^{2+} signaling

In order to provide a first characterization of the Ca^{2+} signaling properties of microglia during aging we performed *in vivo* imaging of the spontaneous Ca^{2+} signals in WT mice, for which we used three different age groups: 2-4 months old ("young adult"), 9-11 months old ("middle-aged") and 18-21 months old ("old") (Olmedillas del Moral et al., 2019; Figure 5A). To this purpose, I loaded cortical microglia with the Ca^{2+} indicator dye Oregon Green 488 BAPTA-1 (OGB-1) by means of single-cell electroporation described in section 2.5 (Eichhoff et al. 2011; Brawek et al. 2019) and measured the somatic Ca^{2+} signaling *in vivo.*

Our results reported that microglia from middle-aged WT mice display significantly higher number of spontaneous Ca^{2+} transients compared to young adult mice (p = 0.0417, Kruskal–Wallis test followed by Dunn's post hoc test). In contrast, old mice displayed microglia with lower frequencies compared to those from middle-aged mice (p = 0.0035, Kruskal–Wallis test followed by Dunn's post hoc test; Figure 5B, C).

Next, we measured the amplitude (% ΔF/F), duration (T-half, s) and area under the curve (AUC, ΔF/F*s) for all detected Ca^{2+} transients (Olmedillas del Moral et al., 2019; Figure 5D). Our results reported that both the durations and AUCs of the Ca^{2+} transients from old mice were also significantly reduced compared to middle-aged mice (p < 0.001 and p = 0.0405, respectively; Kruskal–Wallis test followed by Dunn's post hoc test; Figure 5E, F). No significant differences were found in the amplitudes of the Ca^{2+} transients between the three age groups (p = 0.1562, Kruskal–Wallis test), although there was a trend toward smaller amplitudes in both middle-aged and old mice, compared to young adult mice Figure 5D).
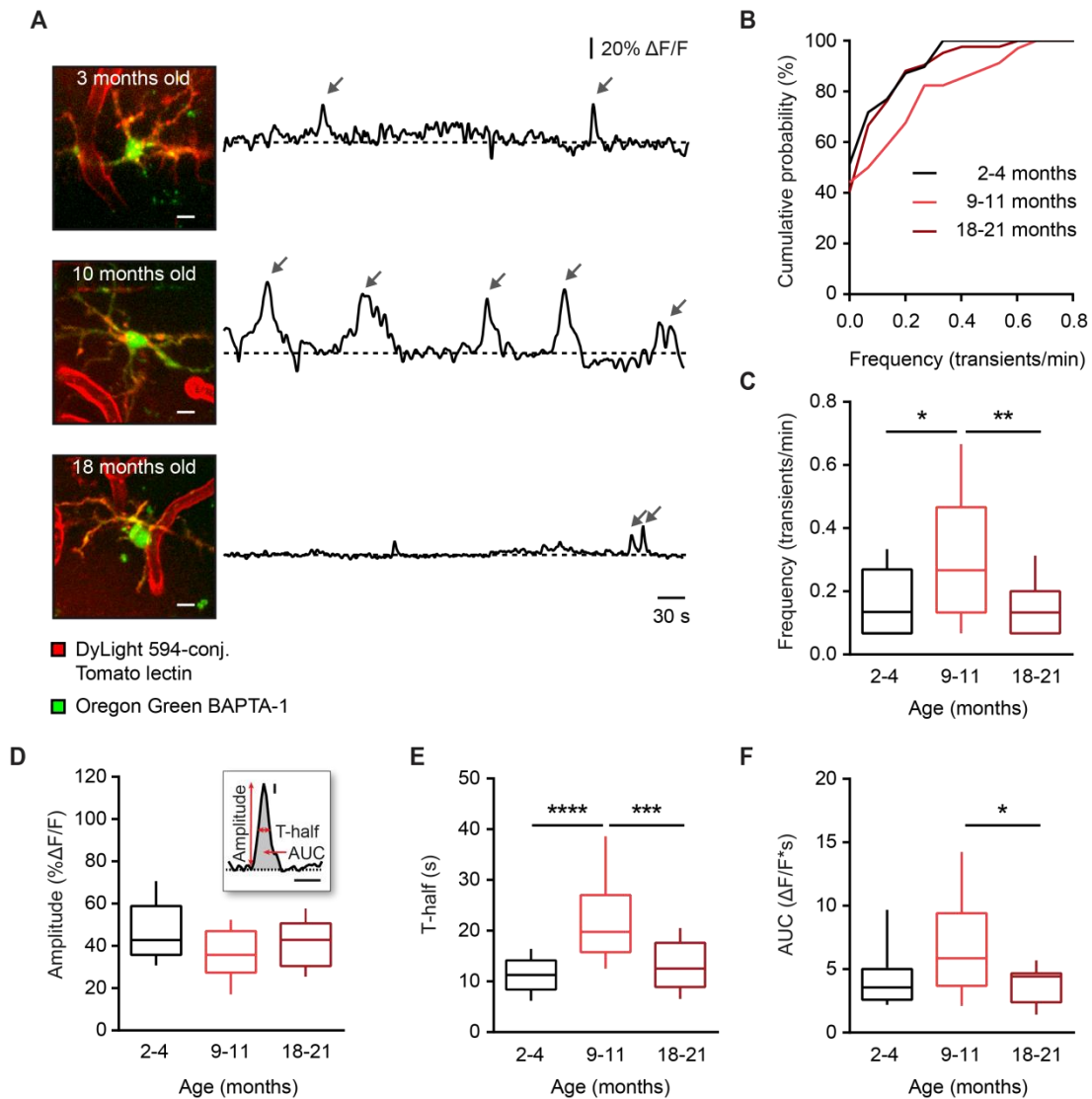
Figure 5. Age-dependent changes of microglial Ca^{2+} signaling properties in WT mice *in vivo.* (**A**) On the left (from top to bottom): maximum intensity projection (MIP) images of representative microglial cells from 3, 10- and 18-month-old mice labeled with DyLight 594-conjugated Tomato lectin and loaded with the Ca^{2+} indicator Oregon Green BAPTA-1 (OGB-1) by means of single-cell electroporation in WT mice (from 82-103 μm, 73-97 μm and 65-87 μm below the cortical surface, respectively). On the right, their respective spontaneous somatic Ca^{2+} transients recorded during a 15-min-long period. The arrows point to the spontaneous Ca^{2+} transients in respective cells. Scale bar: 5 μm. (**B**) Cumulative probability distributions of frequency of spontaneous Ca^{2+} transients in 2–4- (black; n = 39 cells, 11 mice), 9–11- (red; n = 34 cells, 10 mice), and 18–21- (dark red; n = 42 cells, 14 mice) month-old mice. (**C-F**) Box-and-whisker plots illustrating the frequency per cell (**C**), amplitude (**D**), T-half (**E**) and AUC (**F**) of the spontaneous Ca^{2+} transients in spontaneously active microglia from 2–4- (n = 19 cells), 9–11- (n = 19 cells), and 18–21- (n = 28 cells) month-old mice. Amplitude, T-half and AUC show median values per cell. Inset in (**D**) illustrates a schematic example of a Ca^{2+} transient and the parameters analyzed for each Ca^{2+} transient. Scale bars: 5% ΔF/F and 10 s. Statistical differences were determined using Kruskal–Wallis test followed by Dunn's post hoc test for multiple comparisons (*$p < 0.05$, **$p < 0.01$, ***$p < 0.001$).

Taken together, our results revealed that the Ca^{2+} signaling properties of microglia from WT mice follow a bell-shaped relationship with age, with the most frequent and largest spontaneous Ca^{2+} transients observed in middle-aged (9-11 months old) mice, therefore revealing an enhanced spontaneous Ca^{2+} signaling in middle-aged mice (Olmedillas del Moral et al. 2019).

Next, we wanted to validate the aging-related changes observed in WT mice in the widely used Cx$_3$CR1$^{GFP/+}$ mice by using the same methodological approaches (Figure 6A).
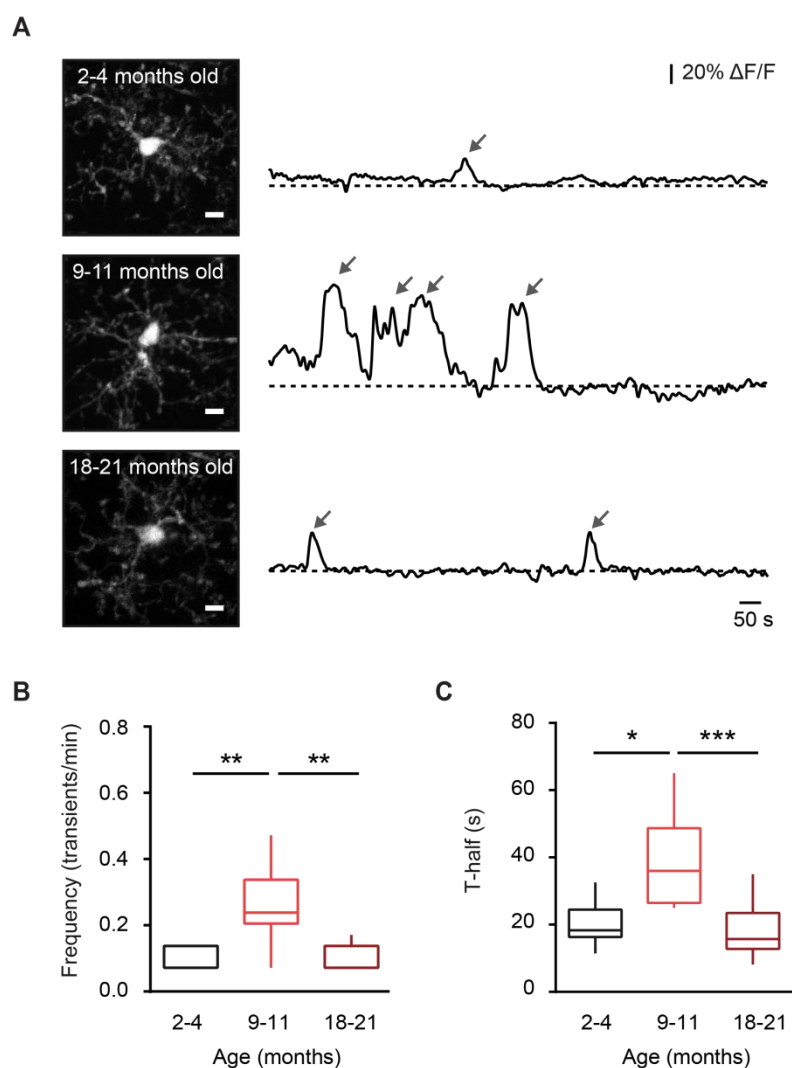
Figure 6. Age-dependent changes of the Ca^{2+} signaling properties of microglia in Cx$_3$CR1$^{GFP/+}$ mice. (**A**) From top to bottom: MIP images of representative microglial cells from 4, 11- and 21-month-old mice (left) from 55-92 µm, 80-110 µm and 106-136 µm below the cortical surface, respectively. On the right, their respective spontaneous somatic Ca^{2+} transients recorded during a 15-min-long period. The arrows point to spontaneous Ca^{2+} transients in respective cells. Scale bar: 5 µm. (**B, C**) Box-and-whisker plot illustrating the median (per cell) (**B**) frequency of Ca^{2+} transients and (**C**) their T-half in microglia from the three age groups. N = 9, 9 and 18 cells from 2–4- (n = 9 mice), 9–11- (n = 5 mice), and 18–21-(n = 9 mice) month-old Cx$_3$CR1$^{GFP/+}$ mice.

Our results showed that the spontaneous Ca^{2+} transients in middle-aged $Cx_3CR1^{GFP/+}$ mice are more frequent and longer compared to those in young adult ($p < 0.01$ and $p < 0.02$, respectively) and middle-aged ($p < 0.01$ and $p < 0.02$, respectively) mice (Figure 6B, C). Thus, consistent with our data obtained in WT mice, microglia from middle-aged $Cx_3CR1^{GFP/+}$ mice has a significantly heightened Ca^{2+} signaling compared to microglia from both young adult and old mice.

In summary, the Ca^{2+} signaling properties of microglia follow a bell-shaped relationship with the animal's age. Microglia from middle-aged WT mice displayed higher frequencies, durations and AUCs of spontaneous Ca^{2+} transients than those of young adult and old WT mice. The widely used $Cx_3CR1^{GFP/+}$ mice recapitulated the aging-related changes of Ca^{2+} signaling properties observed in WT mice, thus validating microglia hyperactivity as a new hallmark of aging in middle-aged mice, which suggests an "reactive-like" or "alerted" phenotype in middle-aged mice.

3.1.1. Sex-specificity of the age-dependent changes in the time course of spontaneous Ca^{2+} signals

Next, we investigated the sex-specificity of the different properties of spontaneous Ca^{2+} transients during aging. Our results showed that males displayed a bell-shaped distribution for the frequency of spontaneous Ca^{2+} transients with significantly higher frequencies in middle-aged mice compared to young adult and old mice ($p = 0.01$ and $p < 0.001$, respectively, Two-way ANOVA followed by Bonferroni's post hoc test; Figure 7A). In contrast, the frequency of the spontaneous Ca^{2+} transients was not affected by age in female mice ($p > 0.99$, two-way ANOVA). Consistently, a significantly higher frequency was observed in male compared to female mice of the middle-age group ($p = 0.03$, two-way ANOVA followed by Bonferroni's post hoc test; Figure 7A). We did not observe any sex- or age-dependent differences for the amplitude of spontaneous Ca^{2+} transients ($p > 0.1$, Two-way ANOVA, Figure 7B). The duration of the transients followed a strong bell-shaped relationship on the age in females but not in males, with significantly higher durations of spontaneous Ca^{2+} transients in middle-aged

females compared to young adult and old females ($p < 0.001$ for both comparisons, Two-way ANOVA followed by Bonferroni's post hoc test; Figure 7C). Similar results were obtained for the AUCs of Ca^{2+} transients in female mice ($p < 0.001$ for both comparisons, Two-way ANOVA followed by Bonferroni's post hoc test; Figure 7D), whereas for male mice we did not observe any sex- or age-dependent differences. Accordingly, the AUCs measured in middle-aged females were significantly higher than those from age-matched males ($p = 0.03$, Two-way ANOVA followed by Bonferroni's post hoc test, Figure 7D).
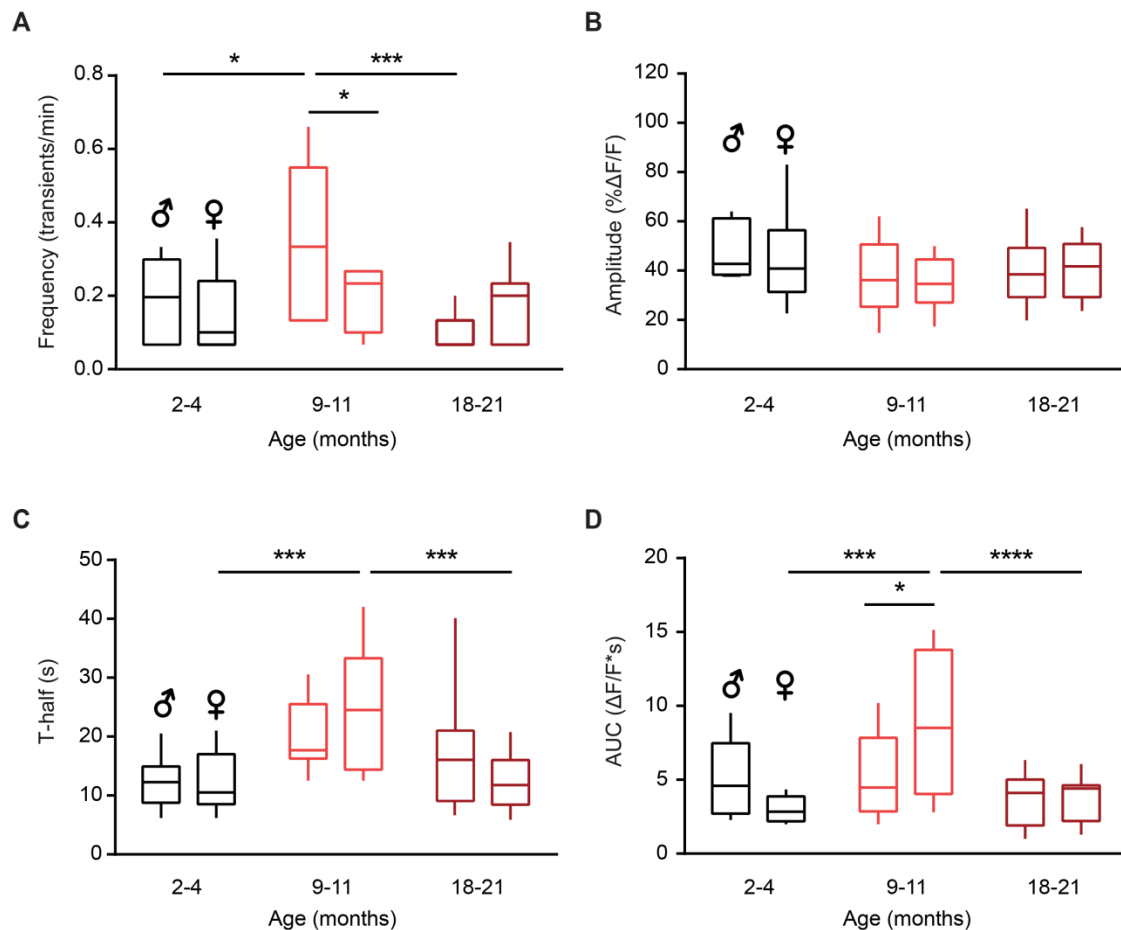
Figure 7. Sex-specificity of the time course of spontaneous Ca^{2+} transients during aging in WT mice. Box-and-whisker plots illustrating the effect of age and sex on the frequency (**A**), amplitude (**B**), T-half (**C**) and AUC (**D**) of the spontaneous Ca^{2+} transients of microglia. Amplitude, T-half and AUC show median values per cell. N = 9 cells (males), 10 cells (females) for 2-4-month old mice; n = 10 cells (males), 9 cells (females) for 9-11-month old mice and n = 10 cells (males), 18 cells (females) for 18-21-month old mice). Statistical differences were determined using two-way ANOVA followed by Bonferroni's post hoc test (*$p < 0.05$, ***$p < 0.001$, **** $p < 10^{-4}$).

Next, we quantified the fraction of spontaneously active microglia in males and females from young adult, middle-aged and old mice. Our data showed that in young adult female mice, (median ± IQR) 33 ± 20% of microglia showed at least one spontaneous Ca^{2+} transient during the recording period (Figure 8A). This fraction was higher in the age-matched males (50 ± 12.15%), but this difference did not reach the statistical significance (p = 0.2264, two-way ANOVA followed by Bonferroni's post hoc test; Figure 8A).
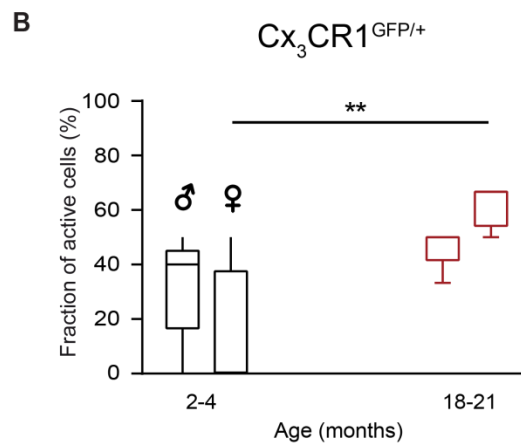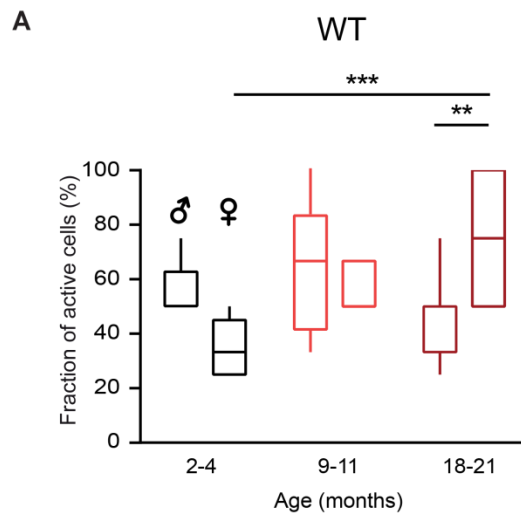
In contrast, the fraction of active microglia in old females was higher than that of old males (75 ± 50% and 33.3 ± 16.7%, respectively, $p = 0.0019$, two-way ANOVA followed by Bonferroni's post hoc test; Figure 8A). Accordingly, aging had a stronger effect on the fraction of active microglia in females compared to males ($p = 0.0006$ for young adult females vs. old females, two-way ANOVA followed by Bonferroni's post hoc test). Additional experiments in $Cx_3CR1^{GFP/+}$ mice reported a significantly higher fraction of active microglia in old females compared to young ones ($p = 0.0015$, two-way ANOVA followed by Bonferroni's post hoc test; Figure 8B), while no differences were found in microglia from old male mice compared to young adult mice ($p = 0.3990$, two-way ANOVA followed by Bonferroni's post hoc test).

Taken together, our data further emphasize the "reactive-like" or "alerted" phenotype of microglia in middle-aged mice of both sexes but also reveal several sex-specific differences in the age-dependent changes of microglial Ca^{2+} signaling.

3.2. Effect of aging on the ATP-directed process outgrowth of microglia

To confirm the age-related changes observed in the Ca^{2+} signaling

Figure 8. Sex-specificity of the fraction of spontaneously active microglia in WT and $Cx_3CR1^{GFP/+}$ mice during aging. (**A**) Box-and-whisker plot illustrating the effect of the interaction between age and sex on the fraction of spontaneously active microglia. N = 5 males, 6 females for 2-4-month old mice; n = 5 males, 5 females for 9-11-month old mice; n = 7 males, 7 females for 18-21-month old mice. (**B**) Box-and-whisker plot illustrating the same effect in $Cx_3CR1^{GFP/+}$ mice. N = 5 males, 4 females for 2-4-month old mice; n = 5 males, 4 females for 18-21-month old mice. Statistical differences were determined using two-way ANOVA and Bonferroni's post hoc test (**$p < 0.01$, ***$p < 0.001$).

properties of microglia, we studied whether ATP-directed process outgrowth, a Ca^{2+}-dependent function, is also affected by age. ATP stimulates directed process extension in microglia, which is accompanied by elevations of $[Ca^{2+}]_i$ driven by the activation of the purinergic receptor $P2Y_{12}$ (Haynes et al. 2006). In the brain, ATP is released from injured cells upon tissue damage, and this situation can be mimicked by locally applying 5 mM ATP with a micropipette into the brain parenchyma of $Cx_3CR1^{GFP/+}$ mice (Davalos et al. 2005;

Olmedillas del Moral et al. 2019). The microglial processes thicken their bulbous endings upon ATP application and move rapidly toward the tip of the micropipette using the chemo-attractant gradient as a directional cue (Davalos et al. 2005; Schwendele et al. 2012; Olmedillas del Moral et al. 2019) (Figure 9A). A spherical containment around the tip of the pipette is then formed, presumably acting as a shield between the healthy and the "injured" tissue (Davalos et al. 2005; Nimmerjahn et al. 2005).
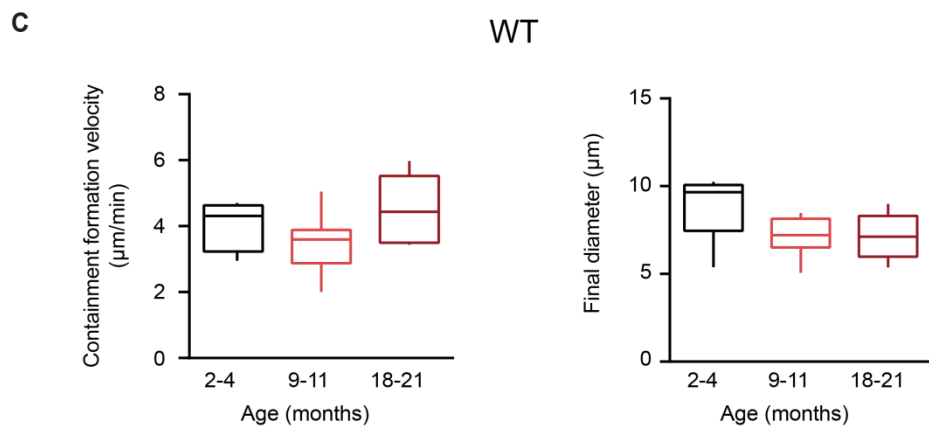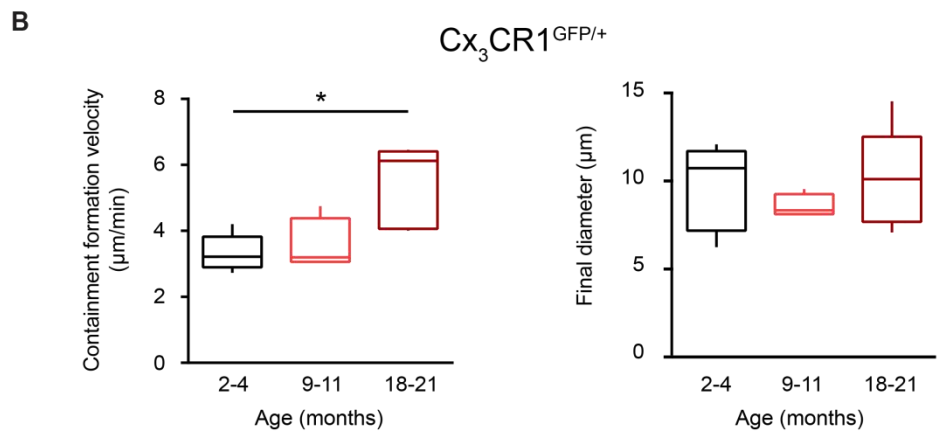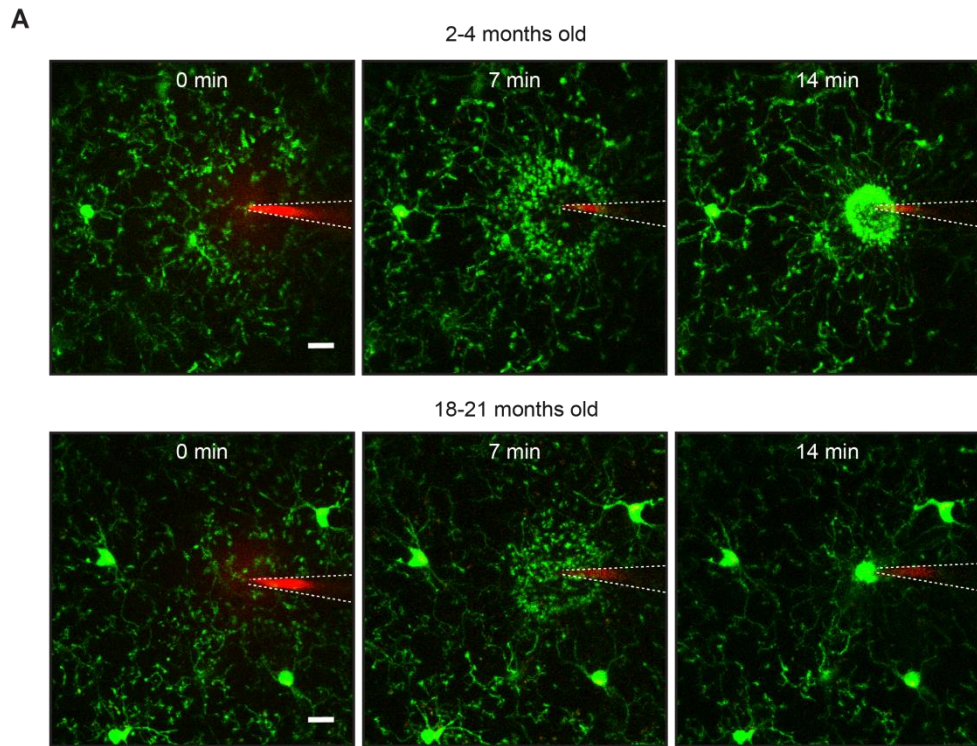
Figure 9. ATP-evoked process extension of microglia during aging. (**A**) MIP images of a Z stack showing exemplifying the formation of the spherical containment in a 2-month-old mouse (top) and 18-month-old mouse (bottom) at three time points after local ATP (5 mM)

application. 3D stacks from 80–100 µm below the cortical surface, 2 µm step size. Scale bar: 10 µm. (**B**) Box-and-whisker plots illustrating median (per mouse) containment formation velocity (left) and the final diameter of the containment formed by the microglial processes around the pipette (right) in 2–4- (n = 5 mice), 9–11- (n = 5 mice) and 18–21- (n = 6 mice) month-old Cx$_3$CR1$^{GFP/+}$ mice. (**C**) Box-and-whisker plot illustrating the median (per mouse) containment formation velocity (left) and the final diameter of the containment (right) in 2–4- (n = 7 mice), 9–11- (n = 8 mice), 18–21- (n = 8 mice) month-old WT mice. Statistical differences were determined using Kruskal–Wallis test followed by Dunn's post hoc test for multiple comparisons, *p < 0.05.

In order to investigate the effect of aging on directed process chemotaxis, I acutely pressure-applied ATP into the brain parenchyma of young adult, middle-aged and old Cx$_3$CR1$^{GFP/+}$ mice. Then, time-lapse images were acquired to monitor the microglial process response using in-vivo two-photon microscopy. The following parameters were analysed: i) the average diameter of the containment formed by microglial processes around the tip of the ATP-containing pipette over time, ii) the speed at which the containment converges around the ATP source, and the iii) final diameter of the containment (Olmedillas del Moral et al. 2019). In order to validate the results obtained, we repeated the same experiments in Tomato-lectin labeled microglia from WT mice.

The results in Cx$_3$CR1$^{GFP/+}$ mice showed that the containment formation velocity increased significantly between the young adult (in median ± IQR, 2.28 ± 0.435 µm/min) and old mice (2.94 ± 0.78 µm/min, p = 0.04 for 2–4- vs.18–21-month-old mice, Kruskal–Wallis test; Figure 9B). However, no differences in the final diameter of the containment surrounding the tip of the ATP-containing pipette were detected between the three age groups (p = 0.17, Kruskal–Wallis test; Figure 9B), suggesting that roughly equal number of microglial processes participate in the containment formation at different ages (Olmedillas del Moral et al. 2019).

Our results from Tomato-lectin-labeled microglia in WT mice reported, however, no differences in the containment formation speed between old (4.434 ± 2.029 µm/min) and young adult (4.308 ± 1.4 µm/min) mice (p > 0.999 Kruskal–Wallis test; Figure 9C). Likewise, the final diameter of the containment was similar between the three age groups (p = 0.0984, Kruskal–Wallis test; Figure 9C).

To study in detail the formation of the process containment we analyzed the full trajectory of the microglial processes during their extension toward the ATP-containing pipette (Olmedillas del Moral et al. 2019), taking the moment of the ATP application as a time point 0 (Figure 10A). Our results in $Cx_3CR1^{GFP/+}$ mice showed that process velocities were slightly but significantly higher in old mice compared to young adult mice ($p = 0.0351$, Kruskal-Wallis test followed by Dunn's post hoc test; Figure 10B), but not to the middle-aged group. WT mice, however, did not reported age-related differences in the process velocity ($p = 0.3521$, Kruskal-Wallis test; Figure 10C). Interestingly, we have observed that processes located in the proximity of the tip of the pipette (e.g. cyan-colored processes in Figure 10A) moved at slower compared to those from further distances (e.g. red- or yellow-colored processes). Moreover, in young adult mice all processes stopped almost simultaneously (Figure 10A, black arrows in right panels), suggesting a high coordination between the microglial processes during the movement (Olmedillas del Moral et al. 2019). In contrast, in old mice the time points when individual processes stopped was not simultaneously, suggesting less coordination between them during the movement toward the pipette.

Correlation analyses in $Cx_3CR1^{GFP/+}$ mice have shown that in young adult mice the initial distance of a process tip to the ATP-containing pipette displayed a strong positive correlation with its mean velocity of extension (Spearman's rank correlation coefficient, $r = 0.84 \pm 0.26$, *(from page 50)*. Figure 11A). In contrast, microglial processes in old mice and middle-aged mice displayed lower correlation coefficients ($r = 0.51 \pm 0.17$ and $r = 0.72 \pm 0.25$, respectively; *(from page 50)*. Figure 11B). The difference between young adult and old mice reached the level of statistical significance ($p = 0.03$, Kruskal-Wallis test followed by Dunn's post hoc test; *(from page 50)*. Figure 11B) (Olmedillas del Moral et al. 2019).
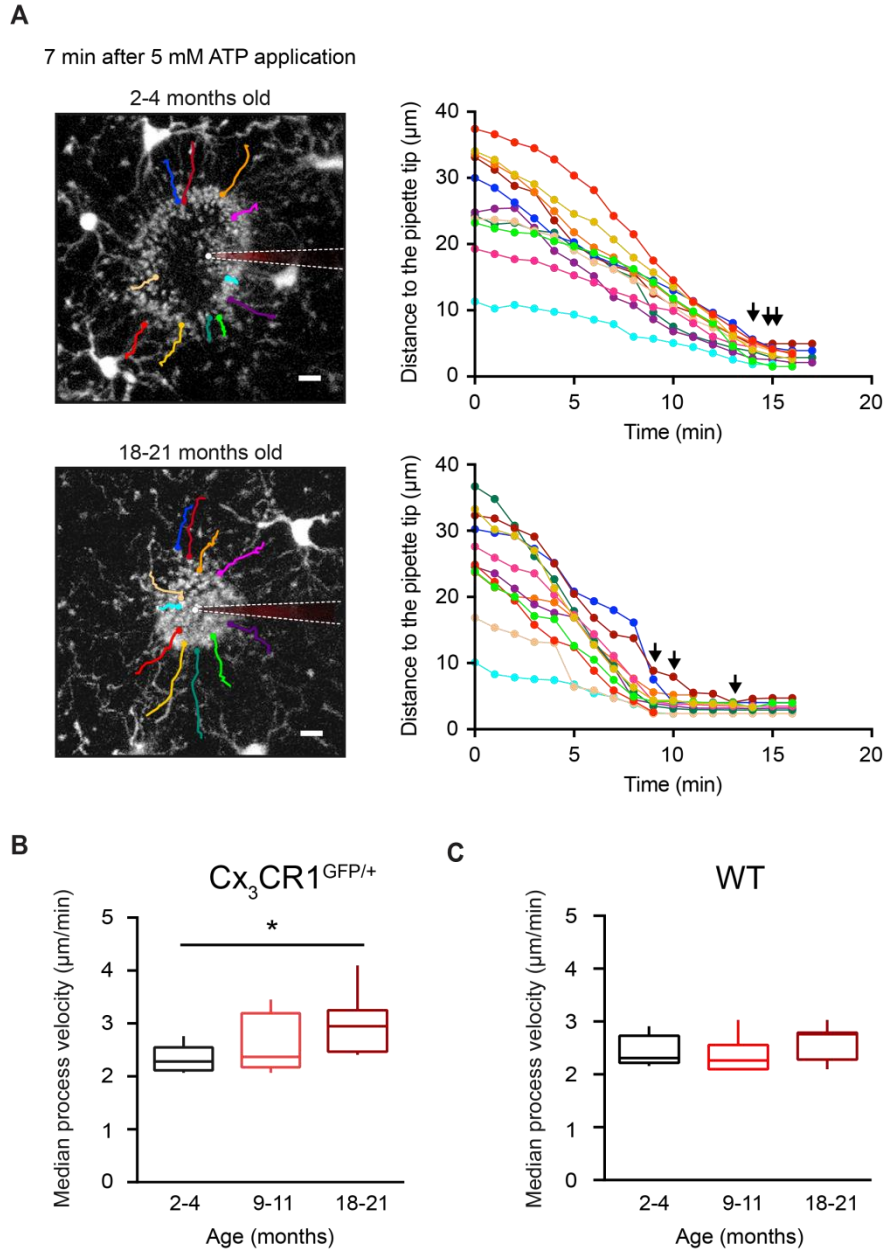
Figure 10. Extension of individual microglial processes involved in the formation of the containment around the ATP-containing pipette. (A) *Left:* MIP images of Z stacks of a 2- (top) and 18- (bottom) month-old mouse at 87–107 µm and 82–102 µm below the cortical surface, respectively, illustrating the shape of the containment 7 min after application of 5 mM ATP. The moment of the ATP application is taken as time point 0. Color lines illustrate trajectories of deliberately chosen individual microglial processes extending toward the pipette tip. White dashed lines emphasize the locations of the ATP-containing pipettes. *Right:* Graphs illustrating the changes in distances of the selected (color-coded as in A, left) microglial processes to the pipette tip over time. Please note that in 18–21-month-old mice the time points at which individual microglial processes reached their final destination (black arrows) scattered much more compared to 2–4-month-old mice. **(B)** Box-and-whisker plot illustrating median (per mouse) process velocity in microglia from 2–4 (n = 151 processes, 5 mice), 9–11 (n = 199 processes, 5 mice) and 18–21 (n = 158 processes, 6 mice)-month-old mice. Statistical differences were determined using Kruskal–Wallis test followed by Dunn's post hoc test for multiple comparisons, $^{**}p < 0.01$.

In WT mice, the initial distance of the microglial processes to the tip of the ATP-containing pipette was, like in Cx₃CR1$^{GFP/+}$ mice, positively correlated with its mean velocity of extension in young adult mice (median ± IQR, r = 0.7461 ± 0.2028), and this correlation was significantly reduced in old mice (r = 0.5466 ± 0.3937, *p* = 0.0412, Kruskal-Wallis test followed by Dunn's post hoc test; *(from page 50).* Figure 11C). Thus, Tomato-lectin-labeled microglial processes in WT mice displayed mean extension velocities and synchronizations that recapitulated those from Cx₃CR1$^{GFP/+}$ mice.
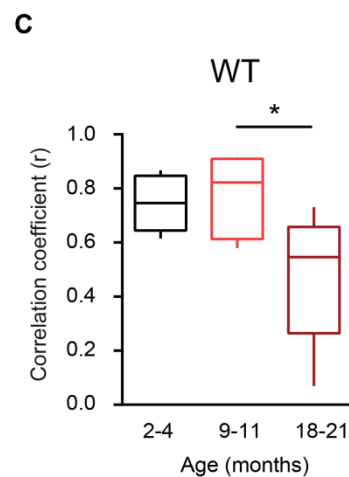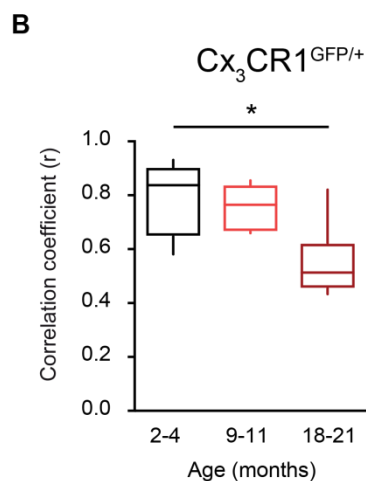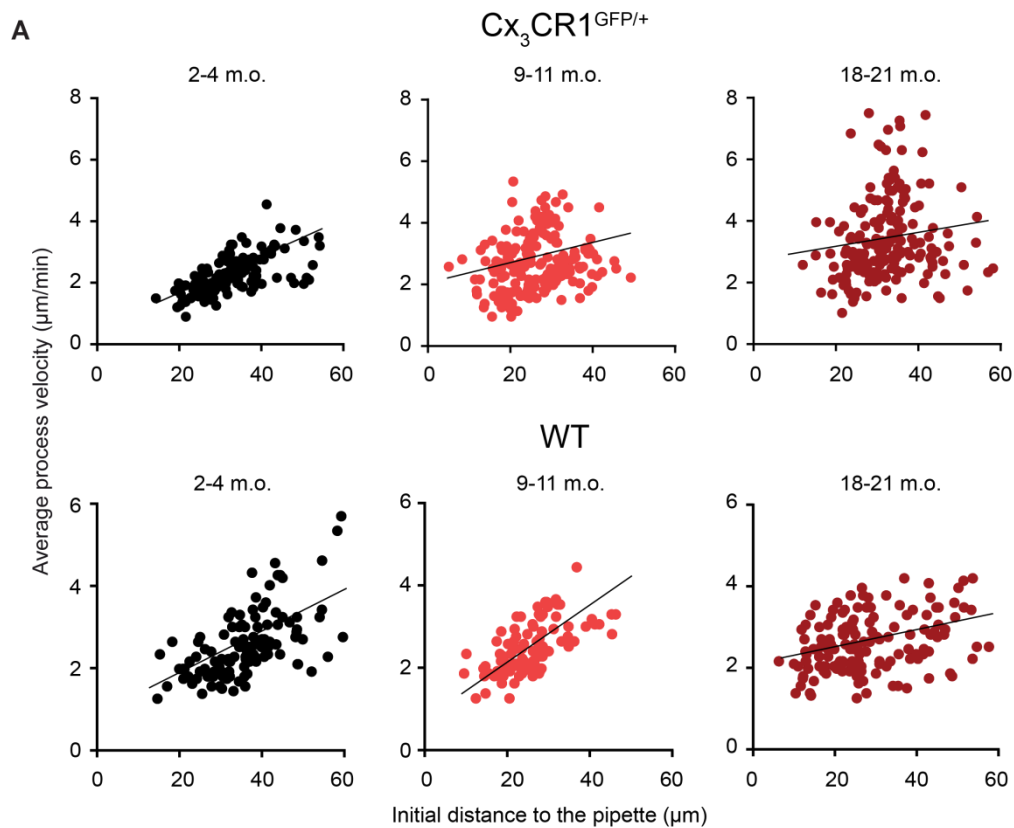
Figure 11. Relationship between the initial distance to the ATP-containing pipette and the process extension velocity. (**A**) Scatter plots illustrating the relationship between the initial distance of all microglial processes to the tip of the ATP-containing pipette (X-axis) and the mean velocity for each process (Y-axis) in 2–4- (n = 6 mice, 118 processes), 9–11- (n = 6 mice, 119 processes), and 18–21- (n = 8 mice, 146 processes) month-old WT mice, and 2–4- (n = 5, 151 processes), 9–11- (n =5, 199 processes), and 18–21- (n = 6 mice, 158 processes) month-old $Cx_3CR1^{GFP/+}$ mice. (**B, C**) Box-and-whisker plot illustrating Spearman's correlation coefficients (per mouse) in (**B**) WT and (**C**) $Cx_3CR1^{GFP/+}$ mice. Statistical differences were determined using Kruskal–Wallis test followed by Dunn's post hoc test for multiple comparisons, $*p < 0.05$.

Finally, we wanted to test whether the observed aging effect on the process synchronization was sex-specific. Because both WT and $Cx_3CR1^{GFP/+}$ mice reported similar results (see *(from page 50).* Figure 11), we pooled the mice together and split them again according to their gender. The results, shown in Figure 12, showed that reduction in the r occurred similarly in males and females, with no sex-differences found at any age ($p = 0.7552$, two-way ANOVA test).
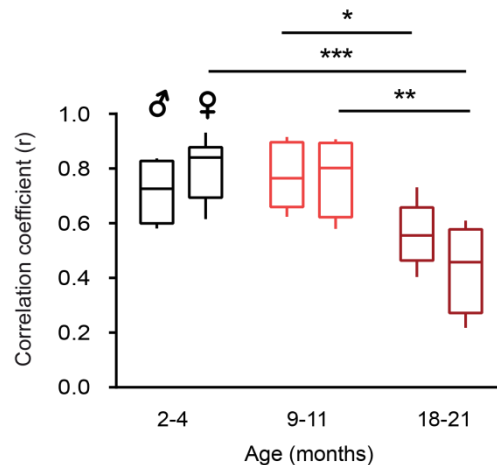
Figure 12. Sex-specificity of the ATP-directed chemotactic properties of microglial processes during aging. Box-and-whisker plot illustrating the effect of the interaction between age and sex on the Spearman's correlation coefficients (per mouse) between the initial distance of microglial processes to the tip of the ATP-containing pipette and the mean process velocity in pooled data from WT and $Cx_3CR1^{GFP/+}$ mice. Statistical differences were determined using two-way ANOVA and Bonferroni's post hoc test ($**p < 0.01$, $***p < 0.001$).

In summary, our data show that ATP-evoked chemotaxis of microglial processes is slightly faster in old mice. However, the formation of the spherical containment as a result of microglial processes fusing together around the ATP-containing pipette, is less synchronized. This effect is recapitulated in Tomato-lectin-labeled WT mice and is sex-independent.

3.3. Ca^{2+} signaling properties of Aβ plaque-associated microglia

Alzheimer's disease (AD) is an age-related disease and its progression is affected by microglia activation. Although an effect of amyloid deposition on the Ca^{2+} signaling properties of microglia has been reported in middle-aged mice (Brawek et al. 2014), what occurs in younger mice remains unclear. To this purpose, we used the APPPS1 mice as a mouse model of AD (here and below "AD mice"). In AD mice, the microglial cells included for the study were located in the vicinity of amyloid plaques and displayed an amoeboid morphology (Figure 13A). After loading of OGB-1 into the cell, somatic Ca^{2+} imaging was performed for a total recording period of 15 minutes per cell in two age groups: 2-4–month–old ("young adult") and 9-11–month–old ("middle-aged") mice (Figure 13B).

Our results showed that plaque-associated microglia from AD mice displayed slightly higher frequencies of spontaneous Ca^{2+} transients in both age groups (0.33 ± 0.27 in young adult and 0.40 ± 0.33 in middle-aged AD mice), compared to the age-matched WT mice (0.13 ± 0.20 in young adult and 0.27 ± 0.33 in middle-aged WT mice), although these differences were not statistically significant ($p = 0.1538$ and $p = 0.6480$ for young adult WT vs young adult AD, and middle-aged WT vs middle-aged AD mice, respectively; two-way ANOVA followed by Bonferroni's post hoc test; Figure 13C).

Next, we quantified the fraction of microglial cells displaying at least one spontaneous Ca^{2+} transient (i.e. % active microglia) in each mouse. Our results showed that the fraction of active microglia per mouse was (median ± IQR) 40 ± 20.84% in young adult WT and 50 ± 16.7% in middle-aged WT mice (Figure 13D). However, the fraction of spontaneously active microglia was higher in the age-matched AD mice (75 ± 70.85%, and 80 ± 33.33%, in young adult and middle-aged mice, respectively; $p = 0.0515$ for young adult WT vs young adult AD mice, and $p = 0.0195$ for middle-aged WT vs middle-aged AD mice, two-way ANOVA followed by Bonferroni's post hoc test). Thus, our data revealed that plaque-associated microglia display enhanced spontaneous activity as soon as mice are in the young adult age.
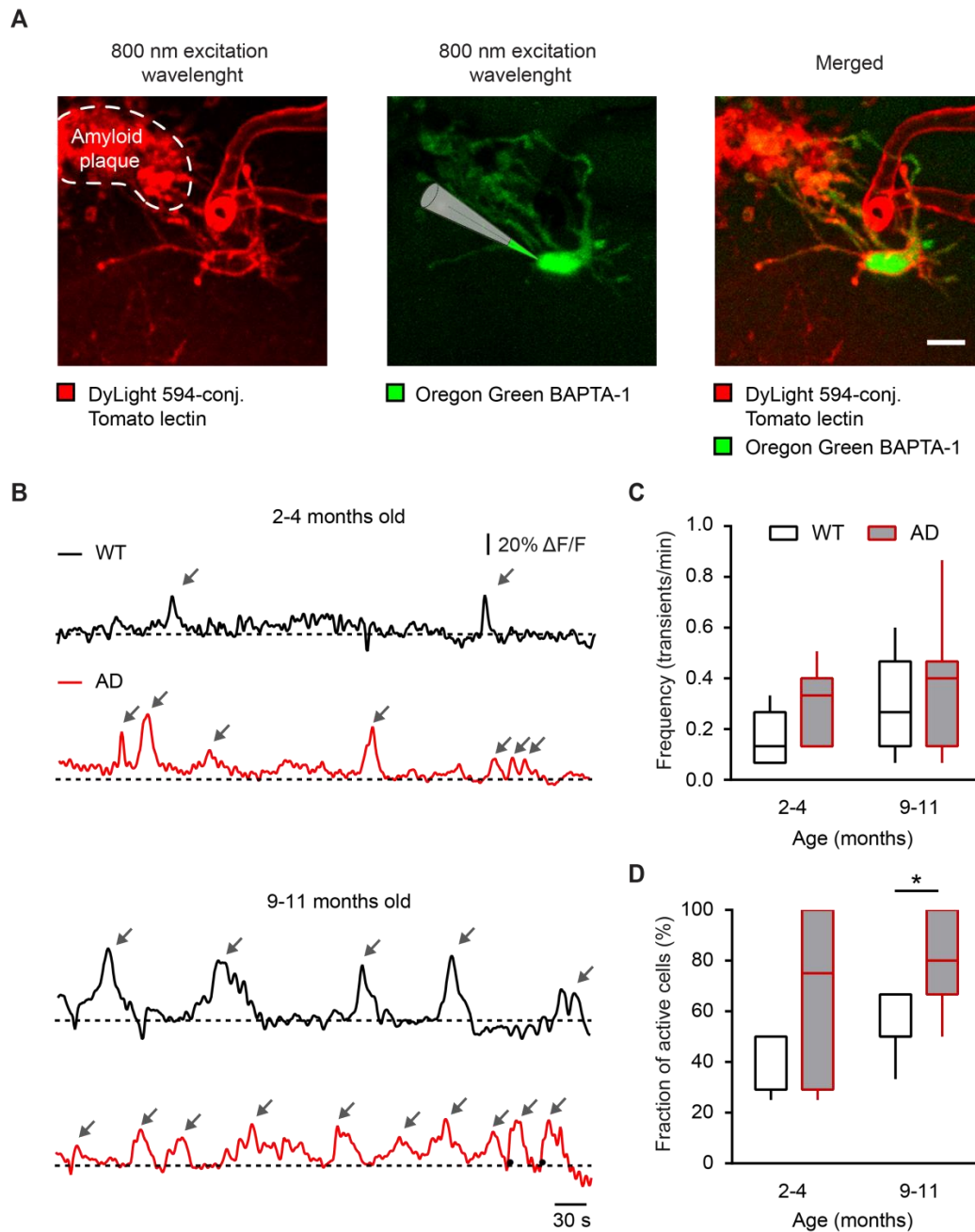
Figure 13. Effect of amyloid-β on microglial hyperactivity and its relationship with aging. (**A**) MIP images of a representative microglial cell labeled with DyLight 594-conjugated Tomato lectin (left) and loaded with the Ca^{2+} indicator OGB-1 by means of single-cell electroporation in an AD mouse (middle). Merged image is shown on the right. (**B**) Representative traces from WT (in black) and AD (in red) mice at 2-4 or 9-11 months of age. The arrows point to the spontaneous Ca^{2+} transients. (**C**) Box-and-whisker plot showing the frequencies (per cell) from 2-4–month old WT and AD mice, and 9-11 –month old WT and AD mice. (**D**) Box-and-whisker plot illustrating the fractions of spontaneously active microglia (per mouse) in 2-4–month old WT and AD mice, and 9-11–month old WT and AD mice. N = 19 and 11 cells from young adult WT (n = 11) and AD (n = 5) mice, respectively; n = 19 and 19 cells from middle-aged WT (n = 10) and AD (n= 8) mice, respectively.

To confirm the presence of early changes in the microglia phenotype in the course of amyloid pathology, we further characterized the time course of the spontaneous Ca^{2+} signals detected in plaque-associated microglia from young adult and middle-aged AD mice. Our data revealed that the amplitudes of the transients were significantly lower in young adult AD mice compared to the young adult WT mice ($p < 0.001$, two-way ANOVA followed by Bonferroni's post hoc test; Figure 14A). However, we did not find statistical differences between WT and AD in neither the duration nor the AUC of the transients in any of the age groups ($p > 0.05$ for both tests, two-way ANOVA; Figure 14B, C). However, our data revealed a strong aging effect on the duration of the spontaneous Ca^{2+} transients of microglia also in AD mice, with significantly longer durations found in middle-aged mice compared to their young adult counterparts ($p = 0.0121$, two-way ANOVA followed by Bonferroni's post hoc test). Likewise, the AUCs of the transients were higher in middle aged AD mice compared to young adult AD mice ($p = 0.0168$, two-way ANOVA followed by Bonferroni's post hoc test; Figure 14C).
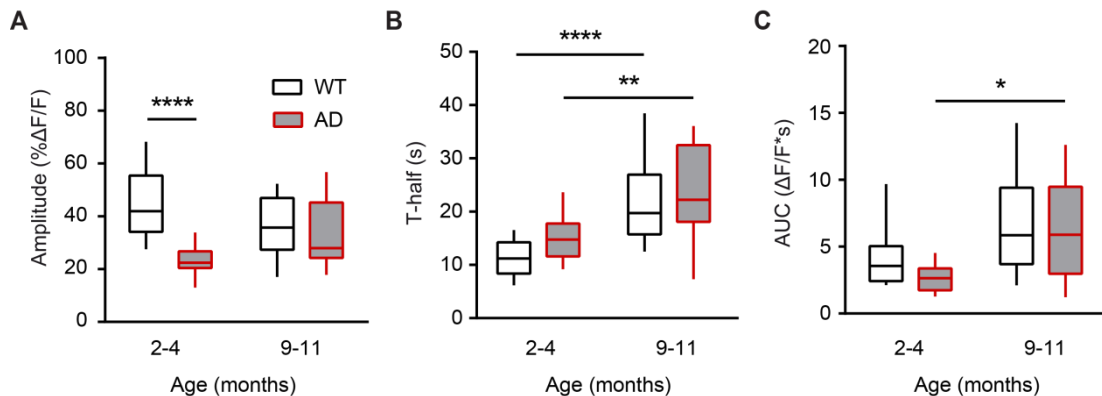
Figure 14. Time course of the spontaneous Ca^{2+} signals in microglia from AD mice. Box-and-whisker plots illustrating the median (per cell) amplitude (**A**), T-half (**B**), and AUC (**C**) of spontaneous Ca^{2+} transients in microglial cells from 2-4- (young adult) and 9-11-month old (middle-aged) WT and AD mice. N = 18 and 18 cells from young adult WT (n = 11) and AD (n = 11) mice, respectively, and n = 19, 19 cells from middle-aged WT (n = 10) and AD (n = 10) mice, respectively. Kruskal–Wallis test followed by Dunn's post hoc test for multiple comparisons, $^*p < 0.05$, $^{**}p < 0.01$, $^{****}p < 10^{-4}$.

Taken together, our data reveal changes in microglial Ca^{2+} signaling in early stages of amyloid-plaque deposition. Most of the microglial cells located in the vicinity of amyloid plaques were spontaneously active with higher

frequencies of Ca^{2+} transients compared to WT mice. Interestingly, a reduction in the amplitude of these transients was found which was much more prominent in young adult than in middle-aged AD mice, thus identifying this phenotype as a new hallmark of amyloid-associated microglia in young adult mice. Aging, however, had a stronger impact on both the duration (T-half) and AUC of the spontaneous Ca^{2+} transients, thus revealing a unique aging- and amyloid-associated effect on the Ca^{2+} signaling properties of microglia.

3.4. Establishment of RGB labeling for microglia *in vivo*

To provide more insights into the functional properties of microglia in AD, we aimed at characterizing microglia dynamics over time from the beginning of plaque deposition. In particular, we were interested in i) the fate of microglia during the pathology, ii) the kinetic properties of the microglia network in the course of the pathology, iii) mechanisms of formation and maintenance of the microglia clusters around amyloid plaques, and iv) how long do microglia survive in the amyloid plaque vicinity. To do so, we first established a method that allowed us to visualize and distinguish single microglial cells unequivocally in order to monitor their behavior longitudinally. Until now, the widely used $Cx_3CR1^{GFP/+}$ or Iba-1-GFP mice, which express GFP constitutively in microglia, have allowed us to visualize these cells *in vivo*. However, unicolor labeling fails to distinguish cells individually, which makes the single-cell tracking difficult and often not reliable. Our new labeling approach is based on red (R), green (G) and blue (B) color coding, and used the miRNA9-regulated lentiviral vectors described elsewhere (Åkerblom et al. 2013). As explained in section 2.6, only cells which express miRNA-9 will induce the suppression of protein translation. Microglia, who lacks miRNA-9 expression, will therefore express the fluorescent reporter marker (Åkerblom et al. 2013).

First, in order to confirm the specificity of RGB labeling for microglia, mice were injected with mVenus-encoding virus in the motor cortex (Figure 15A). Two weeks later the animals were perfused and their brain isolated for

immunostaining. Then, co-stainings against $P2Y_{12}$ and against GFP were performed (Figure 15B). We chose anti-$P2Y_{12}$ because $P2Y_{12}$ is exclusively expressed in microglial cells. Other myeloid cells, like perivascular macrophages, are $P2Y_{12}$ negative (Hickman et al. 2013). We selected fields of view (FOVs) that were at least 100 µm far from the epicenter of the injection site. Among all GFP positive cells, 80.7% were $P2Y_{12}$ positive, meaning that this labeling method is highly specific for microglia. The remaining GFP positive cells were astrocytes (11%), neurons (9%) or perivascular macrophages (2%; data not shown).
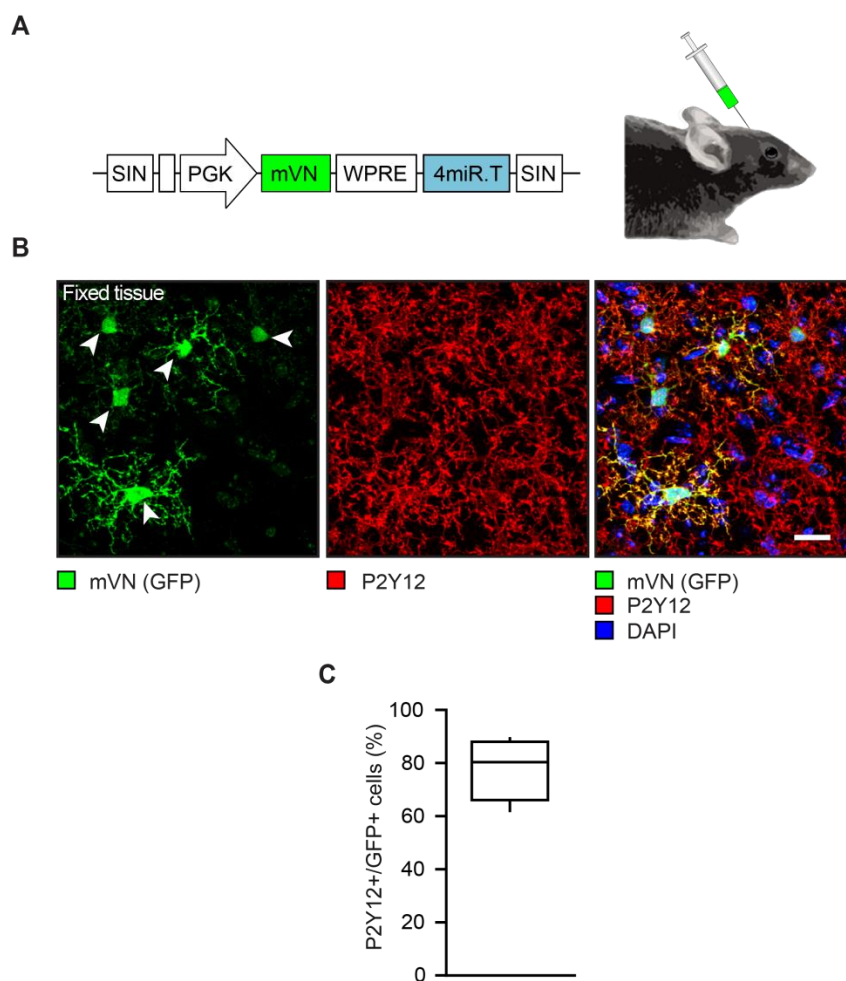
Figure 15. Expression of the LV.miR-9.T vector in the mouse brain tissue. (**A**) Scheme of the LV.PGK.mVN.miR-9.T construct generated from LV.PGK.GFP.miR-9.T (left). A vector solution was injected in the cortex of the mouse brain (AP +1.8 mm, ML 1.0 mm, DV 0.55 mm). (**B**) MIP images illustrating the identity of LV.PGK.mVN.miR-9.T-transduced cells through immunofluorescent staining with an antibody against the microglia-specific marker $P2Y_{12}$. Since rodent microglia lacks miR-9 expression, miR-9-regulated vectors can be used for selective labeling of microglia in the mouse cortex. Scale bar: 10 µm. (**C**) Fraction (per mouse) of $P2Y_{12}$-positive cells among those VN(GFP)-positive.

For multicolor marking *in vivo*, we generated three different constructs, each one coding for a different fluorescent reporter gene: mCherry (mC, red), mVenus (mVN, green) or mTurquoise2 (mTq2, blue) (Figure 16A). A solution with the mixture of the three lentiviral at 1:1:1 proportion was injected into the motor cortex, followed by the implantation of a chronic cranial window (see section 2.2.2). Three weeks later, the transduced cells were visualized through the cranial window and 3D images were acquired (Figure 16B, C). We acquired between one and three FOVs per mouse sized approximately 250 x 250 x 150 μm^3, which reported an average number of tracked cells of (mean ± SEM) 45.25 ± 3.77 per FOV (Table 4).

Table 4. Number of labeled cells in WT mice.

Mouse ID	FOV	Total cells	Volume 3D stack (mm^3)	Cell density (cells/mm^3)
CW20160223	1	72	1.59E-02	4526.94
	2	32	1.99E-02	1609.58
	2	29	8.89E-03	3262.56
CW20170217	1	52	1.19E-02	4359.27
	2	41	1.35E-02	3032.75
	3	49	1.27E-02	3851.04
CW20170222	1	54	1.27E-02	4244.00
	2	39	1.03E-02	3772.45
CW20170220	1	42	1.19E-02	3520.95
CW20170503	1	51	1.11E-02	4590.09
	2	26	9.44E-03	2752.99

We estimated the transduction efficiency based on previously reported microglial density in the mouse cortex, which calculated a microglia density of around 6500 cells/mm^3 (Nimmerjahn, Kirchhoff, and Helmchen 2005; Lawson et al. 1990). Because we obtained density of (mean ± SEM) 3626 ± 297 microglia/mm^3 labeled, we estimate an approximate transduction efficiency of 56 ± 4.56% (Figure 16F).

Data collected from 5 mice (n = 458 cells) indicated that using our experimental setup, around 42% of labeled microglia were either red (in mean ± SEM; R, 4.54 ± 1.28%), green (G, 20.45 ± 2.06%) or blue (B, 18.65 ± 3.81%). Around 22% of the labeled cells were double-labeled (GB 7.95 ±

1.45%; RB 6.51 ± 1.61%; RG 5.57 ± 1.38%) and 36.33 ± 5.11% were RGB labeled (Figure 16D, E).

In summary, we established RGB labeling for microglia *in vivo*. This method labels microglia specifically and has relatively high transduction efficiency. Because viral transduction occurs stochastically, this approach provides a combinatorial expression of the fluorescent genes which results in a wide range colors, giving a unique color identity to each microglial cell.
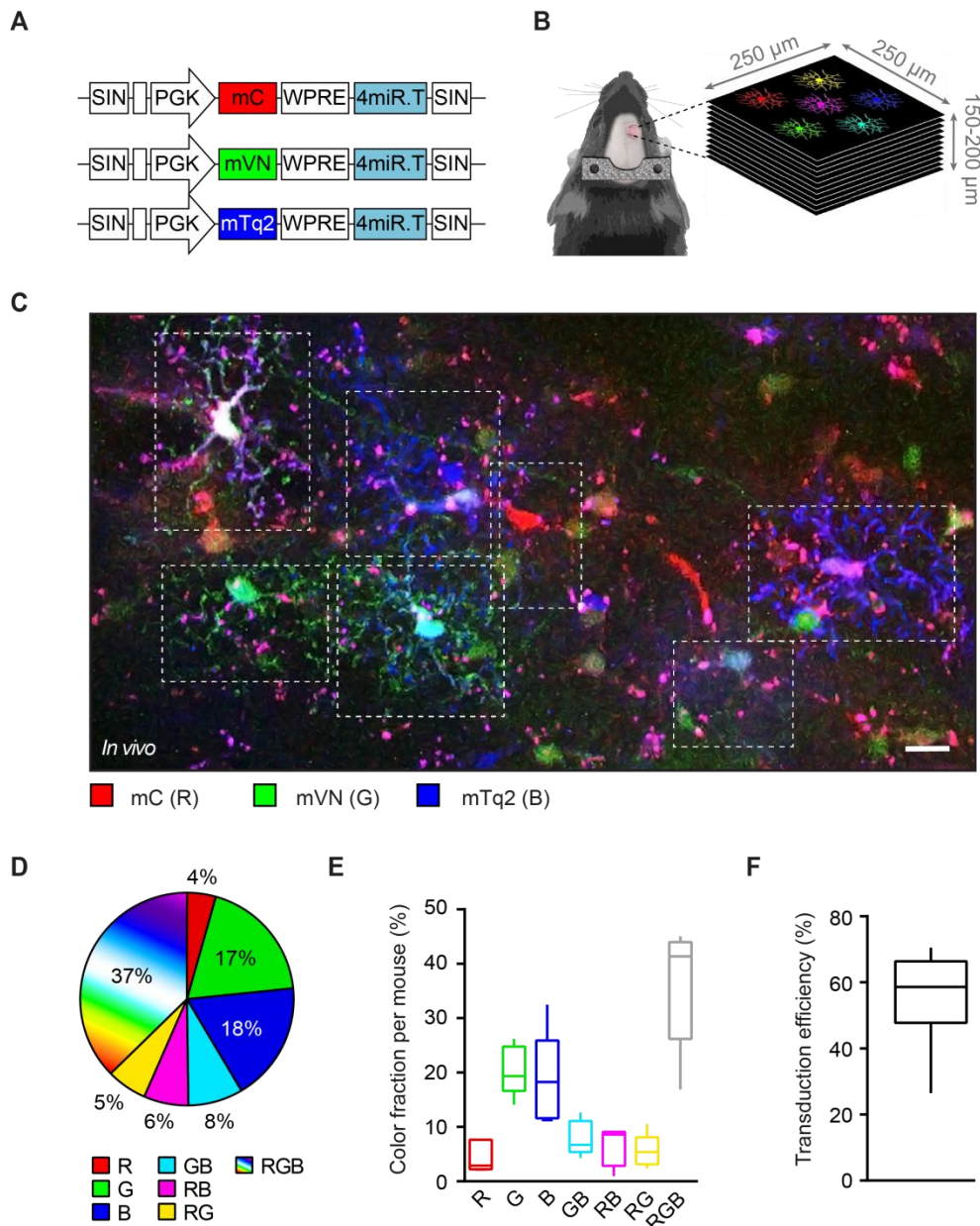
Figure 16. Expression of target genes (mCherry, mVenus and mTurquoise2) in LV.PGK.FP.miR-9.T vector-transduced brain tissue. (**A**) Scheme of the LV.PGK.miR-9.T constructs generated: mC (mCherry), mVN (mVenus), and mTq2 (mTurquoise2). (**B**) Immediately after injection of the viral mix in proportions 1:1:1 into the mouse motorcortex (AP +1.8 mm, ML 1.0 mm, DV 0.55 mm), a chronic cranial window was implanted and a titanium bar was attached onto the skull, enabling repeated long-term imaging of the same *xyz* coordinates. Three weeks later after virus injection and cranial window implantation, 3D stacks were acquired from every FOV, sized 250 × 250 μm², up to a depth of 200 μm from the brain surface. In each mouse, typically one to three positions were selected so that the highest possible number of labeled microglia and color combinations was visible within each stack. Positions were imaged daily for 10-22 days. (**C**) MIP image of a stack Z (32-89 μm below the cortical surface, 2 μm step size) showing an example of RGB-labeled microglial cells. Images were generated by overlaying three images of basic colors red, green and blue acquired with the pre-determined settings (see section 2.7.3). Scale bar: 10 μm. (**D**) Pie chart illustrating the color proportion of each color hues from the in-vivo RGB images collected from n = 458 cells, 5 mice (WT). (**E**) Box-and-whisker plot illustrating the color fraction (per mouse). (**F**) Box-and-whisker plot showing the estimated transduction efficiency *in vivo*, result from dividing the cell density of labeled microglia by the previously reported density of microglia in the mouse cortex (6500 cells/mm³, Nimmerjahn et al. 2005).

59

In order to measure the dynamic properties of RGB-labeled microglial cells, we acquired 3D stacks from each FOV every 24 h for a total period of 10-22 days (Figure 17). A sequential scanning of microglial cells with 800 and 990 nm light was performed to obtain emissions from mCherry (mC), mVenus (mVN) and mTurquoise2 (mTq2). Then, sulforhodamine B was injected i.p. for blood vessel imaging, and excited at 900 nm. Throughout the recording period, a relatively low laser power was always used for excitation in order to avoid photobleaching or phototoxicity. RGB labeling was stable throughout the recording period and lasted up to a year (data not shown).

■ mC ■ mVN ■ mTq2 ☐ Sulforhodamine B
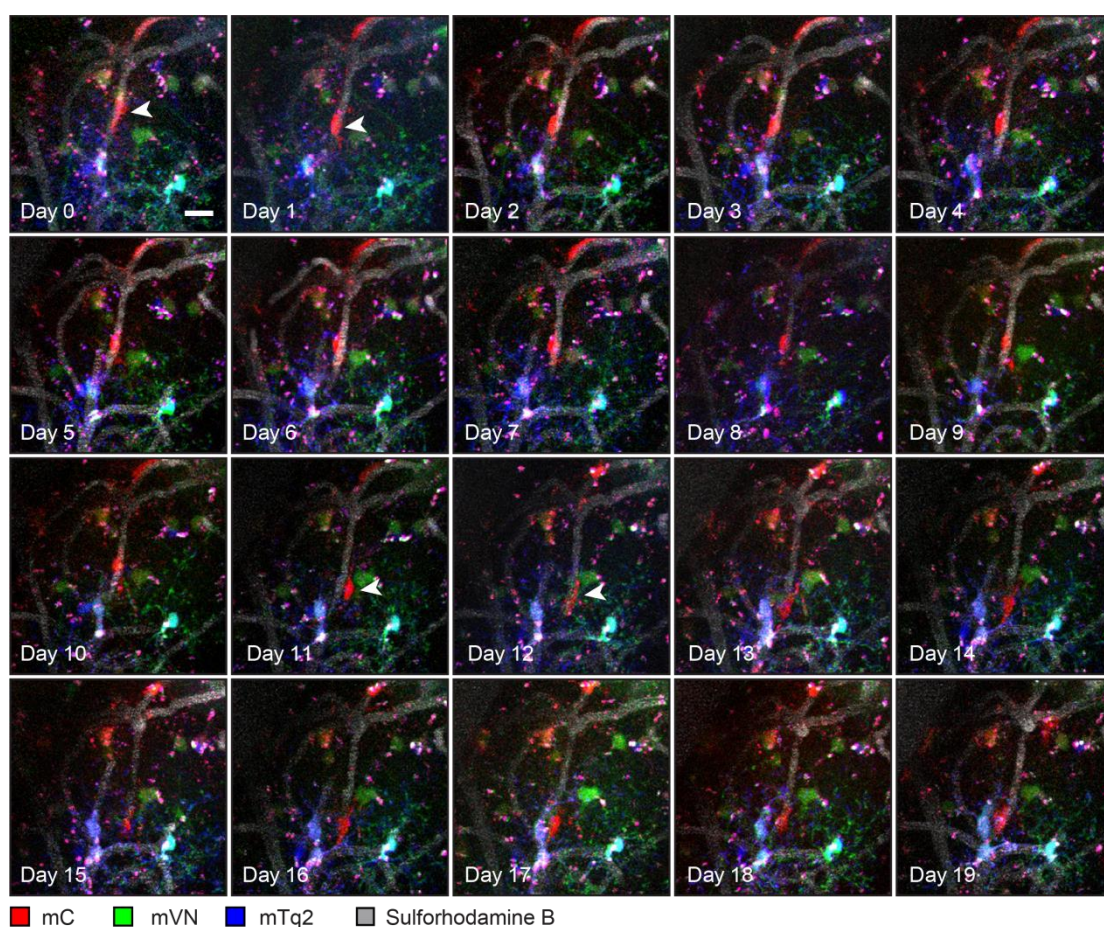
Figure 17. Example of daily image acquisitions of RGB-labeled microglia in WT mice. MIP images of a Z stack (40-76 µm below the cortical surface, 2 µm step size) acquired every 24 h for a total recording period of 20 days. The first time point was labeled as Day 0. White arrow points to a microglial cell that eventually underwent soma translocation (i.e. migration). Note the relative change in position on days 1, 11 and 12, while the neighboring cells remained stationary. A sequential scanning of microglial cells with 800 and 990 nm light was performed to obtain emissions from mCherry (mC), mTurquoise (mTq2) and mVenus (mVN). Then, sulforhodamine B was injected i.p. for blood vessel imaging, and excited at 900 nm. Throughout the recording period, a relatively low laser power was always used for excitation in order to avoid photobleaching or phototoxicity. Our labeling method was stable throughout the recording periods. Because the color hues are different in the neighboring cells, RGB labeling allows single-cell tracking for longitudinal studies. Scale bar: 10 µm.

In summary, RGB labeling provides a reliable and stable multicolor coding of microglia *in vivo*, thus allowing longitudinal single-cell tracking of these cells to quantify their dynamics properties *in vivo*.

3.4.1. Fate determination of microglia during homeostasis

In order to measure the dynamic properties of microglia during homeostatic conditions we first determined the cell fate of microglia in WT mice. To this purpose, we quantified in 6 mice (n = 543 cells) the number of migration, proliferation and cell death events observed in an imaging period of 10-22 days.

The identification of cell division events was possible by following same-colored daughter cells in consecutive time points (Figure 18A). Cell death was defined as cell disappearance within the network of relatively immobile neighboring cells (Figure 18B). Finally, the identification of migration events was possible because each cell tracked had its corresponding 3D coordinates, with the blood vessel pattern providing additional landmarks, and was defined as the translocation of the cell position for ≥ 5 µm (Figure 18C). Our data collected from 6 mice revealed that a fraction of 16% of all cells tracked migrated at least once during the imaging period and, as expected, only around 1-3% of the total cells tracked either divided or died (Figure 18D). Most cells (~80%), however, remained stable throughout the recording period. The median fraction (per mouse) of division and death events per mouse was 0.48 ± 1.79% and 2.48 ± 3.48%, but the difference between these was not significant (p = 0.23, Mann-Whitney test). However, the median fraction (per mouse) of migration events was 15.90 ± 10.68%, which was significantly higher than those observed for division and death rates (p = 0.002 and p = 0.04, Kruskal-Wallis test followed by Dunn's test for multiple comparisons; Figure 18E).
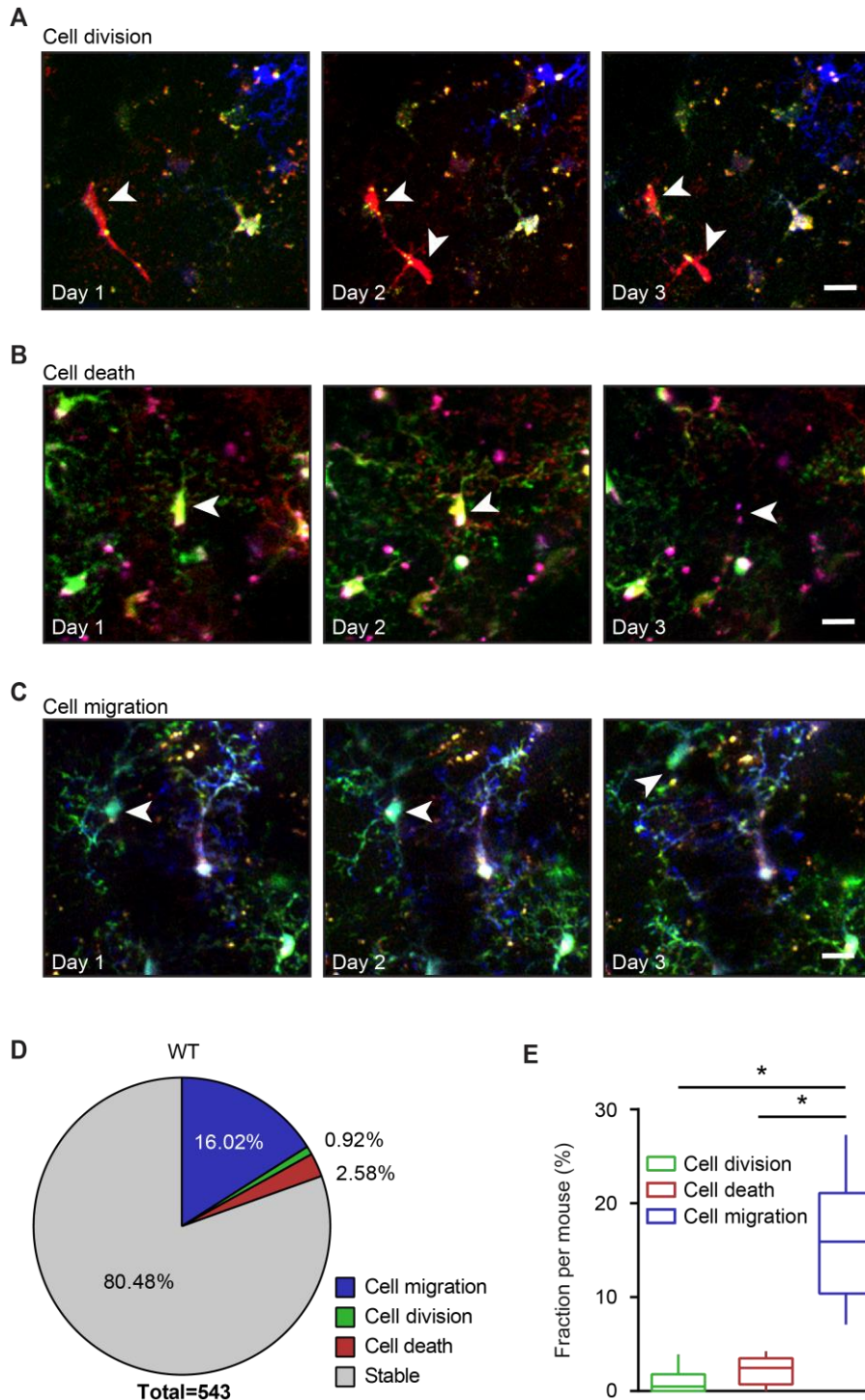
Figure 18. Fate determination of microglia in WT mice under homeostatic conditions.
(**A**) MIP images of a Z stack (30-76 μm below the cortical surface, 2 μm step size) acquired sequentially every 24 h. White arrows point to a cell division event, possible by following same-colored daughter cells in consecutive time points. (**B**) MIP images of a Z stack (48-94 μm below the cortical surface, 2 μm step size) acquired sequentially every 24 h. White arrows point to a cell death event, defined a cell disappearance within the network of immobile neighboring cells. (**C**) MIP images of a Z stack (35-67 μm below the cortical surface, 2 μm step size) acquired sequentially every 24 h. White arrows point to a cell migration event, defined as the translocation of the cell soma position in ≥ 5 μm. (**D**) Pie chart illustrating the total fraction of cells undergoing any of the above mentioned events (cell division, cell death or cell migration) by the end of the total imaging period (10-22 days). (**E**) Box-and-whisker plot illustrating the median fraction per mouse of cell division, cell death and cell migration events (n = 543 cells, 6 mice). Scale bar: 10 μm.

3.4.2. Characterization of the migration properties of WT microglia

Next, we aimed at providing a detailed characterization of the migration properties of microglia in WT mice. Our data acquired from 6 mice (n = 12 FOVs) revealed a total fraction of migrating cells per FOV of (mean ± SEM) 16.03 ± 2.18%, (Figure 19A), corresponding to 16.10 ± 2.81% per mouse (Figure 19B). Although this fraction was positively correlated to the number of days of recoding (Spearman's correlation coefficient, $r = 0.64$, p = 0.02; Figure
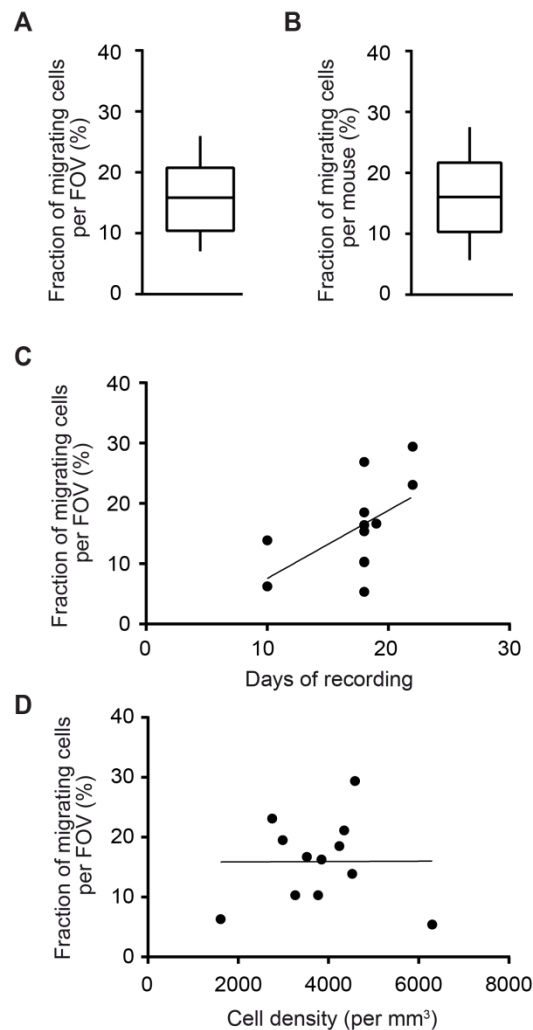
Figure 19. Fraction of migrating microglia in WT mice under homeostatic conditions. Box-and-whisker plots illustrating (**A**) the fraction of migrating cells per FOV (n = 12 FOVs) and (**B**) the median fraction of migrating cells per mouse (n = 6 mice). (**C**) Scatter plot illustration the relationship between the length of the imaging period (days of recording) and the fraction of migrating cells. (**D**) Scatter plot showing the relationship between the cell density and the fraction of migrating cells in each FOV.

19C), it was independent of the cell density (Spearman's correlation coefficient, r = 0.03, p = 0.94; Figure 19D).

In order to provide a detailed characterization of the migration properties of microglia under homeostatic conditions, we measured every 24h the 3D coordinates of each cell tracked (n = 543, 6 mice) and the translocation distance per day (Figure 20A). Our results reported a daily fraction of migrating cells of 0.92% (Figure 20B). More than half (~60%) displayed only one translocation movement throughout the total imaging period, ~22% displayed two translocation movements and the remaining ~18% displayed 3 translocation movements or more (Figure 20C). Thus, migrating events occur eventually in a subset of cells, but then they were mostly stationary. We therefore identified the migration pattern of microglia as saltatory, defined as alternating fast moving and long stationary periods.

The median speed and cumulative translocation distance were 14.0 ± 3.4 µm and 20.75 ± 9.7 µm respectively (Figure 20D, E). The cumulative distance is defined as the total translocation distance during the recording period (Figure 20F). In order to determine the directionality of the movement, we took those cells which displayed at least 2 or more migration events. Our data from 6 mice (n = 32 cells, 1-11 cells per mouse) revealed that 40.6% of these cells had a multidirectional movement, while 59.4% had a unidirectional movement (Figure 20G). Among all cells displaying unidirectional movement, only 14% had a cumulative translocation distance greater than 40 µm, suggesting that most of these cells remain in their territorial domain (data not shown).
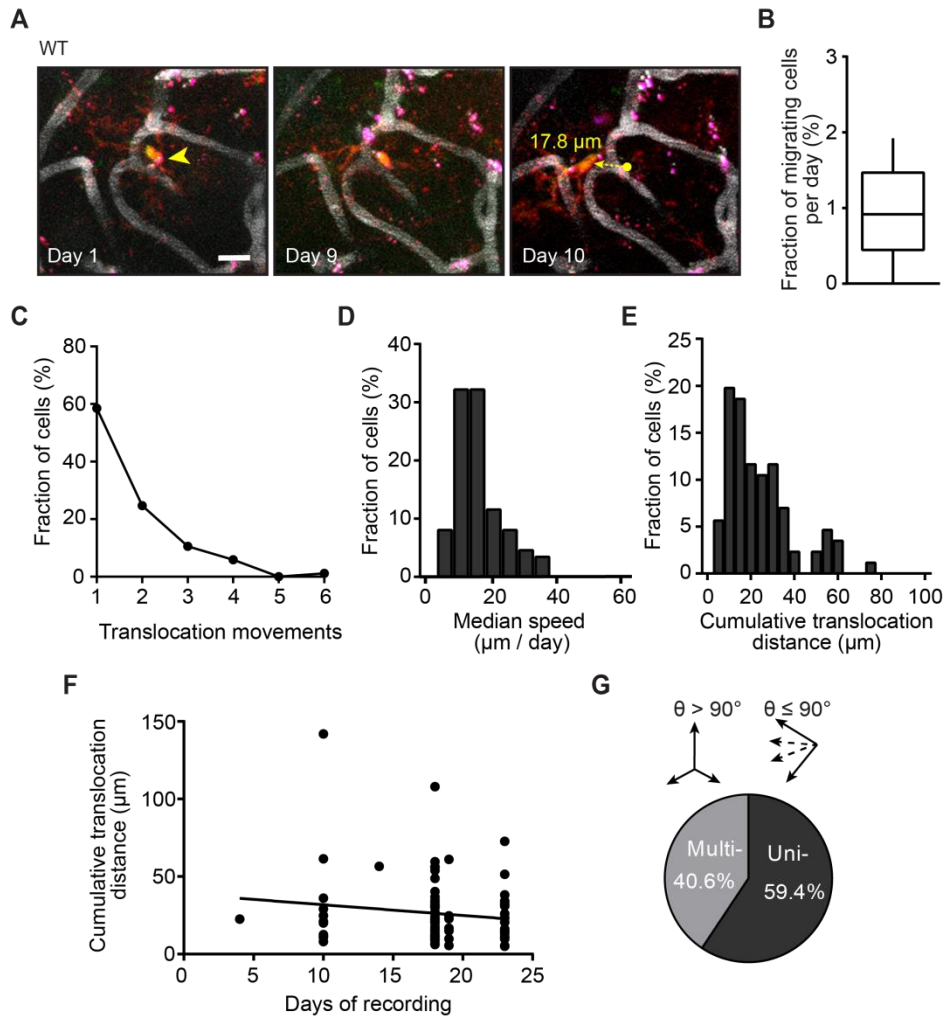
Figure 20. Characterization of the migration properties of microglia in WT mice. (**A**) MIP images of a Z stack (42-71 µm below the cortical surface, 2 µm step size) showing a microglial cell (pointed by yellow arrow) at different time points during the recording period. Note the translocation between day 9 and 10. In yellow, the translocation distance. Scale bar: 10 µm. (**B**) Box-and-whisker plot illustrating the fraction of migrating cells per day and mouse (n = 543 cells, 6 mice). (**C**) Histogram showing the fraction of the number of translocation movements of migrating cells (n = 87 cells, 6 mice). (**D,E**) Histograms showing the fraction distribution of (**D**) the median translocation speed and (**E**) the cumulative translocation distance of migrating microglia (n = 87 cells, 6 mice). (**F**) Scatter plot illustration the relationship between the length of the imaging period (days of recording) and the cumulative distance of migrating cells.

Next, we aimed at characterizing the destination of the migration events observed. Our results reported that nearly 50% of all migration events were related to blood vessels. In particular, cells were observed to migrate "along" blood vessels (cell soma remains in contact with a blood vessel in all translocation movements) or "toward" blood vessels (cell soma in the parenchyma gets directly in contact with a blood vessel after the last translocation movement) (Figure 21A). The remaining half of the migrating

cells was not associated to blood vessels so we labeled them into the category "others". Our results reported that almost half of the migration events were related to blood vessels: 20.69% of all migrating cells were moving along blood vessels, whereas 25.29% moved toward blood vessels (Figure 21B). Importantly, the median speed and the cumulative translocation distance remained similar between the three groups (Figure 21C, D).
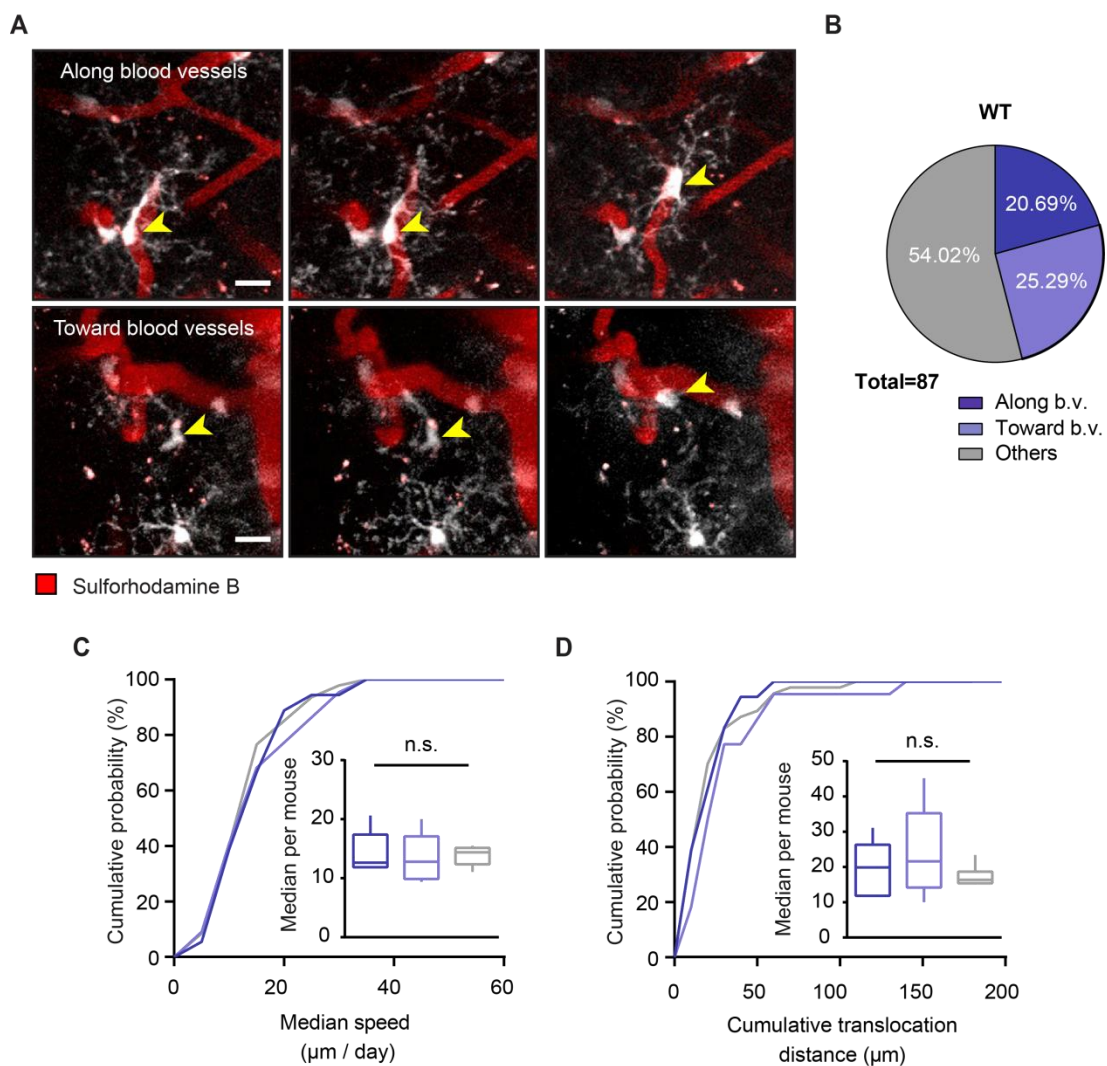
Figure 21. Fraction of blood-vessel related migration of microglia in the mouse brain under homeostatic conditions. (A) MIP images of Z stacks (top, 35-68 μm below the cortical surface; bottom, 41-73 μm below the cortical surface, 2 μm step size) acquired every 24 h showing examples of a cell (yellow arrow) migrating along (top) or toward (bottom) blood vessels. Scale bar: 10 μm. **(B)** Pie chart illustrating the fraction of migrating cells according their destination. **(C,D)** Cumulative probability histograms showing **(C)** the median translocation speed and **(D)** the cumulative translocation distance per cell regardless their destination (n = 87 cells). Insets in C,D indicate the median values per mouse (n = 6).

In summary, longitudinal tracking of single microglia cells via RGB labeling method revealed that under homeostatic conditions i) microglia has low turnover, ii) the fraction of migration events are significantly higher than division and death events, and ii) half of all migrating microglia is associated to blood-vessels.

3.4.3. Dynamic properties of microglia in AD mice

After we characterized the microglia dynamics in WT mice, we then proceed to compare these properties with those from AD mice at the beginning of plaque deposition (4-5 months of age).

We first aimed at determining the fate of these cells at the end of the imaging period. Our data acquired from 6 mice (n = 732 cells) recorded every day for 19-22 days revealed that 20% of microglia migrated, ~4% divided and ~6% died by the end of imaging period (Figure 22A). The median fraction (per mouse) of cell division and cell death events was 2.44 ± 4.93% and 4.88 ± 8.89%, respectively (Figure 22B). Like in WT mice, the median fraction (per mouse) of migration events was significantly higher than those from division and death rates (16.75 ± 19.67%, p = 0.004, Kruskal-Wallis test; Figure 22B).
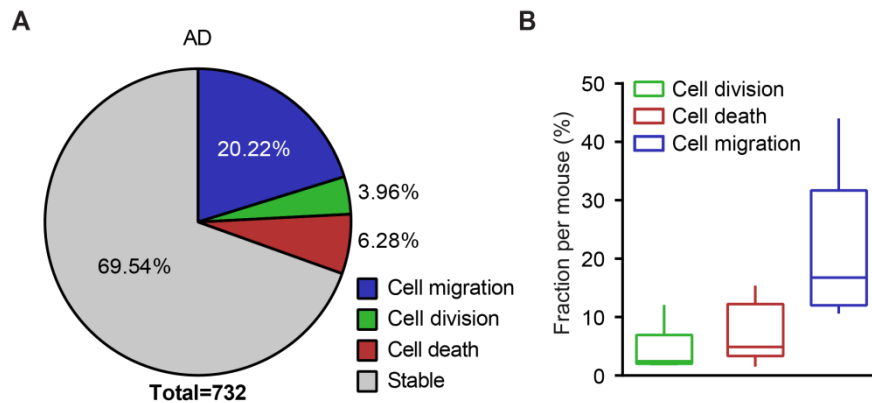
Figure 22. Fate determination of microglia in adult AD mice. (**A**) Pie chart illustrating the total fraction of cells undergoing any of the above mentioned events (cell division, cell death or cell migration) by the end of the total imaging period (19-23 days). (**B**) Box-and-whisker plot illustrating the median fraction per mouse of cell division, cell death and cell migration events (n = 6 mice).

The fractions of cell division and cell death were significantly higher compared to WT mice (p = 0.02 and p = 0.04, respectively, Mann-Whitney test; Figure 23A, B). Thus, the Kaplan-Meyer survival curves of AD mice were, significantly different from those in WT mice and indicated less survival rates for AD mice (p = 0.01, Mantel-Cox test; Figure 23C).
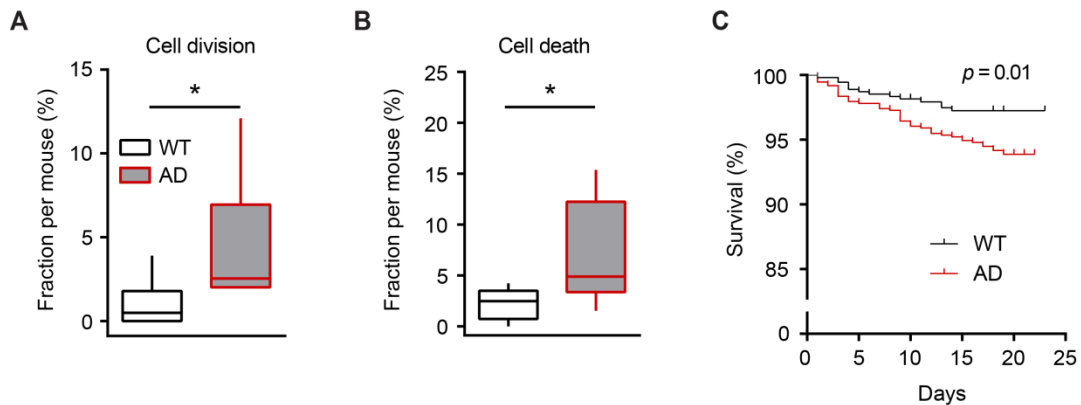
Figure 23. Cell division and death rates in AD mice. (**A,B**) Box-and-whisker plots illustrating the median fraction (per mouse) of (**A**) division and (**B**) death events. (**C**) Kaplan-Meier survival curves of WT (n = 543 cells, 6 mice) vs AD (n = 732, 6 mice) microglia.

Next, we looked at the location of these events in AD mice. Among the total number of divisions observed in 6 mice (n = 29 events), 69% took place on plaque viccinity, 21% on blood vessels and the remaining 10% in other locations (Figure 24A). Likewise, among all death events observed (n = 46 events), 54% took plaque on plaque viccinity, 22% on blood vessels and 24% in other locations (Figure 24B). When only considering APPPS1/Iba1-eGFP mice (n = 4 mice) 94% of all divisions (n = 16 events) and 72% of all deaths (n = 29 events) took place in plaques (data not shown). Thus, the main source of both division and death events in AD mice were the viccinity of amyloid plaques. Finally, when observed the destination of all migration events in AD mice (n = 148 events), 30% of these were blood-vessel related (along or toward blood vessels), another 33% were toward β-amyloid plaques and the remaining fraction was toward other destinations (37%; Figure 24C).

In summary, AD mice displayed higher division, death and migration rates compared to WT mice. Amyloid plaque vicinity harbor highly dynamic microglia, but the survival rates of these cells are significantly reduced compared to those in WT mice.
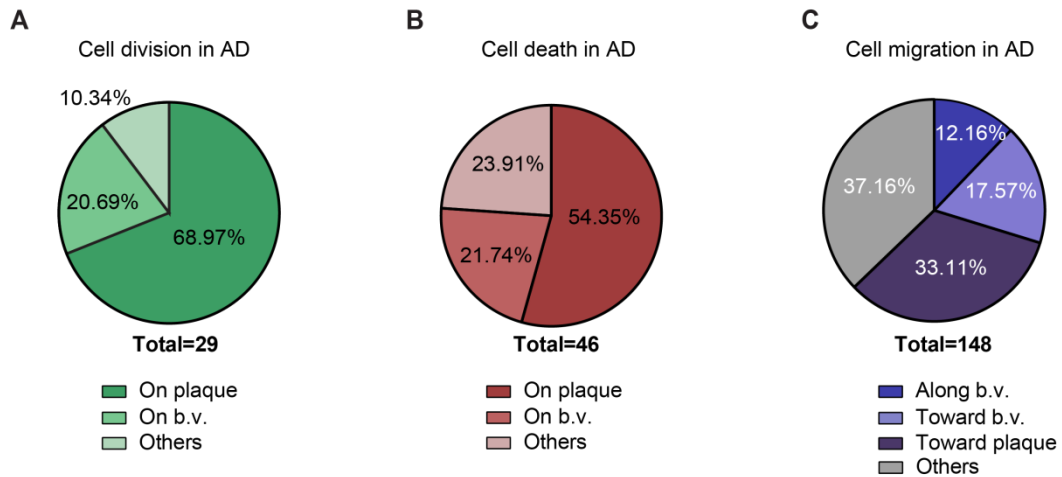
Figure 24. Location of division, death and migration events of microglia in AD mice. Note that the highest fraction of microglia turnover (division (**A**) and death (**B**) events) occured in association with amyloid plaques, and one third of all migration (**C**) events are toward amyloid plaques. N = 6 mice.

Finally, we characterized the migration properties of microglia in AD mice. As mentioned, the main destination of microglial migration in AD mice was β-amyloid plaques (Figure 25A). Indeed, the directionality of the movement was mostly unidirectional (65.5%, Figure 25C). However, our results reported no significant differences in the daily fraction of migrating cells between AD mice (1.41 ± 1.8%) compared to WT mice (0.92 ± 1.02%, p = 0.26, Mann-Whitney test, Figure 25B). Like in WT, most microglia cells had either one or two translocation movements during the total imaging period (60% and 22%, respectively; Figure 25D). The median speed and cumulative translocation distance in AD mice were 14.9 ± 5.45 μm and 20.25 ± 9.6 μm respectively (Figure 25E, F). These values were very similar to those found in WT mice (p = 0.84 for median speed and p = 0.77 cumulative distance, Mann-Whitney test; Figure 25G, H).
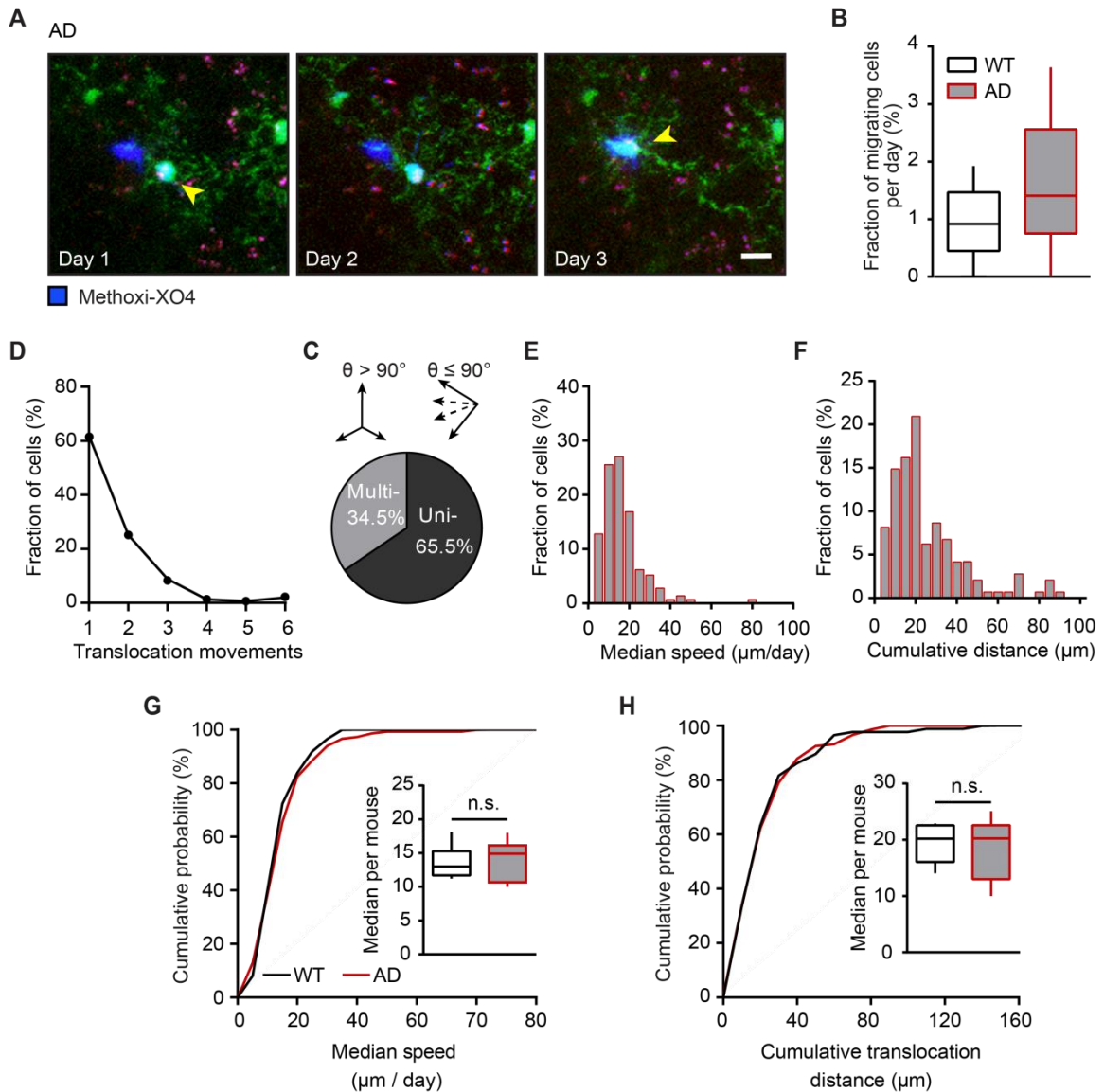
Figure 25. Characterization of the migration properties in AD mice. (**A**) MIP images of a Z stack (63-86 μm below the cortical surface, 2 μm step size) showing a microglial cell (in cyan) at different time points during the recording period. Note that this cell is migrating to an amyloid plaque (stained with Methoxi-XO4). The yellow arrow represents the translocation distance of that cell in relation to the previous time point. Scale bar: 10 μm. (**B**) Histogram showing the fraction of the number of translocation movements of migrating cells per day in WT (n = 87 cells, 6 mice) vs AD (n = 148 cells, 6 mice). (**C**) Box-and-whisker plot illustrating the fraction per day and mouse in WT vs AD. (**D**) Histogram showing the fraction of the number of translocation movements of migrating cells in AD mice (n = 148 cells, 6 mice). (**E,F**) Histograms showing the fraction distribution of (**E**) the median translocation speed and (**F**) the cumulative translocation distance of migrating microglia (n = 148 cells, 6 mice). (**G,H**) Cumulative probability histograms showing (**G**) the median translocation speed and (**H**) the cumulative translocation distance per cell regardless their destination (n = 148 cells). Insets in C,D indicate the median values per mouse (n = 6).

70

Because we found a high migration rate in microglia associated to blood vessels, we wanted to test differences in the migration properties of blood-vessel related migration in AD mice. Our results reported no significant differences between WT and AD mice (data not shown). Thus, no differences were found in the migration properties between young adult AD mice and young adult WT mice.

3.4.3.1. Dynamics of plaque-associated microglia

In order to determine the dynamics of amyloid-associated microglia, we quantified the number of migration, division or death events associated only to amyloid plaques. To this purpose, amyloid plaques were stained *in vivo* with Methoxi XO4. Microglia could easily be recognized in the vicinity of amyloid plaques and was characterized by a hypertrophic morphology with smaller soma and thick processes (Figure 26A). Our data from 6 mice revealed that among all events associated to plaques (n= 94 events), 49% corresponded to migration (cells approaching plaque vicinity), whereas the fraction corresponding to cell division and deaths on plaque was 24% and 22%, respectively (Figure 26B).
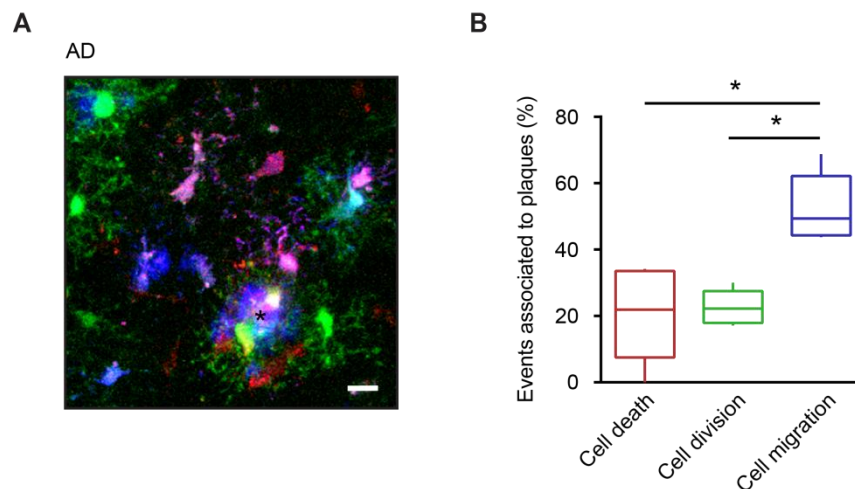
Figure 26. Events associated to amyloid-beta plaques in AD mice. (**A**) MIP image of a Z stack (62-108 μm below the cortical surface, 2 μm step size) showing microglial cells labeled in different colors with RGB labeling method. Note that cells are cluster around an amyloid plaque (stained with Methoxi-XO4, black asterisk points to the center of the plaque). Scale bar: 10 μm. (**B**) Box-and-whisker plot illustrating the median fraction per mouse of cell division, cell death and cell migration events (n = 6 mice).

Next, we generated Kaplan-Meier survival curves from microglia once established in the vicinity of a plaque (i.e. cells that were recruited by migration) and the survival curves from microglia upon they divide on plaque (i.e. cells that divided). Our results reported a reduction of the survival rates in the first five days for both groups, although no significant differences in the survival rates were found between these two groups of cells (p = 0.59, Mantel Cox test, Figure 27)
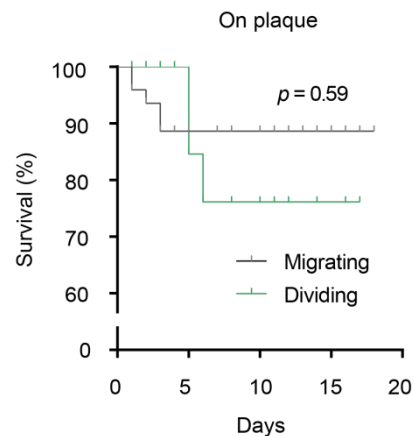
Figure 27. Survival rates of microglia after undergoing division or migration on plaque. Kaplan-Meier survival curves of cells that migrated to plaques (n = 49 cells, 6 mice) vs cells that divided on plaque (n = 29, 6 mice) microglia.

Taken together, recruitment of microglia from plaque vicinity is the main source of plaque-associated microglia. Plaque-associated migration rates are significantly higher than plaque-associated division/proliferation rates. Contact with amyloid plaque vicinity affects microglia survival rates.

CHAPTER 4

Discussion

4.1.   Normal brain aging alters microglia function *in vivo*

In the past years, great efforts have been made to define the aging phenotype of microglia, which will be crucial to understand brain aging and the development of neurodegenerative diseases such as AD. Whereas morphological and transcriptomic changes have been reported in aging microglia, the age-dependent functional changes remain obscure. This work provides new features of the aging phentoype by revealing (i) a bell-shaped relationship between the mouse age and the time course spontaneous Ca^{2+} signals, and (ii) an altered DAMP-induced microglial process extension in old mice (Olmedillas del Moral et al. 2019).

4.1.1.   Middle age as the first turning point in microglia homeostasis

For the first time, we have reported in $Cx_3CR1^{GFP/+}$ and WT mice that normal brain aging is accompanied by an increase in the frequency and duration of the spontaneous Ca^{2+} transients in microglia in middle aged mice compared to young adult mice, identifying microglial hyperactivity as a new hallmark of the aging brain (Olmedillas del Moral et al. 2019).

Microglia hyperactivity has also been observed in amyloid depositing mice (Brawek et al. 2014). Moreover, LPS-injected mice display higher fraction of spontaneously active microglia compared to PBS-injected mice (Pozner et al. 2015). AD and LPS, however, caused higher degrees of microglial hyperactivity than those we observed in middle-aged mice. Thus, we hypothesize that the age-related hyperactivity we observe here is a potential risk factor for the development of neurodegenerative diseases.

Whereas genomic, proteomic as well as morphological analyses have documented changes between young adult and old microglia, the middle-aged microglia is much less characterized. In humans, many age-related neuroinflammatory diseases such as Alzheimer's or Parkinson's disease are known to begin at middle age and, according to epidemiological studies, long-term use of non-steroidal anti-inflammatory drugs during this time period offers some protection against the development of the disease (Perry 2010).

Based on the idea that enhanced intracellular Ca^{2+} signaling accompanies activation of microglia (Brawek et al. 2014; Pozner et al. 2015), we named the phenotype of middle-aged microglia "reactive-like" or "alerted". In agreement with this view, recent data from single RNA-seq have reported a microglia subpopulation with pro-inflammatory features that is highly abundant in middle-aged mice (Sala-Frigerio et al. 2019). Thus, we hypothesize that the Ca^{2+} signals observed in our experiments likely reflect this reactive or pro-inflammatory phenotype.

4.1.2. Dysfunctional microglia in old mice is the second turning point

Whereas middle aged mice display an increased Ca^{2+} signaling activity, old mice had lower frequencies and durations of the spontaneous Ca^{2+} transients compared to those of middle-aged mice. This phenotype was unexpected based on the classical standpoint of "inflammaging", which proposes that aging leads to a more reactive-like microglial phenotype. We therefore aimed at characterizing the microglia response to DAMPs. To this purpose, we used the well-established ATP-directed process chemotaxis assay *in vivo* (Davalos et al. 2005; Schwendele et al. 2012; Olmedillas del Moral et al. 2019). In these experiments we used $CX_3CR1^{GFP/+}$ mice, since they display bright GFP-labeled processes that can be easily tracked. We then monitored the extension of individual microglial processes in mice at different ages. In the youngest mice (2-4 months old), tracking of individual processes over time revealed a high coordination between the processes in their movement toward an ATP-containing pipette. This coordination is documented by a strong monotonic relationship between the initial distance of the process tip to the ATP-containing pipette and its mean extension velocity as well as the simultaneous arrival of individual microglial processes at their final destination" (i.e. the source of ATP) (Olmedillas del Moral et al 2019). Mechanistically, the coordination between microglial processes might be orchestrated by the ATP concentration gradient generated upon application of the ATP-containing solution. Indeed, it was previously shown that microglial processes move fast toward pipettes containing lower

concentrations of ATP but move slower or even stop accounting high ATP concentrations (Davalos et al. 2005). Our data show that such coordination is gradually lost with aging, although the reasons are could not be assessed by the methods used. We propose as underlying mechanisms for this impairment: (i) age-related impairment of actin polymerization, a Ca^{2+}-dependent process required for actin cytoskeleton remodeling that mediates process extension (Larsson 2006; Irino et al. 2008; Hines et al. 2009), (ii) age-related reduction in the homogeneity of the $P2Y_{12}$ receptor expression or (iii) loss of the ATP concentration gradient caused by the aging-induced heterogeneity of the extracellular space. In the literature, we find evidence supporting all the above mentioned mechanisms. For example, transcriptomic analyses of purified human cortical microglia revealed aging-mediated downregulation of the expression of many actin cytoskeleton-associated genes (Galatro et al. 2017). Also gene expression of the $P2Y_{12}$ receptors was significantly reduced both in aged humans (Galatro et al. 2017) as well as in mice (Hickman et al. 2013), although the (in)homogeneity of their expression could not be addressed with the methods used. Finally, aging has been reported to cause a decrease in the volume of the extracellular space and a loss of the extracellular matrix macromolecules (Sykova et al. 2005; Sykova and Nicholson 2008).

These findings together with the bell-shaped relationship between the mouse age and the properties of spontaneous Ca^{2+} transients observed suggest that aging microglia undergo changes in their functional state at least twice (Olmedillas del Moral et al. 2019). In the first turning point, mentioned in the previous section, middle-aged microglia change toward a "reactive-like" phenotype characterized by higher frequencies and durations of spontaneous Ca^{2+} transients than those of young adult mice, with a slight but not significant increase in the response to DAMPs (i.e. ATP). As such, middle-aged microglia might be already "alerted" and react much more vividly to DAMP signals, in the extreme case leading to chronic activation of microglia eventually causing neuronal damage or neurotoxicity. This phenomenon might explain why in humans midlife systemic inflammatory responses

caused by type 2 diabetes, midlife hypertension, or infection, were identified as risk factors for developing neurodegenerative diseases (Perry, Cunningham, and Holmes 2007; Perry 2010; Perry and Teeling 2013; Ott et al. 2016; Abell et al. 2018).

The second switch or turning point in the functional phenotype of microglia appear to occur in older ages. Our results reported that aged microglia display reduced frequencies and durations of spontaneous Ca^{2+} transients, as well as an affected DAMP-induced microglial process extension, compared to middle-aged mice. All these alterations suggest a dysfunctional rather than a reactive-like phenotype in old mice. Interestingly, however, our observation of faster process extension of aged microglia resembles previous findings in the brains suffering from epilepsy (Avignone et al. 2008) or amyloid β-induced inflammation (Brawek et al. 2014). A dysfunctional phenotype can be interpreted as a deficiency in the neuroprotective functions of microglia in older ages, so it is plausible to think that they increase their susceptibility to age-related neurodegenerative diseases. In support of this view, Streit et al reported the presence of dystrophic microglia in aged humans and, later, a similar phenotype in areas of neurodegeneration and tau pathology from AD patients was observed (Streit et al., 2009).

In summary, our results have identified two distinct functional phenotypes of aging microglia (Olmedillas del Moral et al. 2019). The first one is an "alerted" phenotype, characterized by enhanced "spontaneous" intracellular Ca^{2+} signaling, likely reflecting overreacting responses to minor cell or tissue damages occurring in their microenvironment. Unexpectedly, this phenotype was largely present in middle-aged mice, but not in old mice. The second "dysfunctional" phenotype was present in old mice, and was characterized by overall microglial hyperactivity, reduced spontaneous Ca^{2+} signaling and "ataxic" movements of microglial processes. Therefore, this phenotype is likely dysfunctional, and it consists of the second functional phenotype arising with aging.

4.1.3. Sex-specific changes in microglial Ca^{2+} signaling

We have recently reported in $Cx_3CR1^{GFP/+}$ mice that the fraction of spontaneously active microglia increases slightly with aging, with young adult mice displaying a median fraction of 33% ± 45%, and old mice displaying a median fraction of 55% ± 12.5% (Olmedillas del Moral et al. 2019). Despite the variability in young adult mice, the difference between young adult and old mice was statistically significant. However, in our series of experiments in Tomato-lectin labeled microglia from WT mice, in which we used equal number of males and females, the median fraction of spontaneously active microglia in young adult mice was 50 ± 12.5%. The reason for the higher fraction of spontaneously active microglial cells observed in WT compared to $Cx_3CR1^{GFP/+}$ mice remains unclear but it is unlikely due to the presence of Tomato lectin, as microglia from $Cx_3CR1^{GFP/+}$ mice showed similar Ca^{2+} signaling behavior before and after the injection of Tomato lectin (data not shown). Therefore, we split our data from WT mice according to the animal's gender. Surprisingly, our data reported a higher fraction of spontaneously active microglia in males compared to females in young adult mice, which also explains the variability observed in the mice. This data suggest a more sensitized or "alerted" state of young male microglia and are in line with recent single cell RNA-seq data showing that in young adult males, microglia upregulate genes belonging to clusters associated with inflammatory processes, including the regulation of cell migration and cytokine production (Villa et al. 2018). Moreover, male microglia have larger somata and higher expression of MHC molecules as well as purinergic receptors compared with their female counterparts (Guneykaya et al. 2018). In addition, in cortical slices from male mice microglia had higher baseline outward and inward and responded with larger inward K^+ currents to applications of ATP (Guneykaya et al. 2018).

While starting at the higher level in young adult mice, the fraction of active cells in males seem to change little over the life span, much in contrast to female mice, in which this fraction of spontaneously active microglia in old mice roughly doubled those from young adult females. These functional data

are in agreement with recent analyses of microglia single-cell RNA sequencing (Sala Frigerio et al. 2019). The authors identified a subtype of reactive microglia named activated response microglia (ARM), which was more prevalent in old mice (Sala Frigerio et al. 2019). Remarkably, more female microglia fell into the ARM cluster than male microglia. ARMs were characterized by the expression of genes involved in inflammatory processes (*Cst7*, *Clec7a*, and *Itgax*), MHC-II presentation (*Cd74*, *H2-Ab1*, *H2-Aa*, *Ctsb*, and *Ctsd*) and, interestingly, genes involved in tissue regeneration (*Spp1*, *Gpnmb*, and *Dkk2*) (Sala Frigerio et al. 2019). The consequences of more reactive microglia in females might reflect a chronic neuroinflammatory state which, according to the classical view, might be a risk factor to develop age-related neurodegenerative diseases such as AD, which would explain the higher incidence of any dementia and AD in females (Beam et al. 2018). However, this reactive phenotype might also have neuroprotective functions, thus reflecting a better adaptation of female microglia to the new environmental landscape arising with aging.

4.2. Ca^{2+} signaling hyperactivity of microglia in early plaque-deposition

Neuroinflammation is a hallmark of AD in both humans and mouse models of the disease, and it is characterized by the presence of hyperthrophic microglia expressing pro-inflammatory markers. However, little is known about the functional properties of microglia in AD and even less about its interaction with aging. Here we characterized *in vivo* the Ca^{2+} signaling properties of microglia in APPPS1 mice at 2-4 and 9-11 months old. Our data revealed a higher incidence of Ca^{2+} signaling in microglia located in amyloid-plaque vicinity, documented by an increase in the frequency of spontaneous Ca^{2+} signals and a higher fraction of microglial cells displaying spontaneous Ca^{2+} signals. These results are in agreement with those from Brawek et al. 2014, who reported that in middle-aged APPPS1/Iba-1-eGFP mice 80% of the amboeboid microglia in association with amyloid plaques

display spontaneous Ca^{2+} signals compared to ramified microglia from plaque-free cortical areas (Brawek et al. 2014).

Microglia hyperactivity could be understood as the result of the stimulation by DAMPs or PAMPs, based on the analysis of Ca^{2+} signaling after the induction of neuronal damage as well as in LPS-challenged mice (Eichhoff et al. 2011; Pozner et al. 2015). In these studies, microglia increase their incidence of spontaneous Ca^{2+} signals upon the induction of neuronal damage or 12h after the injection of LPS peripherally (Eichhoff et al. 2011; Pozner et al. 2015). These *evoked* Ca^{2+} signals rely on the activation of purinergic receptors and result from the depletion of intracellular Ca^{2+} stores, as application of PPADS (a P2X and P2Y antagonist) reduce the presence of Ca^{2+} signals after LPS challenge (Pozner et al. 2015), and the treatment with thapsigargin (a SERCA inhibitor) blocks damage-induced Ca^{2+} transients (DICTs) (Eichhoff et al. 2011). Similarly, amoeboid microglia in APPPS1/Iba-1-eGFP mice display spontaneous Ca^{2+} transients which depend on purinergic receptors, as PPADS blocked the presence of these transients (Brawek et al. 2014). Spontaneous Ca^{2+} transients in plaque-associated microglia also depend on the depletion of the intracellular stores, as CPA suppresses virtually 100% of all spontaneous Ca^{2+} transients (Brawek et al. 2014). Thus, we hypothesized that hyperactivity in plaque-associated microglia might trigger a Ca^{2+}-dependent release of toxic and/or proinflammatory substances in the vicinity of amyloid plaques. In agreement with this hypothesis, Heneka et al. reported an enhanced activation of caspase-1 and the nucleotide-binding domain, leucine-rich-repeat-containing family, pyrin domain-containing 3 (NLRP3) inflammasome in AD pathology. Indeed, caspase-1$^{-/-}$ and NLRP3$^{-/-}$ mice carrying AD-related mutations increased Aβ clearance and were largely protected from loss of spatial memory and reduction of dendritic spine density *in vivo* (Heneka et al. 2013). Since Ca^{2+} release from the intracellular ER stores seems to mediate the activation of the NLRP3 inflammasome via P2 receptors (Lee et al. 2012; Murakami et al. 2012), it is plausible to think that the Ca^{2+} transients observed in plaque-associated microglia reflect the activation of the NLRP3

inflammasome, which mediate the release of pro-inflammatory cytokines such as IL-1β.

Interestingly, the microglia hyperactivity we found in AD mice was, however, more prominent in young adult mice than in middle-aged mice. This was somewhat unexpected since the plaque density in young adult mice is lower compared to that from older mice (Radde et al. 2006). Moreover, our data revealed a substantial reduction of the amplitude of the spontaneous Ca^{2+} signals in young adult AD mice and, to a lesser extent, in middle-aged mice and old mice. Thus, we have identified a unique phenotype of microglia during early plaque deposition, characterized by Ca^{2+} signaling hyperactivity with small amplitudes. This phenotype differs from that found in normal aging, thus paving the way to the identification of specific targets for the early intervention of AD.

4.3. Establishment of a new labeling method for microglia *in vivo*

In this work, we have also aimed at providing more insights into the functional properties of amyloid-associated microglia during early plaque deposition, which are largely unknown until now. To do so, we first established a method that allowed us to visualize and distinguish single microglial cells unequivocally in order to monitor their behavior longitudinally during amyloid deposition. Until now, the widely used Cx$_3$CR1$^{GFP/+}$ or Iba-1-eGFP mice, which express GFP constitutively in microglia, have allowed us to visualize these cells *in vivo*. However, unicolor labeling fails to distinguish cells individually, which makes the tracking challenging and often not possible. Moreover, other myeloid cells such as perivascular macrophagues also express Iba-1 and the Cx$_3$CR1 receptor, making these approaches not specific for microglia. Our new labeling approach is based on red (R), green (G) and blue (B) color coding, and used the miRNA9-regulated lentiviral vectors described elsewhere (Åkerblom et al. 2013). RGB labeling marked microglia specifically with high efficiency (approximately 60%). Because viral transduction occurs stochastically, this approach provides a combinatorial

expression of the fluorescent genes which results in a wide range colors, giving a unique color identity to each microglial cell. Thus, RGB labeling provides a versatile toolkit for studying live microglia and lay the ground for future analysis of microglia function under disease conditions, in which the issues of cell clonality as well as fate of individual cells become important. RGB labeling allowed us to determine and characterize the fate of microglial cells during homeostasis and AD pathology.

4.3.1. RGB labeling reveals low turnover rates under homeostatic conditions

Longitudinal tracking of single microglia cells via our newly established RGB labeling method revealed that under homeostatic conditions cortical microglia have low turnover, with newly appearing microglia deriving from local cell division events. Our observation of low turnover of cortical microglia in mice is in agreement with previous data using different approaches. For example, most microglial cells could be identified after imaging periods up to 15.5 months in the mouse neocortex and further Kaplan-Meier survival analysis suggested a median microglial lifetime greater than 15 months (Füger et al. 2017). Consistently, Tay et al. also estimated a proliferation rate of less than 1% in the mouse cortex (Tay et al. 2017). Réu et al. isolated microglia from fresh postmortem cortical samples and used traces of carbon-14 left over from atomic bomb tests in the 1950's and '60s to estimate the lifespan of microglia in humans (Réu et al. 2017). The authors estimated that on average 28% of our microglia is replenished every year, which suggests higher levels of microglia turnover in humans compared to mice (Réu et al. 2017).

The low turnover rates observed in cortical areas from mice diverge from those observed in the olfactory bulb, a niche for adult neurogenesis, where microglia was reported to display a daily turnover rate of ~0.4-0.8% (Askew et al. 2017; Tay et al. 2017). This suggests a correlation between neuronal and microglial survival, presumably reflecting an intimate crosstalk between these two cell types along the lifespan of the organism.

4.3.2. RGB labeling reveals a subset of migrating microglia under homeostasis

In the mouse cortex, mature microglia display a highly branched morphology occupying non-overlapping domains of approximately 40-50 µm diameter (Torres-Platas, G, S Comeau et al. 2014). In 2005, Nimmerjahn et al. and Davalos et al. reported the first studies showing that live microglia, far from being resting cells, displayed highly motile processes constantly monitoring their local microenvironment, although their somata were proposed to be largely sessile under homeostatic conditions (Nimmerjahn et al. 2005; Davalos et al. 2005).

Microglial migration occurs during brain development, where they exert important functions for the establishment of the neuronal networks (Okajima & Tsuruta 2018). In addition, microglia are known to surround sites of injury with their processes, as a putative mechanism to "shield" the injury site (Davalos et al. 2005; Nimmerjahn et al. 2005). To the best of our knowledge, migration of microglia (defined as translocation of their soma position in ≥ 5 µm) has not been reported yet under homeostatic conditions, although some studies have already suggested this phenomenon after observing rearrangements in the microglial landscape, which were independent of cell proliferation (Eyo et al. 2018). In the adult brain, soma translocation has been reported in other contexts where major insults occur, and has been shown to be a transition stage of microglia toward an amoeboid/reactive phenotype (Stence et al. 2001). For example, confocal time-lapses of brain slices reported additional transition stages before microglia initiates soma translocation. In the first minutes after acquiring the brain slices, microglia are in the withdrawal stage (W-stage), in which they retract their processes. In the transitional and motile stages (M-stage and T-stage, respectively) microglia generate new protrusions at a fast rate. Finally, hours later, microglia might enter a locomotory stage (L-stage), in which cells acquire a highly motile stage involving soma translocation (Stenceet al. 2001). Microglia soma translocation has also been reported after kainic acid (KA)-

induced seizures (Eyo et al. 2018) and microelectrode implantation (Kozai et al. 2012).

The role of translocating microglia is presumably to restore the homeostatic conditions. For example, microglia migrates to the site of lesion after photoreceptor injury in the mouse retina (Miller et al. 2019). The injured photoreceptors recovered their function to near-baseline levels after microglia had departed the injury locus (Miller et al. 2019). In amyloid depositing mice, microglia is rapidly recruited to amyloid plaques, where they usually transform into an amoeboid phenotype. Plaques which were surrounded by microglia increase in size at a lower speed than those with less microglia attached (Bolmont et al. 2008). Remarkably, whisker trimming also induced a change in the microglia landscape in the barrel cortex presumably due, at least in part, to microglia translocation (Eyo et al. 2018).

In this study, we have characterized for the first time the migration events observed during homeostasis in adult WT mice. We analyzed the migration rate per day, the median speed per day, the cumulative translocation distance, the directionality and destination of the migration. Our results reported that the migration speed and the cumulative translocation distance were 14.2 µm/day and 20.5 µm, respectively, in a total imaging period of 3 weeks approximately. These values were regardless of the directionality, suggesting that most of the migrating cells remain in their territorial domain throughout the recording period. This presumably reflects a new feature of surveillant microglia, which might not just survey their local environment with dynamic processes, but also "patrol" their surroundings. Remarkably, around 14% of migrating microglia that displayed unidirectional movement had cumulative translocation distances greater than 40 µm, suggesting that at least a subset of cells is able to leave their territorial domain. Presumably, this may reflect specific functions associated to this microglia subset, which cannot otherwise be fulfilled by neighboring cells.

Finally, we have reported the destination of all cells migrating within our imaging period. Remarkably, around half of these cells migrated either along or toward blood vessels. Although this type of migration has been similarly

observed during brain development (Grossmann et al. 2002), the reasons for these blood-vessel associated migration in young adult mice remain unclear, but possible mechanisms might include favoring nutrient supply or angiogenesis (Dudvarski Stankovic et al. 2016), although we cannot exclude the possibility of an interaction with the peripheral immune system.

In summary, the migration events we observed are likely related to homeostatic control of their local environment within their territorial domains, thus identifying a new mechanism of microglial surveillance. However, giving the imaging time frame, we cannot exclude the possibility of microglia leaving their territorial domains after longer periods of imaging.

4.3.3. Recruitment rather proliferation is the source of new plaque-associated microglia in young adult AD mice

Microglia have been shown to be rapidly recruited to amyloid plaques *in vivo* (Bolmont et al. 2008). As mentioned above, the role of recruited microglia is to form a barrier which likely protects from spreading amyloid and from neurotoxicity (Bolmont et al. 2008; Condello et al. 2015). Once in the plaque vicinity, microglial processes remain highly dynamic (Bolmont et al. 2008). Plaques that had less microglial coverage increased their volume at a higher rate than those smaller plaques. Although these amyloid-associated microglia has been shown to phagocyte amyloid *in vivo* (Bolmont et al. 2008; Baik et al. 2016), the size of the plaques keeps growing, which has been suggested to reflect the cell's inability to perform clearance.

We have observed significant higher fractions of proliferation and death rates in AD mice *in vivo*, with the highest found in amyloid plaque vicinities. However, the survival rates of microglia in AD are significantly lower compared to WT mice. This results are consistent with *in vivo* studies showing that an excess of the accumulation of Aβ in microglia reached cell death (Baik et al. 2016).

In addition, we have reported that microglia recruited to amyloid plaques is the predominant mechanism by which this barrier is formed and maintained. What occurs with the empty domains left by microglia recruited to plaques remains obscure, but it is possible that in our animal model cells

from periphery infiltrate and participate in the restoration of the microglia mosaic (Unger et al. 2018).

The extent to which migration, proliferation or cell death participate in reestablishing the microglia mosaic is an important focus for subsequent investigations.

4.4. Conclusions

In the last two decades, since the discovery of their extraordinary surveillant ability and their unique origins, the field of microglia research has grown exponentially. In addition, large population studies in humans have recently point to a central role of microglia in age-related neurodegenerative diseases such as AD. The functional role of microglia in the context of AD, however, is far from being elucidated. This is due in large part to our lack of information about the functional properties of these cells during normal aging. This work provides knowledge in this direction by identifying two distinct functional phenotypes of aging microglia. The first, an "alerted" phenotype in midlife might be overreacting to minor cell or tissue damages happening in their microenvironment. The second phenotype, ubiquitously present in old mice, can be considered "dysfunctional" or "senescent". It remains unclear whether this phenotype signals aging-dependent failure of microglial function or it is a normal adaptation to the chronically increased level of DAMPs in the aging brain. Even less clear is to which extent these age-related changes are explained by cell-autonomous aging of microglia versus the contribution of extracellular signals from the microglia environment. In case microglia are drivers for aging in the brain, targeting these cells would provide new anti-aging approaches for brain rejuvenation.

In addition, we have provided evidence for sex differences in the function of microglia and its interaction with aging, which are supported by recently published transcriptomic studies in single microglial cells. The extent to which these intrinsic differences during aging contribute to disease susceptibility remains to be elucidated.

Finally, we have established a new method for *in vivo* labeling of microglia cells for single-cell longitudinal tracking in order to characterize microglia dynamics during early AD pathology. Our results using RGB labeling revealed a subset of microglial cells migrating under homeostatic conditions, thus identifying a new "patrol" feature of microglia. In AD mice, the hotspots for microglia dynamics are the amyloid plaques, in which the highest rate of migration, death and proliferation were found. However, microglia in amyloid plaque vicinity had less survival rates, thus supporting the view of a dysfunctional phenotype in amyloid-plaque vicinity, but it still remains open whether microglial cells are initiators or followers in AD pathology.

Thus, future studies are needed to understand what microglia "are doing" rather than what they express, which will provide more precise information about their roles in health and disease. Examples would be use Tg mice that lack genes involved in aging and pathology (e.g. TREM2). To address the molecular mechanisms, human iPSC-derived microglia for *in vitro* studies of microglia could be a suitable option.

5. Abstract

Microglial cells are the primary macrophages of the central nervous system and, as such, they provide the first line of immune defense in response to injury or disease. Malfunction of microglia was proposed to play a critical role in the development of age-related diseases such as Alzheimer's disease (AD), and recently 'omics' studies have pointed to microglia as causal agents of the disease. The role of microglia in the context of AD and other age-related diseases, however, is far from being elucidated. First, we still lack information about the functional properties of these cells during normal aging. And second, we do not understand how the pathology (e.g. amyloid accumulation) interacts with the organism's age. Detailed knowledge about cellular and physiological properties of microglia is therefore crucial, and this information can only be assessed by studying these cells in their native environment: the intact brain. In this work, we analyze for the first time the in vivo physiological changes of microglia during normal brain aging and provide new insights about their functional changes in AD by using high resolution two-photon imaging and two different approaches: i) characterization of the Ca^{2+} signaling properties of cortical microglia from mice during aging and AD and ii) characterization of microglia dynamics during homeostasis and AD.

Our data revealed a bell-shaped relationship between the properties of the Ca^{2+} signals and the animal's age, with the most frequent and largest Ca^{2+} transients observed in middle-aged (9-11 months old) mice, compared to young adult (2-4 months old) and old (18-21 months old) mice. Interestingly, we also found sex-specific changes in some of the Ca^{2+} signaling properties, such as in the fraction of spontaneously active microglia. Importantly, the reduction of the Ca^{2+} signaling activity in old microglia was accompanied by an impairment of their ATP-directed chemotactic properties. The changes observed in AD mice were different to those observed in normal aging, and were characterized by a higher fraction of spontaneously active microglia with significantly reduced amplitudes of the Ca^{2+} transients, compared to the age-matched WT mice.

In this work, we also characterized for the first time the motility and turnover of microglia in young adult WT mice (i.e. during homeostasis) and AD pathology, by establishing a new labeling method for red (R), green (G) and blue (B) color coding of microglia based on miRNA9-regulated lentiviral vectors. By combining this approach with in vivo two-photon imaging, we characterized the migration, proliferation and death of cortical microglia. Our results revealed that, in the healthy young adult brain, microglia display a daily average migration rate of 1%, with a median translocation distance of ~20 μm. The migration pattern is saltatory, characterized by fast translocation alternating with long stationary periods. In addition, our results from WT mice revealed a high fraction of blood-vessel associated migration (along or toward blood vessels) and low turnover rates. Although in young adult AD mice the daily average migration rate was slightly higher compared to age-matched WT mice, we neither observed significant differences in their pattern, nor in the median speed or cumulative translocation distance. The proliferation and death rates were, however, significantly higher than those from WT mice, leading to significantly lower survival rates of microglia from AD mice. Accordingly, amyloid plaques harbored most of the dynamic microglia but also triggered the highest death rates.

Taken together, this work provides i) a better understanding of the physiological changes in microglia during normal aging and AD, and ii) a versatile toolkit for studying individual live microglia, laying the ground for future analysis in other pathological conditions.

6. Zusammenfassung

Mikrogliazellen sind die primären Makrophagen des Zentralen Nervensystems und bilden als solche die erste Linie der Immunabwehr als Reaktion auf Verletzungen oder Krankheiten. Eine Fehlfunktion der Mikroglia wurde beispielsweise mit der Pathogenese der Alzheimer-Erkrankung (Alzheimer's disease = AD) in Verbindung gebracht, und kürzlich publizierte Daten weisen auf Mikroglia als einer der Kausalfaktoren der Krankheit hin. Die Rolle der Mikroglia im Kontext von AD und anderen altersabhängigen Krankheiten ist bisher allerdings noch nicht vollständig aufgeklärt. Erstens fehlen bisher Informationen über die funktionellen Eigenschaften und Veränderungen dieser Zellen während des normalen Alterungsprozesses. Zweitens ist unklar, wie die pathologischen Merkmale wie das Auftreten von Amyloidablagerungen mit dem Alterungsprozess interagieren. Detaillierte Kenntnisse der zellulären und physiologischen Eigenschaften der Mikroglia sind daher von entscheidender Bedeutung. Diese können nur durch die Untersuchung der Zellen in ihrer natürlichen Umgebung, dem intakten Gehirn, ermittelt werden. In dieser Arbeit analysieren wir erstmalig die physiologischen Veränderungen der Mikroglia im Verlauf der normalen Gehirnalterung in vivo und liefern neue Erkenntnisse über die funktionellen Veränderung im Verlauf der AD. Hierzu verwendeten wir hochauflösende Zwei-Photonen-Bildgebung und zwei unterschiedliche Versuchsansätze: i) Charakterisierung der Ca^{2+} Signalgebung kortikaler Mikroglia in alternden Wildtyp (WT) Mäusen und im Mausmodell der AD, und ii) Charakterisierung der Dynamik von Mikrogliazellen im gesunden Gehirn und im Mausmodell der AD.

Unsere Daten zeigten eine glockenförmige Beziehung zwischen Ca^{2+} Signalgebung und dem Alter der Tiere, wobei die häufigsten und größten Ca^{2+} Transienten bei Mäusen mittleren Alters (9-11 Monate) im Vergleich zu jungen adulten Mäusen (2-4 Monate) und alten Mäusen (18-21 Monate) beobachtet wurden. Interessanterweise fanden wir auch geschlechtsspezifische Veränderungen in einigen Eigenschaften der Ca^{2+} Signalgebung, beispielsweise im Anteil der spontan aktiven Mikrogliazellen.

Interessanterweise ging die Reduzierung der mikroglialen Ca^{2+} Signalgebung in alten Mäusen mit einer Beeinträchtigung ihrer chemotaktischen Eigenschaften einher. Die im Mausmodell der AD beobachteten Veränderungen unterschieden sich von denen während des normalen Alterungsprozesses, und waren gekennzeichnet durch einen höheren Anteil an spontan aktiven Mikroglia mit signifikant reduzierten Amplituden der Ca^{2+} Transienten im Vergleich zu gleichaltrigen WT Mäusen.

In dieser Arbeit charakterisierten wir ebenfalls die Motilität und die Umsatzrate von Mikroglia bei jungen erwachsenen WT Mäusen (d.h. während der Homöostase) und im Mausmodell der AD. Zu diesem Zweck nutzten wir erstmals eine neue Methode zur Markierung, welche auf miRNA9-regulierten lentiviralen Vektoren basiert und die rote (R), grüne (G) und blaue (B) Farbkodierung von Mikroglia ermöglicht. Durch die Kombination dieses Ansatzes mit der in vivo Zwei-Photonen-Bildgebung charakterisierten wir die Migration, Proliferation und den Tod kortikaler Mikrogliazellen. Unsere Ergebnisse zeigten, dass Mikroglia im gesunden jungen erwachsenen Gehirn eine tägliche durchschnittliche Migrationsrate von 1% bei einem mittleren Translokationsabstand von ~20 μm aufweisen. Das Migrationsmuster ist saltatorisch und durch eine schnelle Translokation im Wechsel mit langen stationären Perioden charakterisiert. Ein hoher Anteil der Migration in WT Mäusen war mit Blutgefäßen (entlang oder zu den Blutgefäßen) assoziiert. Die Umsatzrate der Mikroglia in diesen Tieren war niedrig. Obwohl bei jungen erwachsenen AD Mäusen die tägliche durchschnittliche Migrationsrate im Vergleich zu gleichaltrigen WT Mäusen etwas höher war, konnten wir weder signifikante Unterschiede in ihrem Muster noch in der mittleren Geschwindigkeit oder dem kumulativen Translokationsabstand feststellen. Die Proliferations- und Sterberaten waren jedoch signifikant höher als bei WT Mäusen. Dies hatte signifikant niedrigere Überlebensraten der Mikroglia in AD Mäusen zur Folge. Die größte Dynamik der Mikroglia, aber auch die höchsten Todesraten konnten wir in der Umgebung von Amyloidablagerungen nachweisen.

Die hier dargestellten Ergebnisse tragen zu einem besseren Verständnis der physiologischen Veränderungen der Mikroglia während des normalen Alterns und im Verlauf der AD Pathologie bei. Die hier verwendeten Methoden bieten vielseitige Möglichkeiten für die Untersuchung einzelner Mikroglia in vivo unter physiologischen und pathologischen Bedingungen.

7. References

Abell, Jessica G; Mika Kivimäki; Aline Dugravot; Adam G Tabak; Aurore Fayosse; Martin Shipley; Séverine Sabia; and Archana Singh-Manoux. Association between Systolic Blood Pressure and Dementia in the Whitehall II Cohort Study: Role of Age, Duration, and Threshold Used to Define Hypertension. *European Heart Journal* **2018**, 3119–25.

Ajami, Bahareh; Jami L. Bennett; Charles Krieger; Wolfram Tetzlaff; and Fabio M V Rossi. Local Self-Renewal Can Sustain CNS Microglia Maintenance and Function throughout Adult Life. *Nature Neuroscience* **2007** 10 (12): 1538–43.

Åkerblom, Malin; Rohit Sachdeva; Luis Quintino; Erika Elgstrand Wettergren; Katie Z. Chapman; Giuseppe Manfre; Olle Lindvall; Cecilia Lundberg; and Johan Jakobsson. Visualization and Genetic Modification of Resident Brain Microglia Using Lentiviral Vectors Regulated by MicroRNA-9. *Nature Communications* **2013** 4.

Albert, Marilyn S. Cognitive and Neurobiologic Markers of Early Alzheimer Disease. *Proceedings of the National Academy of Sciences of the United States of America* **1996** 93 (24): 13547–51.

Alliot, Francoise; Isabelle Godin; and Bernard Pessac. Microglia Derive from Progenitors, Originating from the Yolk Sac, and Which Proliferate in the Brain. *Developmental Brain Research* **1999** 117 (2): 145–52.

Amit, Ido; Deborah R. Winter; and Steffen Jung. The Role of the Local Environment and Epigenetics in Shaping Macrophage Identity and Their Effect on Tissue Homeostasis. *Nature Immunology* **2016** 17 (1): 18–25.

Askew, Katharine; Kaizhen Li; Adrian Olmos-Alonso; Fernando Garcia-Moreno; Yajie Liang; Philippa Richardson; Tom Tipton; et al. Coupled Proliferation and Apoptosis Maintain the Rapid Turnover of Microglia in the Adult Brain. *Cell Reports* **2017** 18 (2): 391–405.

Avignone, E.; L. Ulmann; F. Levavasseur; F. Rassendren; and E. Audinat. Status Epilepticus Induces a Particular Microglial Activation State Characterized by Enhanced Purinergic Signaling. *Journal of Neuroscience* **2008** 28 (37): 9133–44.

Baik, Sung Hoon; Seokjo Kang; Sung Min Son; and Inhee Mook-Jung. Microglia Contributes to Plaque Growth by Cell Death Due to Uptake of Amyloid β in the Brain of Alzheimer's Disease Mouse Model. *Glia* **2016** 64 (12): 2274–90.

Bartlett, Jeffrey S; R Jude Samulski; and Thomas J Mccown. Selective and Rapid Uptake of Adeno-Associated Virus Type 2 in the Brain. *Human Gene Therapy* **1998** 9: 1181–86.

Bateman, Randall J.; Chengjie Xiong; Tammie L.S. Benzinger; Anne M. Fagan; Alison Goate; Nick C. Fox; Daniel S. Marcus; et al. Clinical and Biomarker Changes in Dominantly Inherited Alzheimer's Disease. *New England Journal of Medicine* **2012** 367 (9): 795–804.

Beam, Christopher R.; Cody Kaneshiro; Jung Yun Jang; Chandra A. Reynolds; Nancy L. Pedersen; and Margaret Gatz. Differences between Women and Men in Incidence Rates of Dementia and Alzheimer's Disease. *Journal of Alzheimer's Disease* **2018** 64 (4): 1077–83.

Bohlen, Christopher J.; F. Chris Bennett; Andrew F. Tucker; Hannah Y. Collins; Sara B. Mulinyawe; and Ben A. Barres. Diverse Requirements for Microglial Survival, Specification, and Function Revealed by Defined-Medium Cultures. *Neuron* **2017** 94 (4): 759-773.e8.

Bolmont, Tristan; Florent Haiss; Daniel Eicke; Rebecca Radde; Chester A. Mathis; William E. Klunk; Shinichi Kohsaka; Mathias Jucker; and Michael E. Calhoun. Dynamics of the Microglial/Amyloid Interaction Indicate a Role in Plaque Maintenance. *Journal of Neuroscience* **2008** 28 (16): 4283–92.

Brawek, Bianca; and Olga Garaschuk. Microglial Calcium Signaling in the Adult, Aged and Diseased Brain. *Cell Calcium* **2013** 53 (3): 159–69.

Brawek, Bianca; and Olga Garaschuk. Single-Cell Electroporation for Measuring In Vivo Calcium Dynamics. In *Methods in Molecular Biology* **2019**, edited by Olga Garaschuk and Alexei Verkhratsky, 1st ed., 2034:231–41. Humana Press.

Brawek, Bianca; Yajie Liang; Daria Savitska; Kaizhen Li; Natalie Fomin-Thunemann; Yury Kovalchuk; Elizabeta Zirdum; Johan Jakobsson; and Olga Garaschuk. A New Approach for Ratiometric in Vivo Calcium Imaging of Microglia. *Scientific Reports* **2017** 7 (1): 1–13.

Brawek, Bianca; Maria Olmedillas del Moral; and Olga Garaschuk. In Vivo Visualization of Microglia Using Tomato Lectin. In *Methods in Molecular Biology* **2019**, edited by Olga Garaschuk and Alexei Verkhratsky, 1st ed., 2034:165–75. Humana Press.

Brawek, Bianca; Bernd Schwendele; Karin Riester; Shinichi Kohsaka; Chommanad Lerdkrai; Yajie Liang; and Olga Garaschuk. Impairment of in Vivo Calcium Signaling in Amyloid Plaque-Associated Microglia. *Acta Neuropathologica* **2014** 127 (4): 495–505.

Brionne, Thomas C.; Ina Tesseur; Eliezer Masliah; and Tony Wyss-Coray. Loss of TGF-B1 Leads to Increased Neuronal Cell Death and Microgliosis in Mouse Brain. *Neuron* **2003** 40 (6): 1133–45.

Butovsky, Oleg; Mark P. Jedrychowski; Craig S. Moore; Ron Cialic; Amanda J. Lanser; Galina Gabriely; Thomas Koeglsperger; et al. Identification of a Unique TGF-β-Dependent Molecular and Functional Signature in Microglia. *Nature Neuroscience* **2014** 17 (1): 131–43.

Cardona, Astrid E.; Erik P. Pioro; Margaret E. Sasse; Volodymyr Kostenko; Sandra M. Cardona; Ineke M. Dijkstra; De Ren Huang; et al. Control of Microglial Neurotoxicity by the Fractalkine Receptor. *Nature Neuroscience* **2006** 9 (7): 917–24.

Cherry, Jonathan D; John A Olschowka; and M Kerry O'Banion. Neuroinflammation and M2 Microglia: The Good, the Bad, and the Inflamed. *Journal of Neuroinflammation* **2014** 11: 98.

Chishti, M.A.; D.S. Yang; C. Janus; A.L. Phinney; P. Horne; J. Pearson; R. Strome; et al. Early-Onset Amyloid Deposition and Cognitive Deficits in Transgenic Mice Expressing a Double Mutant Form of Amyloid Precursor Protein 695. *Journal of Biological Chemistry* **2001** 276: 21562–70.

Condello, Carlo; Peng Yuan; Aaron Schain; and Jaime Grutzendler. Microglia Constitute a Barrier That Prevents Neurotoxic Protofibrillar Aβ42 Hotspots around Plaques. *Nature Communications* **2015** 6 (May 2014).

D'Andrea, Michael R.; Gregory M. Cole; and March D. Ard. The Microglial Phagocytic Role with Specific Plaque Types in the Alzheimer Disease Brain. *Neurobiology of Aging* **2004** 25 (5): 675–83.

Damani, Mausam R.; Lian Zhao; Aurora M. Fontainhas; Juan Amaral; Robert N. Fariss; and Wai T. Wong. Age-Related Alterations in the Dynamic Behavior of Microglia. *Aging Cell* **2011** 10 (2): 263–76.

Davalos, Dimitrios; Jaime Grutzendler; Guang Yang; Jiyun V Kim; Yi Zuo; Steffen Jung; Dan R Littman; Michael L Dustin; and Wen-Biao Gan. ATP Mediates Rapid Microglial Response to Local Brain Injury in Vivo. *Nature Neuroscience* **2005** 8 (6): 752–58.

Denizet, Marie; Laurent Cotter; Pierre Marie Lledo; and Françoise Lazarini. Sensory Deprivation Increases Phagocytosis of Adult-Born Neurons by Activated Microglia in the Olfactory Bulb. *Brain, Behavior, and Immunity* **2017** 60: 38–43.

Dinarello, Charles A. Interleukin 1 and Interleukin 18 as Mediators of Inflammation and the Aging Process. *The American Journal of Clinical Nutrition* **2006** 83 (2): 447S-455S.

Dudvarski Stankovic, Nevenka; Marcin Teodorczyk; Robert Ploen; Frauke Zipp; and Mirko H.H. Schmidt. Microglia–Blood Vessel Interactions: A Double-Edged Sword in Brain Pathologies. *Acta Neuropathologica* **2016** 131 (3): 347–63.

Dunn, Nicholas; Mark Mullee; Hugh Perry; and Clive Holmes. Association between Dementia and Infectious Disease: Evidence from a Case-Control Study. *Alzheimer Disease and Associated Disorders* **2005** 19 (2): 91–94.

Eichhoff, Gerhard; Bianca Brawek; and Olga Garaschuk. Microglial Calcium Signal Acts as a Rapid Sensor of Single Neuron Damage in Vivo. *Biochimica et Biophysica Acta - Molecular Cell Research* **2011** 1813 (5): 1014–24.

Engelhart, Marianne J.; Mirjam I. Geerlings; John Meijer; Amanda Kiliaan; Annemieke Ruitenberg; John C. Van Swieten; Theo Stijnen; Albert Hofman; Jacqueline C.M. Witteman; and Monique M.B. Breteler. Inflammatory Proteins in Plasma and the Risk of Dementia: The Rotterdam Study. *Archives of Neurology* **2004** 61 (5): 668–72.

Eyo, Ukpong B.; Mingshu Mo; Min Hee Yi; Madhuvika Murugan; Junting Liu; Rohan Yarlagadda; David J. Margolis; Pingyi Xu; and Long Jun Wu. P2Y12R-Dependent Translocation Mechanisms Gate the Changing Microglial Landscape. *Cell Reports* **2018** 23 (4): 959–66.

Färber, Katrin; and Helmut Kettenmann. Functional Role of Calcium Signals for Microglial Function. *Glia* **2006** 54 (10): 656–65.

Ferrero, Giuliano; Christopher B. Mahony; Eléonore Dupuis; Laurent Yvernogeau; Elodie Di Ruggiero; Magali Miserocchi; Marianne Caron; et al. Embryonic Microglia Derive from Primitive Macrophages and Are Replaced by Cmyb-Dependent Definitive Microglia in Zebrafish. *Cell Reports* **2018** 24 (1): 130–41.

Franceschi, Claudio; Massimilano Bonafè; Silvana Valensin; Fabiola Olivieri; Maria De Luca; Enzo Ottaviani; and Gliovanna De Benedictis. Inflamm-Aging: An Evolutionary Perspective on Immunosenescence. *Annals of the New York Academy of Sciences* **2000** 908 (1): 244–54.

Füger, Petra; Jasmin K. Hefendehl; Karthik Veeraraghavalu; Ann Christin Wendeln; Christine Schlosser; Ulrike Obermüller; Bettina M. Wegenast-Braun; et al. Microglia Turnover with Aging and in an Alzheimer's Model via Long-Term in Vivo Single-Cell Imaging. *Nature Neuroscience* **2017** 20 (10): 1371–76.

Galatro, Thais F.; Inge R. Holtman; Antonio M. Lerario; Ilia D. Vainchtein; Nieske Brouwer; Paula R. Sola; Mariana M. Veras; et al. Transcriptomic Analysis of Purified Human Cortical Microglia Reveals Age-Associated Changes. *Nature Neuroscience* **2017** 20 (8): 1162–71.

Games, Dora; David Adams; Ree Alessandrini; Robin Barbour; Patricia Borthelette; Catherine Blackwell; Tony Carr; et al. Alzheimer-Type Neuropathology in Transgenic Mice Overexpressing V717F β-Amyloid Precursor Protein. *Nature* **1995** 373 (6514): 523–27.

Garaschuk, Olga. Age-Related Changes in Microglial Physiology: The Role for Healthy Brain Ageing and Neurodegenerative Disorders. *Neuroforum* **2017** 23 (4): 182–91.

Garaschuk, Olga; and Alexei Verkhratsky. Chapter 3 Physiology of Microglia. In *Methods in Molecular Biology* **2019**, edited by Olga Garaschuk and Alexei Verkhratsky, 1st ed., 2034:27–40. Humana Press.

Ginhoux, Florent; Melanie Greter; Marylene Leboeuf; Sayan Nandi; Peter See; Solen Gokhan; Mark F Mehler; et al. Primitive Macrophages. *Science* **2010** 701 (November): 841–45.

Ginhoux, Florent; and Marco Prinz. Origin of Microglia: Current Concepts and Past Controversies. *Cold Spring Harbor Perspectives in Biology* **2015** 7 (8): 1–16.

Goldmann, Tobias; Peter Wieghofer; Philippe F. Müller; Yochai Wolf; Diana Varol; Simon Yona; Stefanie M. Brendecke; et al. A New Type of Microglia Gene Targeting Shows TAK1 to Be Pivotal in CNS Autoimmune Inflammation. *Nature Neuroscience* **2013** 16 (11): 1618–26.

Gosselin, David; Dylan Skola; Nicole G. Coufal; Inge R. Holtman; Johannes C.M. Schlachetzki; Eniko Sajti; Baptiste N. Jaeger; et al. An Environment-Dependent Transcriptional Network Specifies Human Microglia Identity. *Science* **2017** 356 (6344): 1248–59.

Grabert, Kathleen; Tom Michoel; Michail H. Karavolos; Sara Clohisey; J. Kenneth Baillie; Mark P. Stevens; Tom C. Freeman; Kim M. Summers; and Barry W. McColl. Microglial Brain Region-Dependent Diversity and Selective Regional Sensitivities to Aging. *Nature Neuroscience* **2016** 19 (3): 504–16.

Grace, Peter M.; Keith A. Strand; Erika L. Galer; Daniel J. Urban; Xiaohui Wang; Michael V. Baratta; Timothy J. Fabisiak; et al. Morphine Paradoxically Prolongs Neuropathic Pain in Rats by Amplifying Spinal NLRP3 Inflammasome Activation. *Proceedings of the National Academy of Sciences of the United States of America* **2016** 113 (24): E3441–50.

Grossmann, Ruth; Nick Stence; Jenny Carr; Leah Fuller; Marc Waite; and Michael E. Dailey. Juxtavascular Microglia Migrate along Brain Microvessels Following Activation during Early Postnatal Development. *Glia* **2002** 37 (3): 229–40.

Guneykaya, Dilansu; Andranik Ivanov; Daniel Perez Hernandez; Verena Haage; Bartosz Wojtas; Niklas Meyer; Meron Maricos; et al. Transcriptional and Translational Differences of Microglia from Male and Female Brains. *Cell Reports* **2018** 24 (10): 2773-2783.e6.

Haynes, Sharon E.; Gunther Hollopeter; Guang Yang; Dana Kurpius; Michael E. Dailey; Wen Biao Gan; and David Julius. The P2Y12 Receptor Regulates Microglial Activation by Extracellular Nucleotides. *Nature Neuroscience* **2006** 9 (12): 1512–19.

Hefendehl, Jasmin K.; Jonas J. Neher; Rafael B. Sühs; Shinichi Kohsaka; Angelos Skodras; and Mathias Jucker. Homeostatic and Injury-Induced Microglia Behavior in the Aging Brain. *Aging Cell* **2014** 13 (1): 60–69.

Heneka, Michael T.; Markus P. Kummer; Andrea Stutz; Andrea Delekate; Stephanie Schwartz; Ana Vieira-Saecker; Angelika Griep; et al. NLRP3 Is Activated in Alzheimer's Disease and Contributes to Pathology in APP/PS1 Mice. *Nature* **2013** 493 (7434): 674–78.

Henry, Christopher J.; Yan Huang; Angela M. Wynne; and Jonathan P. Godbout. Peripheral Lipopolysaccharide (LPS) Challenge Promotes Microglial Hyperactivity in Aged Mice That Is Associated with Exaggerated Induction of Both pro-Inflammatory IL-1β and Anti-Inflammatory IL-10 Cytokines. *Brain, Behavior, and Immunity* **2009** 23 (3): 309–17.

Hick, Meike; Ulrike Herrmann; Sascha W. Weyer; Jan Philipp Mallm; Jakob Andreas Tschäpe; Marianne Borgers; Marc Mercken; et al. Acute Function of Secreted Amyloid Precursor Protein Fragment APPsα in Synaptic Plasticity. *Acta Neuropathologica* **2015** 129 (1): 21–37.

Hickman, Suzanne E.; Nathan D. Kingery; Toshiro K. Ohsumi; Mark L. Borowsky; Li Chong Wang; Terry K. Means; and Joseph El Khoury. The Microglial Sensome Revealed by Direct RNA Sequencing. *Nature Neuroscience* **2013** 16 (12): 1896–1905.

Hines, Dustin J.; Rochelle M. Hines; Sean J. Mulligan; and Brian A. Macvicar. Microglia Processes Block the Spread of Damage in the Brain and Require Functional Chloride Channels. *Glia* **2009** 57 (15): 1610–18.

Hirasawa, Takae; K. Ohsawa; Y. Imai; Y. Ondo; C. Akazawa; S. Uchino; and Shinichi Kohsaka. Visualization of Microglia in Living Tissues Using Iba1-EGFP Transgenic Mice. *Brain and Nerve* **2007** 59 (7): 763–72.

Hoek, R. H.; S. R. Ruuls; C. A. Murphy; G. J. Wright; R. Goddard; S. M. Zurawski; B. Blom; et al. Down-Regulation of the Macrophage Lineage through Interaction with OX2 (CD200). *Science* **2000** 290 (5497): 1768–71.

Hof, Patrick R.; and John H. Morrison. The Aging Brain: Morphomolecular Senescence of Cortical Circuits. *Trends in Neurosciences* **2004** 27 (10): 607–13.

Hoffmann, Anja; Oliver Kann; Carsten Ohlemeyer; Uwe Karsten Hanisch; and Helmut Kettenmann. Elevation of Basal Intracellular Calcium as a Central Element in the Activation of Brain Macrophages (Microglia): Suppression of Receptor-Evoked Calcium Signaling and Control of Release Function. *Journal of Neuroscience* **2003** 23 (11): 4410–19.

Holcomb, Leigh; Marcia N Gordon; Eileen Mcgwan; X I N Yu; Stan Benkovic; Paul Antzen; Kristal Wright; et al. Accelerated Alzheimer-Type Phenotype in Transgenic Mice Carrying Both Mutant Amyloid Precursor Protein and Presenilin 1 Transgenes. **1998** 4: 97–100.

Hsiao, Karen; Paul Chapman; Steven Nilsen; Chris Eckman; Yasuo Harigaya; Steven Younkin; Fusheng Yang; and Greg Cole. Amyloid Plaques in Transgenic Mice. *Science* **1996** 274 (October): 99–102.

Irino, Yasuhiro; Yasuko Nakamura; Kazuhide Inoue; Shinichi Kohsaka; and Keiko Ohsawa. Akt Activation Is Involved in P2Y12 Receptor-Mediated Chemotaxis of Microglia. *Journal of Neuroscience Research* **2008** 86 (7): 1511–19.

Jankowsky, Joanna L.; and Hui Zheng. Practical Considerations for Choosing a Mouse Model of Alzheimer's Disease. *Molecular Neurodegeneration* **2017** 12 (1): 1–22.

Jung, S.; J. Aliberti; P. Graemmel; M. J. Sunshine; G. W. Kreutzberg; A. Sher; and D. R. Littman. Analysis of Fractalkine Receptor CX3CR1 Function by Targeted Deletion and Green Fluorescent Protein Reporter Gene Insertion. *Molecular and Cellular Biology* **2000** 20 (11): 4106–14.

Keren-Shaul, Hadas; Amit Spinrad; Assaf Weiner; Orit Matcovitch-Natan; Raz Dvir-Szternfeld; Tyler K. Ulland; Eyal David; et al. A Unique Microglia Type Associated with Restricting Development of Alzheimer's Disease. *Cell* **2017** 169 (7): 1276-1290.e17.

Kettenmann, H.; U.-K. Hanisch; M. Noda; and A. Verkhratsky. Physiology of Microglia. *Physiological Reviews* **2011** 91 (2): 461–553.

Klunk, William E.; Brian J. Bacskai; Chester A. Mathis; Stephen T. Kajdasz; Megan E. McLellan; Matthew P. Frosch; Manik L. Debnath; Daniel P. Holt; Yanming Wang; and Bradley T. Hyman. Imaging Aβ Plaques in Living Transgenic Mice with Multiphoton Microscopy and Methoxy-X04, a Systemically Administered Congo Red Derivative. *Journal of Neuropathology and Experimental Neurology* **2002** 61 (9): 797–805.

Korvers, Laura; Amanda de Andrade Costa; Martin Mersch; Vitali Matyash; Helmut Kettenmann; and Marcus Semtner. Spontaneous Ca2+transients in Mouse Microglia. *Cell Calcium* **2016** 60 (6): 396–406.

Kovalchuk, Yury; Ryota Homma; Yajie Liang; Anatoliy Maslyukov; Marina Hermes; Thomas Thestrup; Oliver Griesbeck; Jovica Ninkovic; Lawrence B. Cohen; and Olga Garaschuk. In Vivo Odourant Response Properties of Migrating Adult-Born Neurons in the Mouse Olfactory Bulb. *Nature Communications* **2015** 6.

Kozai, Takashi D.Yoshida; Alberto L. Vazquez; Cassandra L. Weaver; Seong Gi Kim; and X. Tracy Cui. In Vivo Two-Photon Microscopy Reveals Immediate Microglial Reaction to Implantation of Microelectrode through Extension of Processes. *Journal of Neural Engineering* **2012** 9 (6).

Krabbe, Grietje; Annett Halle; Vitali Matyash; Jan L. Rinnenthal; Gina D. Eom; Ulrike Bernhardt; Kelly R. Miller; Stefan Prokop; Helmut Kettenmann; and Frank L. Heppner. Functional Impairment of Microglia Coincides with Beta-Amyloid Deposition in Mice with Alzheimer-Like Pathology. *PLoS ONE* **2013** 8 (4).

Larsson, Christer. Protein Kinase C and the Regulation of the Actin Cytoskeleton. *Cellular Signalling* **2006** 18 (3): 276–84.

Lawson, L.J.; V.H. Perry; P. Dri; and S. Gordon. Heterogeneity in the Distribution and Morphology of Microglia in the Normal Adult Mouse Brain. *Neuroscience* **1990** 39 (1): 151–70.

Lazarini, Françoise; Marie Madeleine Gabellec; Nicolas Torquet; and Pierre Marie Lledo. Early Activation of Microglia Triggers Long-Lasting Impairment of Adult Neurogenesis in the Olfactory Bulb. *Journal of Neuroscience* **2012** 32 (11): 3652–64.

Lee, Geun Shik; Naeha Subramanian; Andrew I. Kim; Ivona Aksentijevich; Raphaela Goldbach-Mansky; David B. Sacks; Ronald N. Germain; Daniel L. Kastner; and Jae Jin Chae. The Calcium-Sensing Receptor Regulates the NLRP3 Inflammasome through Ca2+ and CAMP. *Nature* **2012** 492 (7427): 123–27.

Li, Qingyun; and Ben A. Barres. Microglia and Macrophages in Brain Homeostasis and Disease. *Nature Reviews Immunology* **2018** 18 (4): 225–42.

Li, Ying; Xu Fei Du; Chang Sheng Liu; Zi Long Wen; and Jiu Lin Du. Reciprocal Regulation between Resting Microglial Dynamics and Neuronal Activity In Vivo. *Developmental Cell* **2012** 23 (6): 1189–1202.

Liang, Yajie; Kaizhen Li; Kristoffer Riecken; Anatoliy Maslyukov; Diego Gomez-Nicola; Yury Kovalchuk; Boris Fehse; and Olga Garaschuk. Long-Term in Vivo Single-Cell Tracking Reveals the Switch of Migration Patterns in Adult-Born Juxtaglomerular Cells of the Mouse Olfactory Bulb. *Cell Research* **2016** 26 (7): 805–21.

Lopez-Atalaya, Jose P.; Katharine E. Askew; Amanda Sierra; and Diego Gomez-Nicola. Development and Maintenance of the Brain's Immune Toolkit: Microglia and Non-Parenchymal Brain Macrophages. *Developmental Neurobiology* **2018** 78 (6): 561–79.

Mandrekar, Shweta; Qingguang Jiang; C. Y.Daniel Lee; Jessica Koenigsknecht-Talboo; David M. Holtzman; and Gary E. Landreth. Microglia Mediate the Clearance of Soluble Aβ through Fluid Phase Macropinocytosis. *Journal of Neuroscience* **2009** 29 (13): 4252–62.

Mangialasche, Francesca; Alina Solomon; Bengt Winblad; Patrizia Mecocci; and Miia Kivipelto. Alzheimer's Disease: Clinical Trials and Drug Development. *The Lancet Neurology* **2010** 9 (7): 702–16.

Marín-Teva, José Luis; Isabelle Dusart; Catherine Colin; Annie Gervais; Nico Van Rooijen; and Michel Mallat. Microglia Promote the Death of Developing Purkinje Cells. *Neuron* **2004** 41 (4): 535–47.

Menassa, David A.; and Diego Gomez-Nicola. Microglial Dynamics during Brain Development. *Neural Regeneration Research* **2018** 13 (2): 222–23.

Michaud, Jean Philippe; Marc André Bellavance; Paul Préfontaine; and Serge Rivest. Real-Time in Vivo Imaging Reveals the Ability of Monocytes to Clear Vascular Amyloid Beta. *Cell Reports* **2013** 5 (3): 646–53.

Miller, Eric B.; Pengfei Zhang; Karli Ching; Edward N. Pugh; and Marie E. Burns. In Vivo Imaging Reveals Transient Microglia Recruitment and Functional Recovery of Photoreceptor Signaling after Injury. *Proceedings of the National Academy of Sciences of the United States of America* **2019** 116 (33): 16603–12.

Mittelbronn, M.; K. Dietz; H. J. Schluesener; and R. Meyermann. Local Distribution of Microglia in the Normal Adult Human Central Nervous System Differs by up to One Order of Magnitude. *Acta Neuropathologica* **2001** 101 (3): 249–55.

Mogensen, Trine H. Pathogen Recognition and Inflammatory Signaling in Innate Immune Defenses. *Clinical Microbiology Reviews* **2009** 22 (2): 240–73.

Montagna, Elena; Mario M. Dorostkar; and Jochen Herms. The Role of APP in Structural Spine Plasticity. *Frontiers in Molecular Neuroscience* **2017** 10 (May): 1–7.

Moya, K. L.; L. I. Benowitz; G. E. Schneider; and B. Allinquant. The Amyloid Precursor Protein Is Developmentally Regulated and Correlated with Synaptogenesis. *Developmental Biology* **1994**.

Mucke, L; E Masliah; GQ Yu; M Mallory; and EM Rockenstein. High-Level Neuronal Expression of Aβ1–42 in Wild-Type..Synaptotoxicity without Plaque Formation.Pdf. *J Neurosci* **2000** 20 (11): 4050–58.

Mukherjee, Shradha; Christine Klaus; Mihaela Pricop-Jeckstadt; Jeremy A. Miller; and Felix L. Struebing. A Microglial Signature Directing Human Aging and Neurodegeneration-Related Gene Networks. *Frontiers in Neuroscience* **2019** 13 (JAN): 1–12.

Murakami, T; J Ockinger; J Yu; V Byles; A McColl; A M Hofer; and T Horng. Critical Role for Calcium Mobilization in Activation of the NLRP3 Inflammasome. *Proc Natl Acad Sci U S A* **2012** 109 (28): 11282–87.

Navarro, Victoria; Elisabeth Sanchez-Mejias; Sebastian Jimenez; Clara Muñoz-Castro; Raquel Sanchez-Varo; Jose C. Davila; Marisa Vizuete; Antonia Gutierrez; and Javier Vitorica. Microglia in Alzheimer's Disease: Activated, Dysfunctional or Degenerative. *Frontiers in Aging Neuroscience* **2018** 10 (MAY): 1–8.

Nie, Xiang; Shiho Kitaoka; Kohei Tanaka; Eri Segi-Nishida; Yuki Imoto; Atsubumi Ogawa; Fumitake Nakano; et al. The Innate Immune Receptors TLR2/4 Mediate Repeated Social Defeat Stress-Induced Social Avoidance through Prefrontal Microglial Activation. *Neuron* **2018** 99 (3): 464-479.e7.

Nimmerjahn, Axel; Frank Kirchhoff; and Fritjof Helmchen. Resting Microglial Cells Are Highly Dynamic Surveillants of Brain Parenchyma in Vivo. *Science* **2005** 308 (May): 1314–19.

Oakley, Holly; Sarah L. Cole; Sreemathi Logan; Erika Maus; Pei Shao; Jeffery Craft; Angela Guillozet-Bongaarts; et al. Intraneuronal β-Amyloid Aggregates, Neurodegeneration, and Neuron Loss in Transgenic Mice with Five Familial Alzheimer's Disease Mutations: Potential Factors in Amyloid Plaque Formation. *Journal of Neuroscience* **2006** 26 (40): 10129–40.

Oddo, Salvatore; Antonella Caccamo; Jason D. Shepherd; M. Paul Murphy; Todd E. Golde; Rakez Kayed; Raju Metherate; Mark P. Mattson; Yama Akbari; and Frank M. LaFerla. Triple-Transgenic Model of Alzheimer's Disease with Plaques and Tangles: Intracellular Aβ and Synaptic Dysfunction. *Neuron* **2003** 39 (3): 409–21.

Okajima, Tomomi; and Fuminori Tsuruta. Microglial Dynamics during Brain Development. *Neural Regeneration Research* **2018** 13 (2): 222–23.

Olah, Marta; Ellis Patrick; Alexandra Chloe Villani; Jishu Xu; Charles C. White; Katie J. Ryan; Paul Piehowski; et al. A Transcriptomic Atlas of Aged Human Microglia. *Nature Communications* **2018** 9 (1): 1–8.

Olmedillas del Moral, Maria; Nithi Asavapanumas; Néstor L. Uzcátegui; and Olga Garaschuk. Healthy Brain Aging Modifies Microglial Calcium Signaling in Vivo. *International Journal of Molecular Sciences* **2019** 20 (3).

Orre, Marie; Willem Kamphuis; Lana M. Osborn; Jeroen Melief; Lieneke Kooijman; Inge Huitinga; Jan Klooster; Koen Bossers; and Elly M. Hol. Acute Isolation and Transcriptome Characterization of Cortical Astrocytes and Microglia from Young and Aged Mice. *Neurobiology of Aging* **2014** 35 (1): 1–14.

Ott, A.; R.P. Stolk; F. van Harskamp; H.A.P. Pols; A. Hofman; and M.M.B. Breteler. Diabetes Mellitus and the Risk of Dementia : The Rotterdam Study. **2016** 53 (December 1999): 1937–42.

Overmyer, M; S Helisalmi; H Soininen; M Laakso; P Riekkinen; and I Alafuzoff. Reactive Microglia in Aging and Dementia: An Immunohistochemical Study of Postmortem Human Brain Tissue. *Acta Neuropathologica* **1999** 97 (4): 383–92.

Paolicelli, Rosa Chiara; Kanchan Bisht; and Marie Ève Tremblay. Fractalkine Regulation of Microglial Physiology and Consequences on the Brain and Behavior. *Frontiers in Cellular Neuroscience* **2014** 8 (MAY): 1–10.

Parkhurst, Christopher N.; Guang Yang; Ipe Ninan; Jeffrey N. Savas; John R. Yates; Juan J. Lafaille; Barbara L. Hempstead; Dan R. Littman; and Wen Biao Gan. Microglia Promote Learning-Dependent Synapse Formation through Brain-Derived Neurotrophic Factor. *Cell* **2013** 155 (7): 1596–1609.

Perry, V. Hugh. Contribution of Systemic Inflammation to Chronic Neurodegeneration. *Acta Neuropathologica* **2010**.

Perry, V. Hugh; Colm Cunningham; and Clive Holmes. Systemic Infections and Inflammation Affect Chronic Neurodegeneration. *Nature Reviews Immunology* **2007**. Nature Publishing Group.

Perry, V Hugh; and Clive Holmes. Microglial Priming in Neurodegenerative Disease. *Nature Reviews. Neurology* **2014** 10 (4): 217–24.

Perry, V Hugh; and Jessica Teeling. Microglia and Macrophages of the Central Nervous System: The Contribution of Microglia Priming and Systemic Inflammation to Chronic Neurodegeneration. *Seminars in Immunopathology* **2013**.

Pozner, Amir; Ben Xu; Sierra Palumbos; J. Michael Gee; Petr Tvrdik; and Mario R. Capecchi. Intracellular Calcium Dynamics in Cortical Microglia Responding to Focal Laser Injury in the PC::G5-TdT Reporter Mouse. *Frontiers in Molecular Neuroscience* **2015** 8 (May): 1–10.

Priller, Christina; Thomas Bauer; Gerda Mitteregger; Bjarne Krebs; Hans A. Kretzschmar; and Jochen Herms. Synapse Formation and Function Is Modulated by the Amyloid Precursor Protein. *The Journal of Neuroscience : The Official Journal of the Society for Neuroscience* **2006** 26 (27): 7212–21.

Prince, Martin; Gemma Claire Ali; Maëlenn Guerchet; A. Matthew Prina; Emiliano Albanese; and Yu Tzu Wu. Recent Global Trends in the Prevalence and Incidence of Dementia, and Survival with Dementia. *Alzheimer's Research and Therapy* **2016** 8 (1).

Radde, Rebecca; Tristan Bolmont; Stephan A. Kaeser; Janaky Coomaraswamy; Dennis Lindau; Lars Stoltze; Michael E. Calhoun; et al. Aβ42-Driven Cerebral Amyloidosis in Transgenic Mice Reveals Early and Robust Pathology. *EMBO Reports* **2006** 7 (9): 940–46.

Réu, Pedro; Azadeh Khosravi; Samuel Bernard; Jeff E. Mold; Mehran Salehpour; Kanar Alkass; Shira Perl; et al. The Lifespan and Turnover of Microglia in the Human Brain. *Cell Reports* **2017** 20 (4): 779–84.

Río-Hortega, P. (**1919**) El "Tercer Elemento" de los Centros Nerviosos. I. La Microglía en Estado Normal, Boletín de la Sociedad Española de Biología VIII, pp. 67–82, (in Spanish).

Rosario, Awilda M.; Pedro E. Cruz; Carolina Ceballos-Diaz; Michael R. Strickland; Zoe Siemienski; Meghan Pardo; Keri Lyn Schob; et al. Microglia-Specific Targeting by Novel Capsid-Modified AAV6 Vectors. *Molecular Therapy - Methods and Clinical Development* **2016** 3 (February): 16026.

Sala Frigerio, Carlo; Leen Wolfs; Nicola Fattorelli; Nicola Thrupp; Iryna Voytyuk; Inga Schmidt; Renzo Mancuso; et al. The Major Risk Factors for Alzheimer's Disease: Age, Sex, and Genes Modulate the Microglia Response to Aβ Plaques. *Cell Reports* **2019** 27 (4): 1293-1306.e6.

Sasaguri, Hiroki; Per Nilsson; Shoko Hashimoto; Kenichi Nagata; Takashi Saito; Bart De Strooper; John Hardy; Robert Vassar; Bengt Winblad; and Takaomi C Saido. APP Mouse Models for Alzheimer's Disease Preclinical Studies . *The EMBO Journal* **2017** 36 (17): 2473–87.

Schafer, Dorothy P.; Emily K. Lehrman; Amanda G. Kautzman; Ryuta Koyama; Alan R. Mardinly; Ryo Yamasaki; Richard M. Ransohoff; Michael E. Greenberg; Ben A. Barres; and Beth Stevens. Microglia Sculpt Postnatal Neural Circuits in an Activity and Complement-Dependent Manner. *Neuron* **2012** 74 (4): 691–705.

Schmidt, Reinhold; Helena Schmidt; J. David Curb; Kamal Masaki; Lon R. White; and Lenore J. Launer. Early Inflammation and Dementia: A 25-Year Follow-up of the Honolulu-Asia Aging Study. *Annals of Neurology* **2002** 52 (2): 168–74.

Schwendele, Bernd; Bianca Brawek; Marina Hermes; and Olga Garaschuk. High-Resolution in Vivo Imaging of Microglia Using a Versatile Nongenetically Encoded Marker. *European Journal of Immunology* **2012** 42 (8): 2193–96.

Seifert, Stefanie; Maria Pannell; Wolfgang Uckert; Katrin Färber; and Helmut Kettenmann. Transmitter- and Hormone-Activated Ca2+ Responses in Adult Microglia/Brain Macrophages in Situ Recorded after Viral Transduction of a Recombinant Ca2+ Sensor. *Cell Calcium* **2011** 49 (6): 365–75.

Selkoe, Dennis J; and John Hardy. The Amyloid Hypothesis of Alzheimer's Disease at 25 Years. **2016** 8: 595–608.

Serneels, Lutgarde; Jérôme Van Biervliet; Katleen Craessaerts; Tim Dejaegere; Katrien Horré; Tine Van Houtvin; Hermann Esselmann; et al. γ-Secretase Heterogeneity in the Aph1 Subunit: Relevance for Alzheimer's Disease. **2009** 324 (May): 639–43.

Sierra, Amanda; Juan M. Encinas; Juan J.P. Deudero; Jessica H. Chancey; Grigori Enikolopov; Linda S. Overstreet-Wadiche; Stella E. Tsirka; and Mirjana Maletic-Savatic. Microglia Shape Adult Hippocampal Neurogenesis through Apoptosis-Coupled Phagocytosis. *Cell Stem Cell* **2010** 7 (4): 483–95.

Sierra, Amanda; Andrés C. Gottfried-Blackmore; Bruce S. Mcewen; and Karen Bulloch. Microglia Derived from Aging Mice Exihibit an Altered Inflammatory Profile. *Glia* **2007** 55: 412–24.

Sierra, Amanda; Rosa C. Paolicelli; and Helmut Kettenmann. Cien Años de Microglía: Milestones in a Century of Microglial Research. *Trends in Neurosciences* **2019** 42 (11): 778–92.

Simard, Alain R.; Denis Soulet; Genevieve Gowing; Jean Pierre Julien; and Serge Rivest. Bone Marrow-Derived Microglia Play a Critical Role in Restricting Senile Plaque Formation in Alzheimer's Disease. *Neuron* **2006** 49 (4): 489–502.

Singh, Tushar; and Anne B. Newman. Inflammatory Markers in Population Studies of Aging. *Ageing Research Reviews* **2011** 10 (3): 319–29.

Slifkin, M.; and R. J. Doyle. Lectins and Their Application to Clinical Microbiology. *Clinical Microbiology Reviews* **1990** 3 (3): 197–218.

Sochocka, Marta; Breno Satler Diniz; and Jerzy Leszek. Inflammatory Response in the CNS: Friend or Foe? *Molecular Neurobiology* **2017** 54 (10): 8071–89.

Song, Wilbur M.; and Marco Colonna. The Identity and Function of Microglia in Neurodegeneration. *Nature Immunology* **2018** 19 (10): 1048–58.

Sousa, Carole; Knut Biber; and Alessandro Michelucci. Cellular and Molecular Characterization of Microglia: A Unique Immune Cell Population. *Frontiers in Immunology* **2017** 8 (MAR).

Stebbing, Martin James; Jennifer Marie Cottee; and Indrajeetsinh Rana. The Role of Ion Channels in Microglial Activation and Proliferation - a Complex Interplay between Ligand-Gated Ion Channels, K+ Channels, and Intracellular Ca2+. *Frontiers in Immunology* **2015** 6 (OCT): 1–7.

Stence, Nick; Marc Waite; and Michael E. Dailey. Dynamics of Microglial Activation: A Confocal Time-lapse Analysis in Hippocampal Slices. *Glia* **2001** 33 (3): 256–66.

Stevens, Beth; Nicola J. Allen; Luis E. Vazquez; Gareth R. Howell; Karen S. Christopherson; Navid Nouri; Kristina D. Micheva; et al. The Classical Complement Cascade Mediates CNS Synapse Elimination. *Cell* **2007** 131 (6): 1164–78.

Streit, Wolfgang J.; Nicole W. Sammons; Amanda J. Kuhns; and D. Larry Sparks. Dystrophic Microglia in the Aging Human Brain. *Glia* **2004** 45 (2): 208–12.

Streit, Wolfgang J.; Qing Shan Xue; Jasmin Tischer; and Ingo Bechmann. Microglial Pathology. *Acta Neuropathologica Communications* **2014** 2 (1): 1–17.

Strooper, B. De; M. Simons; G. Multhaup; F. Van Leuven; K. Beyreuther; and C. G. Dotti. Production of Intracellular Amyloid-Containing Fragments in Hippocampal Neurons Expressing Human Amyloid Precursor Protein and Protection against Amyloidogenesis by Subtle Amino Acid Substitutions in the Rodent Sequence. *The EMBO Journal* **1995** 14 (20): 4932–38.

Strooper, Bart De; and Wim Annaert. Proteolytic Processing and Cell Biological Functions of the Amyloid Precursor Protein. *Journal of Cell Science* **2000** 113 (11): 1857–70.

Sturchler-Pierrat, Christine; Dorothee Abramowski; Mairead Duke; Karl Heinz Wiederhold; Claudia Mistl; Sabin Rothacher; Birgit Ledermann; et al. Two Amyloid Precursor Protein Transgenic Mouse Models with Alzheimer Disease-like Pathology. *Proceedings of the National Academy of Sciences of the United States of America* **1997** 94 (24): 13287–92.

Sykova, E.; and Charles Nicholson. Diffusion in Brain Extracellular Space. *Physiological Reviews* **2008** 88 (4): 1277–1340.

Sykova, E.; I. Vorisek; T. Antonova; T. Mazel; M. Meyer-Luehmann; M. Jucker; M. Hajek; M. Ort; and J. Bures. Changes in Extracellular Space Size and Geometry in APP23 Transgenic Mice: A Model of Alzheimer's Disease. *Proceedings of the National Academy of Sciences* **2005** 102 (2): 479–84.

Tay, Tuan Leng; Dominic Mai; Jana Dautzenberg; Francisco Fernández-Klett; Gen Lin; S. Sagar; Moumita Datta; et al. A New Fate Mapping System Reveals Context-Dependent Random or Clonal Expansion of Microglia. *Nature Neuroscience* **2017** 20 (6): 793–803.

Timmerman, Raissa; Saskia M. Burm; and Jeffrey J. Bajramovic. An Overview of in Vitro Methods to Study Microglia. *Frontiers in Cellular Neuroscience* **2018** 12 (August): 1–12.

Torres-Platas, G, S Comeau, S; A Rachalski; G Bo, D; C Cruceanu; G Turecki; B Giros; and N Mechawar. Morphometric Characterization of Microglial Phenotypes in Human Cerebral Cortex. *Journal of Neuroinflammation* **2014** 11:12.

Tremblay, Marie-Ève; Martha L Zettel; James R Ison; Paul D Allen; and Ania K Majewska. Effects of Aging and Sensory Loss on Glial Cells in Mouse Visual and Auditory Cortices. *Glia* **2012** 60 (4): 541–58.

Tremblay, Marie Ève; Rebecca L. Lowery; and Ania K. Majewska. Microglial Interactions with Synapses Are Modulated by Visual Experience. *PLoS Biology* **2010** 8 (11).

Tvrdik, Petr; and M. Yashar S. Kalani. In Vivo Imaging of Microglial Calcium Signaling in Brain Inflammation and Injury. *International Journal of Molecular Sciences* **2017** 18 (11).

Tyan, Sheue Houy; Ann Yu Jung Shih; Jessica J. Walsh; Hiroko Maruyama; Floyd Sarsoza; Lawrence Ku; Simone Eggert; Patrick R. Hof; Edward H. Koo; and Dara L. Dickstein. Amyloid Precursor Protein (APP) Regulates Synaptic Structure and Function. *Molecular and Cellular Neuroscience* **2012** 51 (1–2): 43–52.

Unger, M. S.; P. Schernthaner; J. Marschallinger; H. Mrowetz; and L. Aigner. Microglia Prevent Peripheral Immune Cell Invasion and Promote an Anti-Inflammatory Environment in the Brain of APP-PS1 Transgenic Mice. *Journal of Neuroinflammation* **2018** 15 (1): 1–23.

Verderio, C.; and M. Matteoli. ATP Mediates Calcium Signaling Between Astrocytes and Microglial Cells: Modulation by IFN- . *The Journal of Immunology* **2001** 166 (10): 6383–91.

Verkhratsky, Alexei; and Vladimir Parpura. Store-Operated Calcium Entry in Neuroglia. *Neuroscience Bulletin* **2014** 30 (1): 125–33.

Villa, Alessandro; Paolo Gelosa; Laura Castiglioni; Mauro Cimino; Nicoletta Rizzi; Giovanna Pepe; Federica Lolli; et al. Sex-Specific Features of Microglia from Adult Mice. *Cell Reports* **2018** 23 (12): 3501–11.

Villa, Alessandro; Sara Della Torre; and Adriana Maggi. Sexual Differentiation of Microglia. *Frontiers in Neuroendocrinology* **2019** 52 (November 2018): 156–64.

Virgilio, Francesco Di. Purinergic Mechanism in the Immune System: A Signal of Danger for Dendritic Cells. *Purinergic Signalling* **2005** 1 (3): 205–9.

Wake, H.; A. J. Moorhouse; S. Jinno; S. Kohsaka; and J. Nabekura. Resting Microglia Directly Monitor the Functional State of Synapses In Vivo and Determine the Fate of Ischemic Terminals. *Journal of Neuroscience* **2009** 29 (13): 3974–80.

Walz, W.; S. Ilschner; C. Ohlemeyer; R. Banati; and H. Kettenmann. Extracellular ATP Activates a Cation Conductance and a K Conductance in Cultured Microglial Cells from Mouse Brain. *Journal of Neuroscience* **1993** 13 (10): 4403–11.

Wang, Zilai; Baiping Wang; Li Yang; Qinxi Guo; Nadia Aithmitti; Zhou Songyang; and Hui Zheng. Presynaptic and Postsynaptic Interaction of the Amyloid Precursor Protein Promotes Peripheral and Central Synaptogenesis. *Journal of Neuroscience* **2009** 29 (35): 10788–801.

Weyer, Sascha W.; Marta Zagrebelsky; Ulrike Herrmann; Meike Hick; Lennard Ganss; Julia Gobbert; Morna Gruber; et al. Comparative Analysis of Single and Combined APP/APLP Knockouts Reveals Reduced Spine Density in APP-KO Mice That Is Prevented by APPsα Expression. *Acta Neuropathologica Communications* **2014** 2 (1): 1–15.

Wohleb, Eric S.; and Jonathan P. Godbout. Basic Aspects of the Immunology of Neuroinflammation. *Inflammation in Psychiatry* **2013** 28: 1–19.

Yona, Simon; Ki Wook Kim; Yochai Wolf; Alexander Mildner; Diana Varol; Michal Breker; Dalit Strauss-Ayali; et al. Fate Mapping Reveals Origins and Dynamics of Monocytes and Tissue Macrophages under Homeostasis. *Immunity* **2013** 38 (1): 79–91.

Zöller, Tanja; Abdelraheim Attaai; Phani Sankar Potru; Tamara Ruß; and Björn Spittau. Aged Mouse Cortical Microglia Display an Activation Profile Suggesting Immunotolerogenic Functions. *International Journal of Molecular Sciences* **2018** 19 (3): 1–11.

Zusso, Morena; Laurent Methot; Rita Lo; Andrew D. Greenhalgh; Samuel David; and Stefano Stifani. Regulation of Postnatal Forebrain Amoeboid Microglial Cell Proliferation and Development by the Transcription Factor Runx1. *Journal of Neuroscience* **2012** 32 (33): 11285–98.

8. Publications

Parts of this thesis have been published in form of the following scientific articles:

Research article:

Olmedillas del Moral M., Asavapanumas N., Uzcátegui N. L., Garaschuk O. Healthy Brain Aging Modifies Microglial Calcium Signaling In Vivo. *Int. J. Mol. Sci.* 2019, 20 (3).

Book chapter:

Brawek B., **Olmedillas del Moral M.**, Garaschuk O. (2019) In Vivo Visualization of Microglia Using Tomato Lectin. In: Garaschuk O., Verkhratsky A. (eds) Microglia. Methods in Molecular Biology, vol 2034. Humana, New York, NY.

9. Declaration of contribution

The dissertation work was carried out in the Institute of Physiology, Department of Neurophysiology, at the Eberhard Karls Universität Tübingen under the supervision of Professor Olga Garaschuk. The study was conceived by Professor Olga Garaschuk. Dr. Kaizhen Li contributed to the generation of the lentiviral vectors used in this study. I accomplished anything else (~95%) in this study. I hereby declare that I have produced the work entitled "Changes of *in vivo* functional properties of microglia in aging and Alzheimer's disease", submitted for the award of a doctorate on my own, have used only the sources and aids I indicated and have marked passages included from other works. I sear upon oath that these statements are true and that I have not concealed anything. I am aware that making false declaration under oath is punishable by a term of imprisonment of up to three years or by a fine.

Tübingen, 15.12.2019

Signature:

10. Aknowledgements